

**Development of a Flow Injection Analysis Fourier
Transform Mass Spectrometry (FIA-FTMS)
Method to Quantify Lipid Species Profiles
of Biological Samples**



Dissertation
zur Erlangung des Doktorgrades
der Biomedizinischen Wissenschaften
(Dr. rer. physiol.)

der
Fakultät für Medizin
der Universität Regensburg

vorgelegt von
Marcus Höring
aus Würzburg

im Jahr
2019

**Development of a Flow Injection Analysis Fourier
Transform Mass Spectrometry (FIA-FTMS)
Method to Quantify Lipid Species Profiles
of Biological Samples**



Dissertation
zur Erlangung des Doktorgrades
der Biomedizinischen Wissenschaften
(Dr. rer. physiol.)

der
Fakultät für Medizin
der Universität Regensburg

vorgelegt von
Marcus Höring
aus Würzburg

im Jahr
2019

Dekan: Prof. Dr. Dr. Torsten E. Reichert

Betreuer: PD Dr. Gerhard Liebisch

Tag der mündlichen Prüfung: 13.09.2019

I Zusammenfassung

Eine genaue und reproduzierbare Quantifizierung von Lipidspezies ist von entscheidender Bedeutung für ein besseres Verständnis der funktionellen Bedeutung von Lipidspezies. Die Massenspektrometrie stellt dafür das wichtigste analytische Verfahren dar. Die folgende Arbeit beschreibt die Entwicklung einer Fließ-Injektion-Analyse Fourier-Transformation Massenspektrometrie Methode (FIA-FTMS) zur Messung und Quantifizierung von Lipidspeziesprofilen in biologischen Proben mit einem hohen Probendurchsatz. Die Methode wurde an einer Q Exactive Orbitrap mit einer maximalen Auflösung von 140,000 bei m/z 200 entwickelt. Um einen hohen Probendurchsatz zu erreichen wurde eine einfache Aufarbeitung (Bligh & Dyer Extraktion), kurze Messzeiten von weniger als 4 Minuten und eine selbst programmierten Daten Auswertung in Microsoft Excel verwendet.

Ein wichtiger Schritt in der Datenauswertung von lipidomischen Daten stellt die Isotopenkorrektur dar, die zum einen für das natürliche Vorkommen der Isotope (Isotopenkorrektur Typ I) und zum anderen für den Überlapp des zweiten Isotops einer Spezies mit einer zusätzlichen Doppelbindung (Isotopenkorrektur Typ II) korrigiert. Durch Experimente mit synthetischen Standards konnte gezeigt werden, dass eine Reihe von Lipidspezies von Peak Koaleszenz betroffen ist. Dabei handelt es sich um ein Phänomen, welches für Fourier-Transformation Massenspektrometer als konstruktive und/oder destruktive Interferenz von Peaks beschrieben wurde. Peak Koaleszenz kann bei nah-isobaren Ionen auftreten, wie z.B. dem Typ II-Überlapp in Doppelbindungsserien ($\Delta m/z$ 0.00894 für einen Überlapp resultierend aus zwei ^{13}C -Atomen). Im Rahmen dieser Arbeit konnte gezeigt werden, dass trotz Peak Koaleszenz eine akkurate Quantifizierung von Lipidspezies über einen weiten Bereich möglich ist. Wie erwartet ist für Spezies mit $m/z < 600$ keine Typ-II Korrektur notwendig, da die Massenauflösung ausreichend für eine Trennung der isobaren Peaks innerhalb einer Doppelbindungsreihe ist. Unerwartet war, dass für Spezies mit $m/z > 800$ keine Typ-II Korrektur nötig ist, obwohl isobare Spezies hier z.T. vollständig überlappen. Im Massenbereich von m/z 600 bis 800 kommt es zu einem partiellen Überlapp von isobaren Peaks. Hier konnte gezeigt werden, dass mittels „I/A“-Korrektur die Richtigkeit der ermittelten

Konzentrationen deutlich verbessert wird. Dafür wird ein Korrekturfaktor aus Intensität und Fläche der isobaren Peaks bestimmt und mit der Konzentration multipliziert.

Außerdem konnten wir zeigen, dass Cholesterin Ester (CE) wesentliche Unterschiede in der analytischen Response in Bezug auf Kettenlänge, Zahl der Doppelbindungen, infundierte CE Gesamtkonzentration und das Vorhandensein zusätzlicher Lipidklassen aufweisen. Als Hauptgrund für die Response Unterschiede konnten wir Fragmentierungsprozesse in der Ionenquelle während der Elektrospray-Ionisation nachweisen. Die Fragmentierung in der Ionenquelle nimmt insbesondere mit der Zahl der Doppelbindungen in den CE Spezies ab. Mit Hilfe synthetischer Standards konnten Responsefaktoren zur Korrektur der CE Spezies berechnet werden. Erst durch Anwendung dieser Responsefaktoren konnte eine gute Übereinstimmung von Serum-Konzentration mittels FTMS und einem zertifizierten enzymatischen Test erreicht werden. Die Bestimmung von freiem Cholesterin (FC) erfolgt über die gleichzeitige Sammlung und Fragmentierung der Vorläuferionen von FC und D₇-FC (FIA-MSX/FTMS). Die Quantifizierung mit den spezifischen Cholestadiene Fragmenten zeigte im Vergleich mit einer etablierten Acetylchlorid-Derivatisierung übereinstimmende Resultate.

Eine abschließende Methodvalidierung demonstrierte, dass FIA-FTMS und FIA-MSX/FTMS zur Quantifizierung von Lipidspezies in biologischen Proben wie Plasma, Serum, Geweben oder Zellhomogenaten in wissenschaftlichen und klinischen Studien geeignet sind. Die Methoden überzeugen durch hohe Reproduzierbarkeit und ausreichende Sensitivität.

II Abstract

A key requirement to get more insight into the functional role of lipid species is their accurate and precise quantification in biological samples. Considering that, mass spectrometry provides the main analytical tool. The following work describes the development of a flow injection analysis Fourier-Transform mass spectrometry (FIA-FTMS) method to analyze and quantify lipid species profiles of biological samples in high throughput. The method applied a Q Exactive Orbitrap with a maximum resolution of 140,000 at m/z 200, a simple lipid extraction (Bligh and Dyer), short analysis times of less than 4 min and an automated data evaluation with self-programmed macros in Microsoft Excel.

Data deconvolution of lipidomic data includes isotope correction as a crucial step, which comprises the correction of the natural abundance of isotopes (type I effect) and the overlap resulting from the second isotope of a species with one additional double bond (type II effect). Experiments with synthetic standards revealed peak coalescence for a number of lipid species, a phenomenon described for Fourier-Transform mass spectrometry (FTMS) as constructive and/or destructive interference of peaks. Peak coalescence occurs for near-isobaric ions e.g. related to type II overlap in double bond series with $\Delta m/z$ 0.00894 (for isotopic peaks resulting from incorporation of two ^{13}C -atoms). Here, we could demonstrate that, despite peak coalescence, accurate quantification is possible for a wide range of lipid species. As expected, peaks with $m/z < 600$ require no type II correction due to sufficient mass resolution to resolve isobaric peaks within a double bond series. Unexpected, peaks with $m/z > 800$ did not require type II isotope correction despite completely overlapping isobaric peaks within a double bond series. In the mass range m/z 600-800, accuracy of the concentrations of partially overlapping peaks could be improved by the so-called I/A correction (developed in this thesis). The I/A correction applies a correction factor that is calculated from the intensity and area of the overlapping peaks.

Furthermore, we could show that, upon full scan FTMS quantification, cholesteryl esters (CE) show substantial differences in their analytical response depending on the number of double bonds (DB), length of the acyl chain,

infused lipid concentration, and other lipid components. A major determinant for these response differences is their susceptibility to in-source fragmentation. In particular, introduction of DB lowers the degree of in-source fragmentation. Moreover, the results obtained by synthetic standards allowed the calculation of response factors, whose application corrected for the analytical response differences, as the comparison with a certified enzymatic test confirmed. The determination of free cholesterol (FC) was performed by simultaneous collection and fragmentation of precursor ions of FC and D₇-FC (FIA-MSX/FTMS). The quantification matched the results obtained with an established acetyl chloride derivatization method, which improved signal intensities by ~400 fold.

Finally, method validation demonstrated that FIA-FTMS and FIA-MSX/FTMS are applicable for quantification of lipid species in biological samples used in basic science as well as in clinical studies such as cultured cells, tissue homogenates, plasma, and serum. The method showed a high reproducibility and sufficient sensitivity for precise and accurate quantification.

III Index of Abbreviations

AGC	Automated Gain Control
ATP	Adenosine Triphosphate
B&D	Bligh and Dyer
BMI.....	Body-Mass-Index
Calcd.....	Calculated
CL	Cardiolipin
CE	Cholesteryl Ester
Cer	Ceramide
CV	Coefficient of Variation
DB	Double Bond
DBA.....	Double Bond Ambiguity
DC.....	Direct Current
DG.....	Diacylglycerol
DMEM	Dulbecco's Modified Eagle Medium
ESI	Electro-Spray-Ionization
FA	Fatty Acyl
FAME	Fatty Acid Methyl Esters
FC	Free Cholesterol
FIA	Flow Injection Analysis
FT.....	Fourier Transform
FWHM.....	Full Width at Half Maximum
GC-MS	Gas Chromatography Mass Spectrometry
GL	Glycerolipids
GP.....	Glycerophospholipids
HCD	Higher-Energy Collisional Dissociation
HexCer.....	Hexosylceramide

Index of Abbreviations

HR	High Resolution
I/A	Intensity/Area
IS	Internal Standard
IT	Injection Time
LC	Liquid Chromatography
LOD	Limit of Detection
LOQ	Limit of Quantification
LPC	Lysophosphatidylcholine
LPE	Lysophosphatidylethanolamine
M+0	Monoisotopic Peak of Molecule M
M+2	Second Isotope of Molecule M
MG	Monoacylglycerol
MS	Mass Spectrometry
MSX	Multiplexed MS/MS
MUFA	Monounsaturated Fatty Acid
MW	Molecular Weight
PC	Phosphatidylcholine
PE	Phosphatidylethanolamine
PG	Phosphatidylglycerol
PI	Phosphatidylinositol
PK	Polyketides
PR	Prenol Lipids
PS	Phosphatidylserine
PRM	Parallel Reaction Monitoring
PUFA	Polyunsaturated Fatty Acid
RF	Radio Frequency
RIA	Relative Isotopic Abundance

Index of Abbreviations

SD	Standard Deviation
SL.....	Saccharolipids
SM.....	Sphingomyelin
SP	Sphingolipids
ST	Sterol Lipids
TC	Total Cholesterol
TG	Triacylglycerol
TOF	Time-of-Flight

IV Table of Content

I	ZUSAMMENFASSUNG.....	I
II	ABSTRACT	III
III	INDEX OF ABBREVIATIONS	V
IV	TABLE OF CONTENT.....	IX
1	INTRODUCTION	1
1.1	Chemistry and Biology of Mammalian Lipids	1
1.1.1	Main Categories of Lipids	1
1.1.1.1	Fatty Acyls (FA)	2
1.1.1.2	Glycerolipids (GL)	2
1.1.1.3	Glycerophospholipids (GP)	3
1.1.1.4	Sterol Lipids (ST)	5
1.1.1.5	Sphingolipids (SP)	6
1.2	Principles of Mass Spectrometry and Types of Mass Spectrometers	7
1.2.1	Electro-Spray-Ionization.....	7
1.2.2	Quadrupole Mass Analyzers	8
1.2.3	Orbitrap Mass Analyzers.....	10
1.2.4	The Q Exactive Orbitrap Mass Spectrometer.....	11
1.3	Lipidomics.....	13
1.3.1	Definition and Principles	13
1.3.2	LC-based vs Shotgun Lipidomics.....	14
1.3.3	Lipid Nomenclature	15
1.4	Aim of this Work.....	16
2	MATERIALS AND METHODS.....	17
2.1	Chemicals	17
2.2	Internal Standards.....	17
2.3	Laboratory Equipment.....	18
2.3.1	Laboratory at the University Hospital Regensburg.....	18

Table of Content

2.3.2	Mass Spectrometry at the University of Southern Denmark	19
2.4	Biological Samples	20
2.5	Sample Preparation	20
2.5.1	Tissue Homogenization	20
2.5.2	Lipid Extraction	20
2.6	Lipid Species Quantification by FIA-FTMS	21
2.6.1	FIA-FTMS	21
2.6.2	Lipid Class Determination	21
2.6.3	Data Processing and Quantification	22
2.6.3.1	Calculation of Isotopic Probabilities	22
2.6.3.2	Peak Assignment and Offset Correction	22
2.6.3.3	Isotope Correction	23
2.6.3.4	Sodium Correction	24
2.6.3.5	Quantification	25
2.6.3.6	Cholesteryl Ester Response Correction	25
2.6.3.7	Background Correction	25
2.6.4	Method Validation	25
2.7	Instrument Response of Cholesteryl Esters	27
2.7.1	Preparation of Standard Mixtures and Matrix Spikes	27
2.7.2	FIA-FTMS using a Q Exactive Orbitrap	27
2.7.3	Nano-ESI-FIA-FTMS using an Orbitrap Fusion	27
2.7.4	Data Processing and Determination of Response	28
2.8	Evaluation of Isotope Correction Algorithm	28
2.8.1	Preparation of Standard Mixtures and Matrix Spikes	28
2.8.2	FIA-FTMS using a Q Exactive Orbitrap	29
2.8.3	Data Processing	29
3	RESULTS AND DISCUSSION	30
3.1	Isotope Correction Algorithm for FIA-FTMS	30
3.1.1	Peak Picking and Constellations	30
3.1.2	Intensity/Area Ratio	33
3.1.3	Comparison of Isotope Correction Algorithms	35
3.1.3.1	Type II Correction of Isotopic Overlap	43
3.1.3.2	Concentrations without Type II Correction	43

Table of Content

3.1.3.3	Peak Coalescence in FTMS.....	44
3.1.3.4	The “I/A Correction”	44
3.1.4	Resolution dependent Isotope Correction	46
3.1.5	Influence of Sample Matrix	49
3.1.6	Summary of Isotope Correction Algorithm for FIA-FTMS.....	60
3.2	Quantification of Cholesterol and Cholesteryl Ester.....	62
3.2.1	Quantification of Free Cholesterol by FIA-MSX/FTMS.....	62
3.2.2	Analytical Response of Cholesteryl Esters quantified by FIA-ESI-FTMS..	64
3.2.2.1	Effect of Acyl Chain Composition and Ionization Adduct	65
3.2.2.2	Effect of Total CE Concentration.....	70
3.2.2.3	Influence of Sample Matrix.....	72
3.2.2.4	Quantification of CE Species in a Dilution Series of Human Serum...	73
3.2.2.5	Model Compilation for calculating Species-specific Responses.....	76
3.2.2.6	Application of Response Correction on Human Serum Samples	77
3.2.2.7	Response Comparison with Chip-based Infusion nano ESI-FTMS....	78
3.3	Method Validation	81
3.3.1	Intraday and Day-to-Day Reproducibility	81
3.3.2	Limits of Quantification.....	93
3.3.3	Dynamic Range of Quantification.....	97
4	CONCLUSION.....	100
5	BIBLIOGRAPHY	103
V	ACKNOWLEDGEMENT	XIII
VI	LEBENS LAUF.....	XV
VII	SELBSTÄNDIGKEITSERKLÄRUNG	XVII

1 Introduction

1.1 Chemistry and Biology of Mammalian Lipids

A simple definition for lipids is that they are soluble in nonpolar solvents like chloroform or alcohols. However, this definition is quite broad and can be misleading since many substances are nowadays regarded as lipid that may also be soluble in water, for example bile acid conjugates. Newer definitions from LipidMaps (<https://www.lipidmaps.org>) with the purpose of creating a comprehensive classification define lipids as hydrophobic or amphiphatic small molecules that may originate entirely or in part by carbanion-based condensations of thioesters and/or by carbocation-based condensations of isoprene units (Fahy et al., 2005; Fahy et al., 2009).

1.1.1 Main Categories of Lipids

In 2005, the LipidMaps consortium has published a chemically based classification system for lipids (Fahy et al., 2005). Following the publication, lipid species are placed into eight lipid categories: fatty acyls (FA), glycerolipids (GL), glycerophospholipids (GP), sphingolipids (SP), sterol lipids (ST), prenol lipids (PR), saccharolipids (SL), and polyketides (PK). This chapter will briefly introduce the mammalian lipid categories FA, GL, GP, SP, and ST (Figure 1.1).

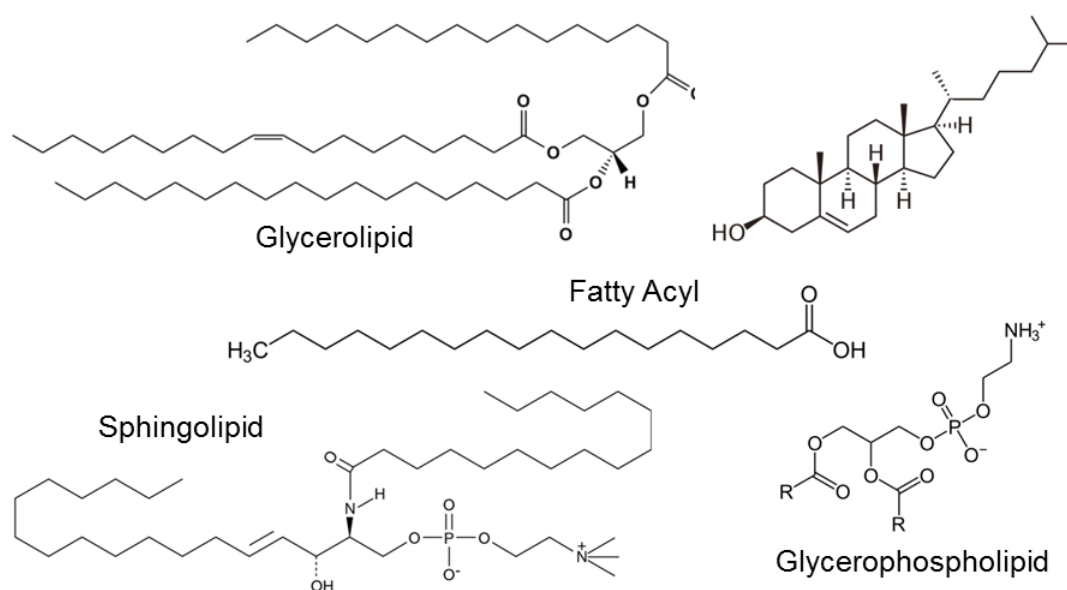


Figure 1.1 Examples of species of the main mammalian lipid categories.

1.1.1.1 Fatty Acyls (FA)

Fatty acyls are synthesized by chain elongation (addition of C_2 units) of an acetyl-CoA with a malonyl-CoA or methylmalonyl-CoA group (Fahy et al., 2005). Depending on the chemical structure, the lipid category consists of various subgroups, for example eicosanoids or fatty alcohols. However, the most prominent members are fatty acids, which contain a carboxyl group. The fatty acids are classified concerning their degree of saturation, branched chains or additional functional groups. In general, fatty acids are main components of most natural lipids in the human body and play crucial roles in health and disease. First, fatty acids serve as source of energy in the β -oxidation. Full oxidation of one molecule palmitic acid ($C_{16}H_{32}O_2$) yields in total 106 molecules ATP. For comparison, full oxidation of one molecule glucose ($C_6H_{12}O_6$) by cellular respiration yields in total only 32 molecules ATP. Furthermore, the fatty acid composition of membrane lipids is one of the regulatory principles of the biophysical membrane properties, which are also important to regulate the activity of membrane proteins (Stubbs & Smith, 1984). However, dysregulation of the fatty acid homeostasis can lead to severe diseases. For example atherosclerosis, neurodegenerative diseases, or various types of cancer are often related to an uncontrolled endogenous palmitic acid biosynthesis (Carta, Murru, Banni, & Manca, 2017).

1.1.1.2 Glycerolipids (GL)

The molecules of this category (GL) are composed of glycerol attached with one, two, or three substitutes. The most relevant substitutes are fatty acids esterified to glycerol (Coleman & Lee, 2004). In some cases, fatty alcohols can be attached via ether bonds to the glycerol. Depending on the number of attached fatty acids the lipid classes are referred to as monoradylglycerol, diradylglycerol, or triradylglycerol (Liebisch et al., 2013). Further subclasses are represented by glycosylradylglycerols, which are characterized by the linkage of one or more sugar residues attached via glycosidic linkage. The chemical structure of exemplary species of monoacylglycerols (MG), diacylglycerols (DG), and triacylglycerols (TG) is shown in Figure 1.2.

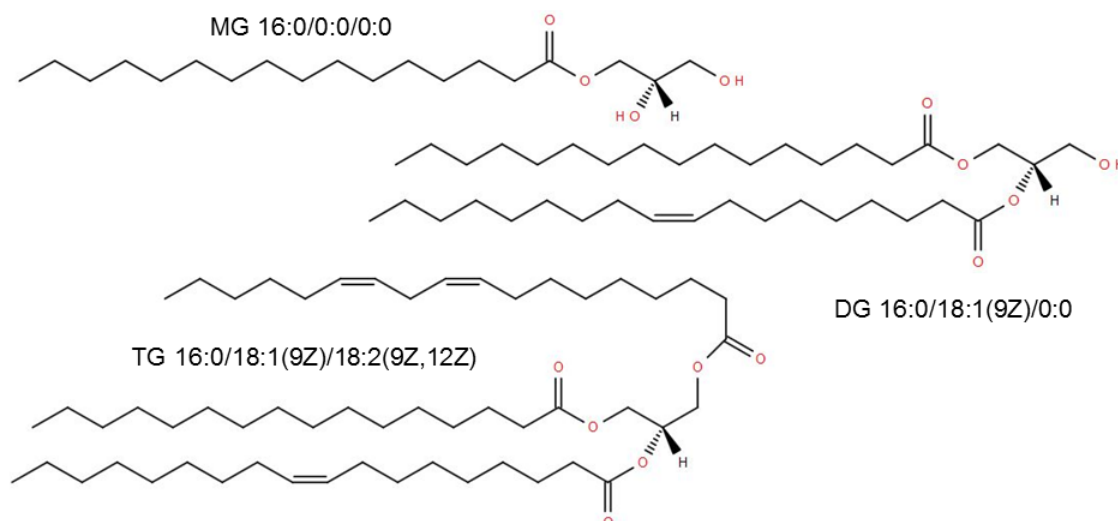


Figure 1.2 Examples of mammalian glycerolipid species.

The daily consumption of fat in humans is about 90-120 g/day with an absorption rate of 95% (Pan & Hussain, 2012). Fats and oils originating from animals or plants are mostly consisting of different TG species. The uptake of dietary lipids occurs mainly in the small intestine. First step of the intestinal digestion is the emulsification with bile salts to make them accessible for the hydrolysis by lipases (Hussain, 2014; Mu & Hoy, 2004; Pan & Hussain, 2012). Pancreatic lipases hydrolyze TG species resulting in the corresponding fatty acids and 2-monoacylglycerol. The free fatty acids are taken up into the enterocytes by active transport and/or diffusion processes (Glatz, Luiken, & Bonen, 2010). After uptake, TGs are resynthesized at the endoplasmic reticulum by acyltransferases before they are either stored in lipid droplets or packed into chylomicrons and secreted to the lymph. Triacylglycerols are accumulated in adipose tissue and are the major form of energy storage in mammals. The energy release is achieved by TG hydrolysis and subsequent β -oxidation of the attached fatty acids.

1.1.1.3 Glycerophospholipids (GP)

Glycerophospholipids are characterized by the presence of a phosphate or phosphonate group esterified to one hydroxyl group of the glycerol (Fahy et al., 2005). The main subclasses in eukaryotic cells are phosphatidylcholines (PC), phosphatidylethanolamines (PE), phosphatidylglycerols (PG), phosphatidylinositols (PI), and phosphatidylserines (PS) (Figure 1.3).

1.1 Chemistry and Biology of Mammalian Lipids

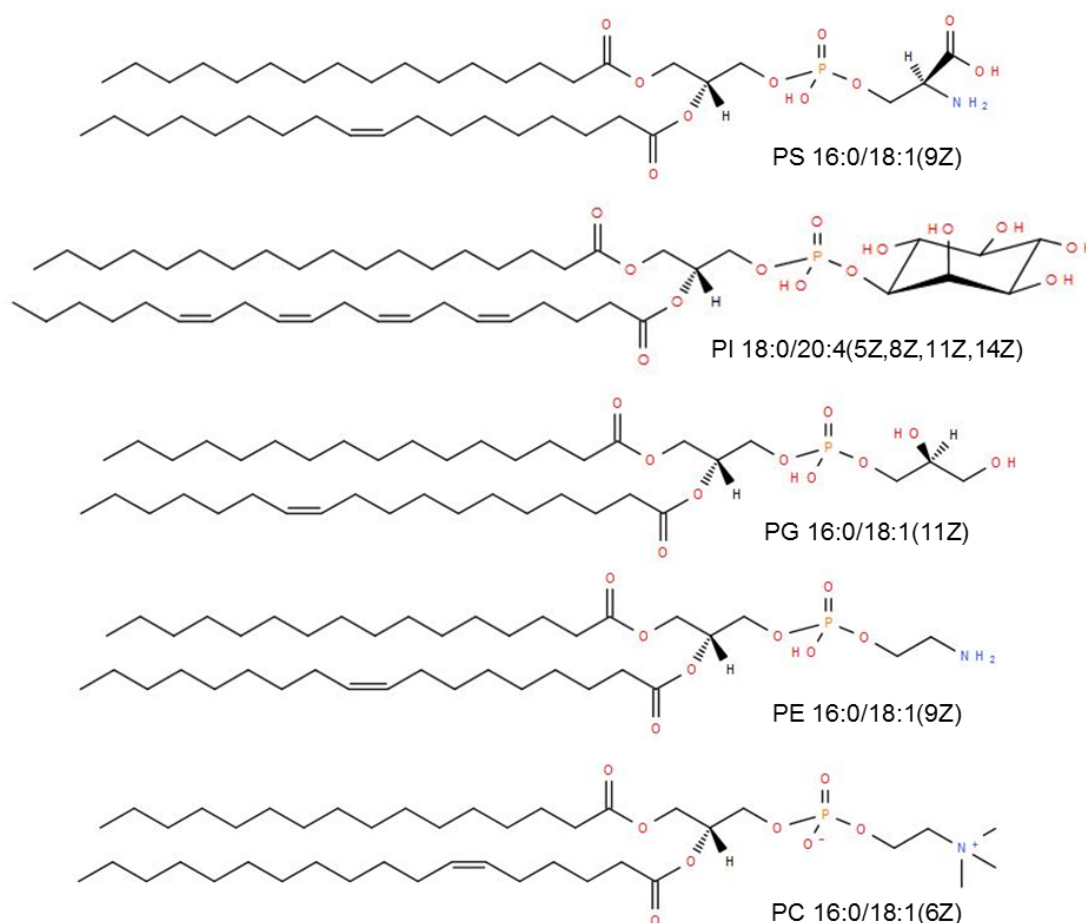


Figure 1.3 Examples of mammalian glycerophospholipid species.

Lipids of this category are the main components of biological membranes (Cooper, 2000). These membranes are usually composed of two layers of lipid molecules (lipid bilayer). The amphiphilic character of phospholipids, consisting of a hydrophilic head group and a lipophilic tail, induces bilayer formation. Biological membranes form physical barriers separating the interior of a cell from the exterior (plasma membrane) as well as different compartments within a cell, for example endoplasmic reticulum, golgi apparatus, or nucleus. Furthermore, proteins are incorporated in plasma membranes to regulate active transport of molecules and/or signaling processes. The phospholipid composition of membranes can be highly diverse for different cell types, organelles, and inner/outer membranes (Hishikawa, Hashidate, Shimizu, & Shindou, 2014). Structural differences and lipid species composition can have a huge influence on membrane fluidity/rigidity and therefore on the regulation of cellular processes. Several PC species contain an ether bond at the *sn*-1

position (Paltauf, 1994), which may serve as precursor for the generation of the platelet-activating factor (Prescott, Zimmerman, Stafforini, & McIntyre, 2000).

1.1.1.4 Sterol Lipids (ST)

The biosynthetic pathway of ST involves the polymerization of dimethylallyl pyrophosphate / isopentenyl pyrophosphate (Fahy et al., 2005). The sterol lipids can be classified to sterols, steroids, steroid conjugates, secosteroids and bile acids. The chemical structure of important sterol lipids is shown in Figure 1.4. The most abundant member of the polycyclic sterol group in mammals is cholesterol. Cholesterol is an essential lipid component in mammalian cells and occurs mainly as non-esterified, free cholesterol (FC) in membranes and as cholesteryl esters (CE) stored in lipid droplets or transported in lipoprotein particles (van Meer, Voelker, & Feigenson, 2008).

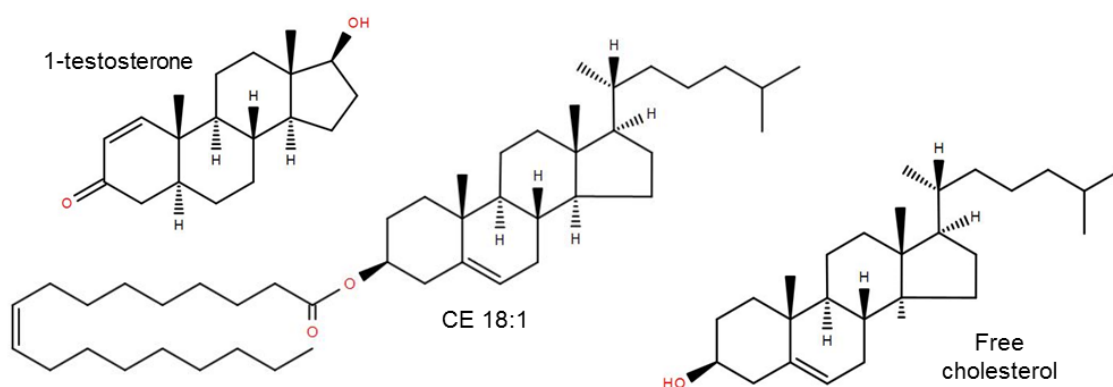


Figure 1.4 Examples of mammalian sterol lipid species.

FC has unique biophysical properties, which play together with the phospholipids an important role in regulation of membrane fluidity and cellular lipid homeostasis (Horton, Goldstein, & Brown, 2002). Small changes in its content may influence membrane properties significantly. Moreover, blood and lipoprotein cholesterol concentrations are applied in patient diagnostics and treatment for decades (Stone et al., 2014). Beside the function within biological membranes, cholesterol serves as precursor for steroid hormones, for example testosterone. These hormones are powerful signaling molecules that regulate various organismal functions.

1.1.1.5 Sphingolipids (SP)

The category of sphingolipids is defined by a long chain base as core structure. The simplest class of SL are ceramides, which contain a sphingosine or a related base linked to a fatty acid via amide bond. Ceramides are used as precursors to form either phospho- or glycosphingolipids by attaching different head groups that provide a number of unique physical properties (Merrill, 2011). For example mammalian sphingomyelins (SM), ceramides (Cer) and hexosylceramides (HexCer) frequently contain a dihydroxy C_{18} sphingosine base but differ by their head groups (Figure 1.5).

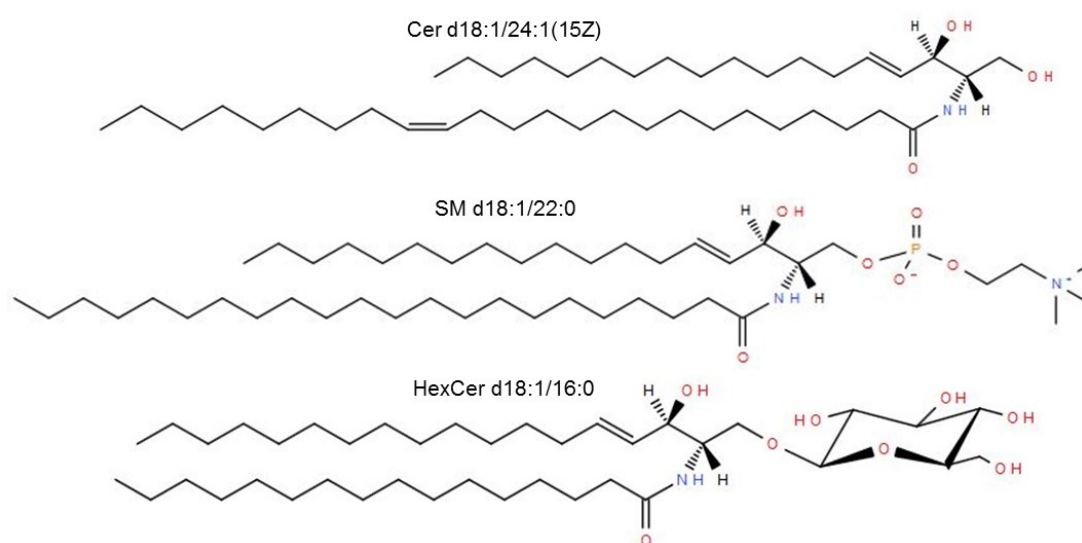


Figure 1.5 Exemplary species of important mammalian sphingolipids.

SP are essential molecules incorporated in membranes and critical signaling molecules whose abundance is tightly regulated (Aguilera-Romero, Gehin, & Riezman, 2014). Ceramides are extremely hydrophobic and increase the molecular order (rigidity) of phospholipid containing membranes (Alonso & Goni, 2018). However, ceramides are minor components within the membrane, but their physical and chemical properties may induce microdomains (Cer-rich platforms) (Staneva, Momchilova, Wolf, Quinn, & Koumanov, 2009). Moreover, Cer concentrations may increase by tenfold and higher under stress or apoptosis conditions. Therefore, Cer has received considerable interest as key regulator of programmed cell death (Alonso & Goni, 2018; Mullen & Obeid, 2012).

1.2 Principles of Mass Spectrometry and Types of Mass Spectrometers

Mass spectrometry is an analytical technique to measure mass-to-charge ratios (m/z) of ions. In general, a mass spectrometer consists of an ion source, a mass analyzer, and a detector. The ion source is the part of the mass spectrometer that ionizes molecules within a sample. Nowadays, the most common applied ionization techniques are electro-spray-ionization (ESI), atmospheric pressure chemical ionization, and matrix-assisted laser desorption ionization (Dass, 2006). The mass analyzer separates the transferred ions according to their specific m/z . Several types of mass analyzers have been developed and all of them have in common that they use electric and/or magnetic fields to resolve ions. Each mass analyzer has its characteristics regarding the mass resolution (resolving power), mass accuracy, sensitivity, mass range, and analysis speed (scans per time unit). Examples of typically used mass analyzers in lipidomics are time-of-flight (TOF) analyzers, quadrupole analyzers, and ion trap analyzers. The molecules within a sample are ionized, separated according to their specific m/z , and detected by a capable detector (for example electron multiplier).

This work has been performed with a heated ESI-source coupled to a Q Exactive Orbitrap mass spectrometer, a hybrid instrument consisting of a quadrupole and an Orbitrap mass analyzer using Fourier Transform mass spectrometry. The following chapter will briefly introduce the applied techniques.

1.2.1 Electro-Spray-Ionization

ESI is a “soft” ionization technique producing intact ions. Therefore, it is possible to analyze large and fragile molecules occurring in biological systems, like proteins and lipids, without fragmentation. ESI is a convenient technique for ionizing polar compounds and is also suitable for any non-polar compound that makes a preformed ion in solution (adduct formation). To enter the gaseous phase, the sample solution is sprayed by the ESI needle, to which a high voltage is applied, creating small droplets that are electrically charged on the surface (Figure 1.6). The solvent slowly evaporates increasing the electrical charge density in the droplets up to the Rayleigh stability limit. The Rayleigh

limit describes the point at which the Coulomb repulsion becomes of the same order as the surface tension. Further solvent evaporation results in an instability (“Coulomb explosion”) that dissociates the droplets in smaller ones. Finally, droplet radius is small enough and the charge density strong enough to desorb the ions from the droplet into the ambient gas to enter the mass spectrometer (Fenn, Mann, Meng, Wong, & Whitehouse, 1989).

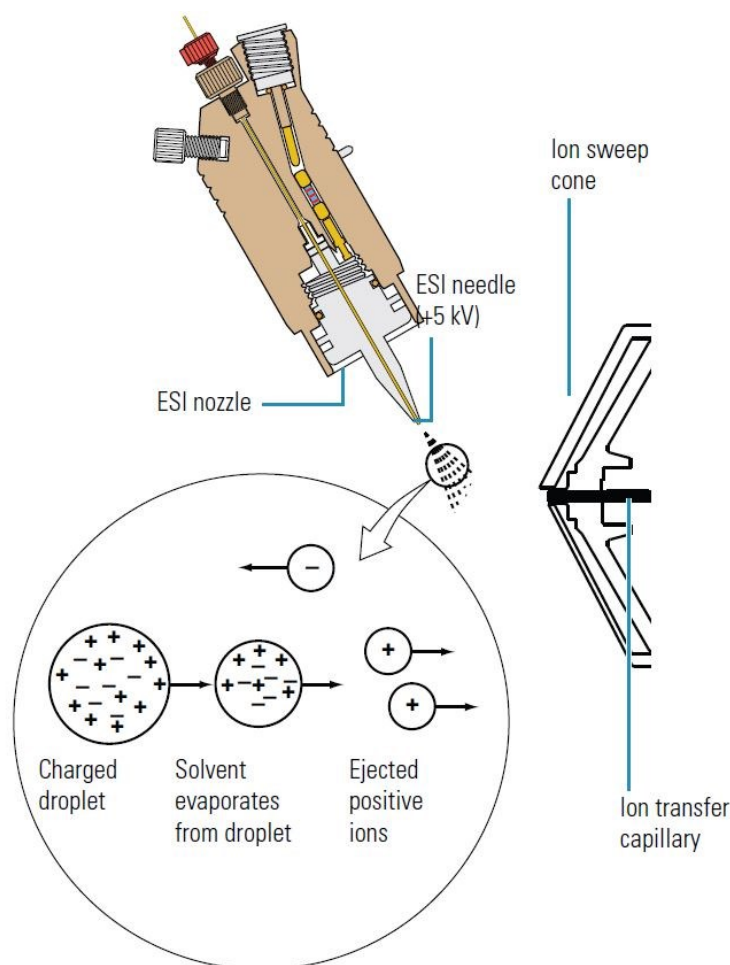


Figure 1.6 ESI process in positive ion polarity mode. Reprinted with permission from Thermo Fisher Scientific. Copyright 2008 Thermo Fisher Scientific.

1.2.2 Quadrupole Mass Analyzers

The quadrupole mass spectrometry was invented in the early 1950s by Wolfgang Paul, who was awarded with the Nobel Prize for his discovery many years later (1989) (Finnigan, 1994). In general, quadrupole mass analyzers consist of four parallel hyperbolic/circular rods (Figure 1.7). A direct current

(DC) voltage and a radio frequency (RF) voltage of the same amplitude and sign are applied to the electrically connected opposing rods. The DC and RF voltages applied to the other rod pair have the same amplitude but differ in their polarity. Subjected ions travel down the electric field of the quadrupole. The applied ratio of voltages allows certain ions of a specific m/z ratio to reach the detector. Ions of different m/z have unstable trajectories and will neutralize by colliding with the rods.

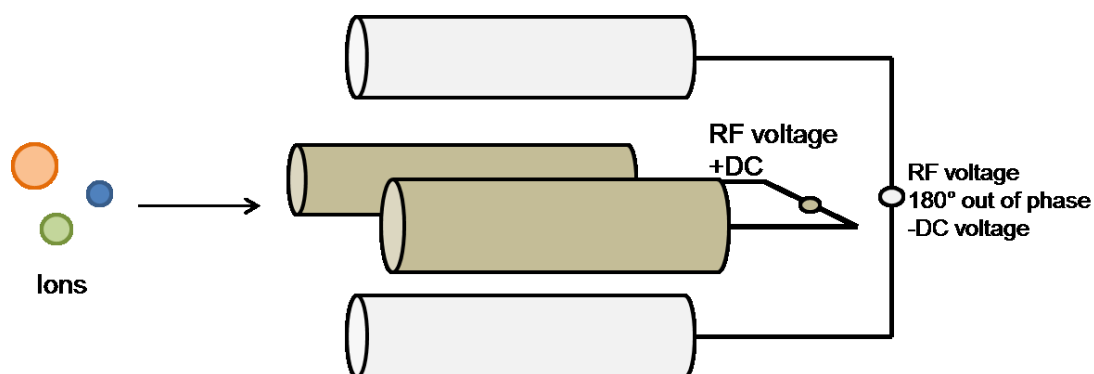


Figure 1.7 Schematic of a quadrupole mass analyzer.

A commonly used mass spectrometer in lipidomics is the triple quadrupole MS. This instrument consists of two quadrupole mass analyzers (Q1 and Q3) controlled by DC and RF voltages and a third quadrupole, the collision cell (q2) to which only a RF voltage is applied (Figure 1.8). The first quadrupole Q1 selects ions at defined m/z . The following quadrupole q2 is filled with an inert gas like argon or nitrogen. The collision with the gas molecules induces formation of fragment ions. These fragments are then analyzed by Q3.

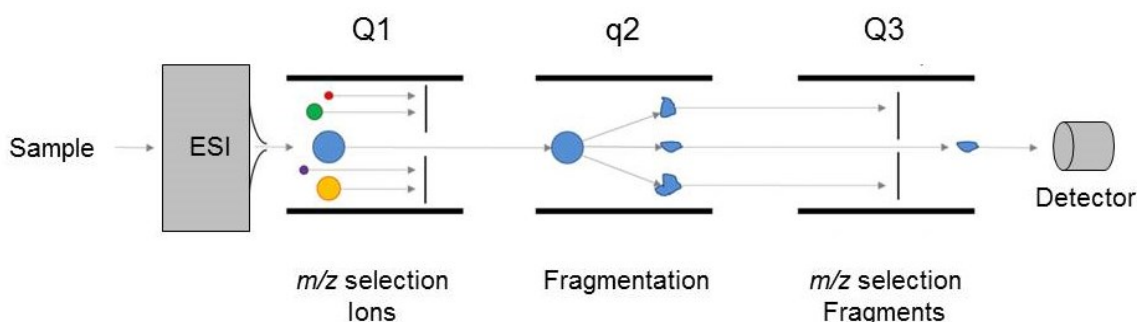


Figure 1.8 Schematic of a triple quadrupole mass spectrometer.

1.2.3 Orbitrap Mass Analyzers

The concept of an orbital trapping device for application to mass analysis has been first published 2000 by Alexander Makarov (Makarov, 2000). The key elements of an Orbitrap are a barrel-like outer electrode and a spindle-like inner electrode along the axis (Figure 1.9).

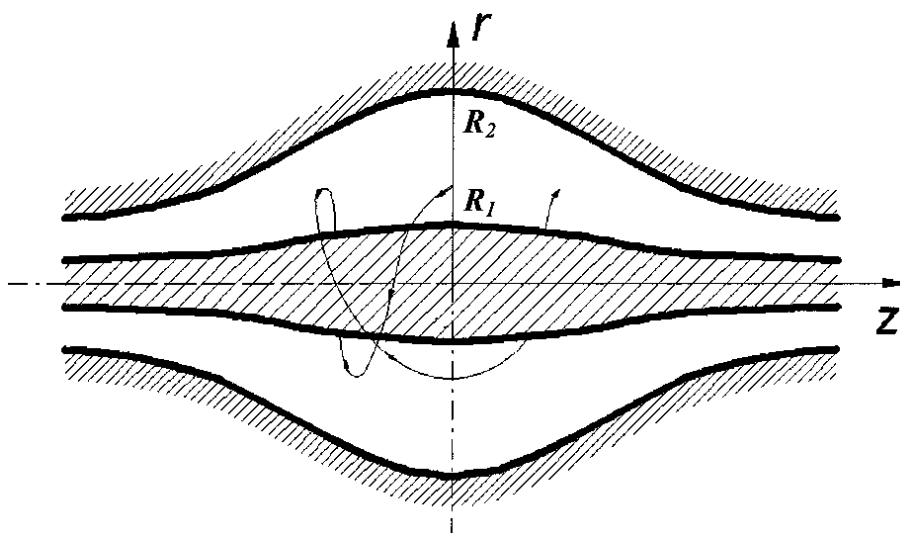


Figure 1.9 Schematic of an Orbitrap and an example of stable ion trajectory. Reprinted with permission from (Makarov, 2000). Copyright 2000 American Chemical Society.

The applied electric field consists of a quadrupole field of the trap and an additional logarithmic field of the cylindrical capacitor (quadro-logarithmic field). The shape of the electrodes and the equipotentials of the quadro-logarithmic field induce stable ion trajectories with a harmonic oscillation along the z-axis (Makarov, 2000). The angular frequency ω of this oscillation is only depending on the ion-specific m/z ratio and the instrument settings (constant k):

$$\omega = \sqrt{\frac{z}{m} * k}$$

Ions of the same m/z ratio will oscillate in-phase along the z-axis for thousands of oscillations. There are two different modes of mass analysis in Orbitrap instruments. The first one is image current detection using Fourier Transform mass spectrometry (FTMS) and the second mode is a detection based on a secondary electron multiplier (Figure 1.10).

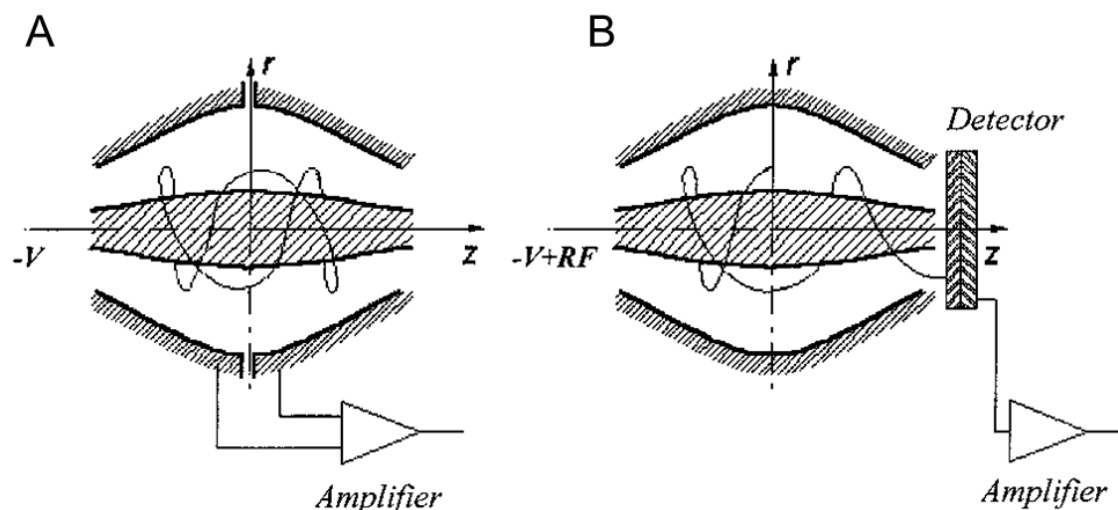


Figure 1.10 Modes of mass analysis in the Orbitrap: (A) Fourier Transform mass spectrometry and (B) detection using a secondary electron multiplier. Reprinted (adapted) with permission from (Makarov, 2000). Copyright 2000 American Chemical Society.

1.2.4 The Q Exactive Orbitrap Mass Spectrometer

The Q Exactive Orbitrap mass spectrometer, which was used for lipid analysis in this thesis, combines a high resolution Orbitrap mass analyzer with a quadrupole for precursor selection and is therefore referred to as hybrid instrument (Figure 1.11). The mode of analysis of the instrument is image current detection (FTMS). Two split halves outer electrodes are used to detect the image current and a differential amplifier for amplification (Figure 1.10A). The application of FT determines the frequency of the harmonic oscillations and allows the calculation of m/z ratios of subjected ions (Zubarev & Makarov, 2013).

Further components of the Q Exactive are the C-trap (curved linear trap filled with nitrogen) and the HCD collision cell (higher-energy collisional dissociation). The C-trap dissipates the kinetic energy of injected ions by collision with nitrogen molecules and bundles them on the trap axis. The ion bundles are then subjected orthogonal to the z -axis of the Orbitrap for FTMS analysis or, if MS/MS spectra are acquired, the ions are first transferred to the HCD collision cell for ion fragmentation.

1.2 Principles of Mass Spectrometry and Types of Mass Spectrometers

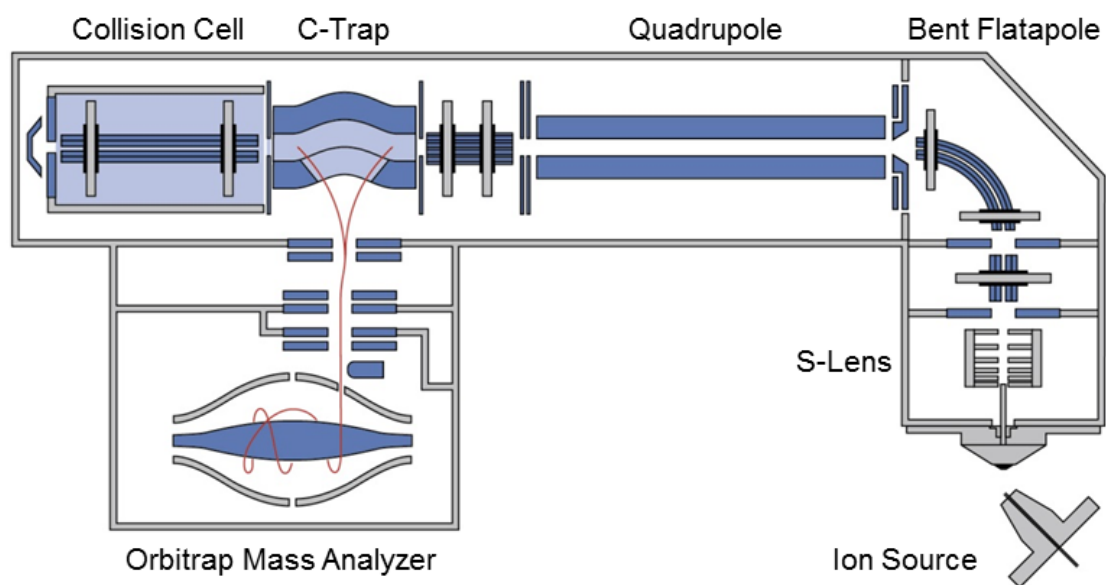


Figure 1.11 Schematic of the Q Exactive Orbitrap mass spectrometer. Reprinted (adapted) with permission from Thermo Fisher Scientific. Copyright 2012 Thermo Fisher Scientific.

1.3 Lipidomics

1.3.1 Definition and Principles

The extensive field of “omics” aims at the analysis of biological molecules that provide functionality, structure, and/or dynamic procedures to organisms. In general, the cascade of omics reaches from the genome through the transcriptome, proteome to the metabolome (Davis, Bathe, Schiller, Slupsky, & Sawyer, 2011). The field of lipidomics is a subset of metabolomics and has recently emerged with the great advances in mass spectrometry (Blanksby & Mitchell, 2010; Han, Yang, & Gross, 2012; Lagarde, Geloën, Record, Vance, & Spener, 2003). An up to date review by Yang and Han defines lipidomics as large-scale study of pathways and networks of cellular lipids in biological systems and denotes the actual research as study of structure and function of the complete set of lipids (lipidome) in a single cell or organism as well as their interaction with other cellular components (Yang & Han, 2016). This involves the quantitative molecular characterization of cellular lipid species in biological systems. According to several estimations, the lipidome of an eukaryotic cell contains up to 100,000 individual molecular lipid species (van Meer, 2005; Wenk, 2005; Yetukuri, Ekroos, Vidal-Puig, & Oresic, 2008). Therefore, the reliable and accurate quantification of lipid species is a key tenet that requires convenient species assignment and depending on the instrument resolution isotopic deconvolution (Bielow, Mastrobuoni, Orioli, & Kempa, 2017).

Cellular lipid composition plays crucial roles in dynamic processes and is influenced by physiological, pathophysiological, and/or environmental conditions. An imbalance in lipid homeostasis for example is involved in various pathophysiological conditions such as Alzheimer disease, atherosclerosis, cardiovascular diseases or diabetes (Dawber, Moore, & Mann, 1957; Ekroos, Janis, Tarasov, Hurme, & Laaksonen, 2010; Hopkins et al., 2003; Kohno, Keenan, Ntambi, & Miyazaki, 2018; Mapstone et al., 2014). Furthermore, lipids are involved in basic processes essential for tumor development, for example cell growth, proliferation, differentiation, and motility (Santos & Schulze, 2012). Several mass spectrometric lipidomic methods with scientific and clinical

application have been developed over the last decades (Hu & Zhang, 2018; Krautbauer & Liebisch, 2018; Matysik & Liebisch, 2017).

1.3.2 LC-based vs Shotgun Lipidomics

In general, biological samples comprise a complex mix of different lipids considering the number of classes, subclasses and species composition. A common way to reduce the complexity of lipid extracts for MS based approaches is the utilization of chromatographic separation, most important liquid chromatography (LC) (Myers, Ivanova, Milne, & Brown, 2011; Schott, Krautbauer, Horing, Liebisch, & Matysik, 2018; Sokol et al., 2013). In contrast, shotgun lipidomics is a direct-infusion based approach without any pre-separation prior to mass spectrometric analysis. The crude lipid extract is directly infused into a mass spectrometer and the identification of individual species relies on their accurately determined masses on MS level or specific fragment ions in MS/MS spectra (Han & Gross, 2003, 2005). The application on MS level gained increasing interest with the development of high resolution mass spectrometers. The technical simplicity allows the detection of multiple lipid classes in parallel in a single analysis with rather short measurement times. Moreover, the lipid concentration and composition of analytes in shotgun approaches does not change over time simplifying species quantification (Yang & Han, 2016). A summary of advantages and limitations of LC-based MS and shotgun MS lipidomic approaches is shown in Figure 1.12.

Nowadays, shotgun MS analysis of biological samples is routinely applied to investigate samples in high throughput (Jung et al., 2011). However, to our knowledge, all lipidomic approaches on a high resolution FTMS instrument use chip-based nano-ESI. (Ejsing et al., 2009; Grzybek et al., 2019; Schuhmann et al., 2017; Surma et al., 2015). Accordingly, the application described in this thesis presents the first application using a conventional LC pump system to infuse crude lipid extracts of biological samples, as it is commonly performed on other instruments (Bowden, Bangma, & Kucklick, 2014; Liebisch, Lieser, Rathenberg, Drobnik, & Schmitz, 2004).

<i>LC-based MS</i>	<i>Shotgun MS</i>
Advantages	
<ul style="list-style-type: none"> • Separation of isomers/isobars • Reduction of sample matrix • Reduction of ion suppression • High sensitivity 	<ul style="list-style-type: none"> • High throughput • Simple and straightforward • Untargeted approach • Simplified quantification
Limitations	
<ul style="list-style-type: none"> • Low throughput • Targeted approach • Complex data processing • Effects of mobile phase 	<ul style="list-style-type: none"> • Ion suppression • Higher matrix effects • Isobaric interference • Isomeric overlap

Figure 1.12 Comparison of LC-based and shotgun MS lipidomic approaches.

1.3.3 Lipid Nomenclature

Lipid nomenclature of this work is based on the comprehensive classification system for lipids presented by the International Lipid Classification and Nomenclature Committee (Fahy et al., 2005; Fahy et al., 2009). Additionally, shorthand notations reflecting the structural information of lipid species derived from mass spectrometric analysis have been applied (Liebisch et al., 2013). For example, PC 34:1 denotes the lipid class (PC, phosphatidylcholine) and indicates the total number of carbon atoms (34) and double bonds (1) of the acyl chains. However, it does not provide further information about the individual fatty acyl chain composition. Possible acyl combinations for example could be PC 16:0/18:1 and PC 18:1/16:0 (different sn-positions of the fatty acyls). The application of high resolution mass spectrometry allows a clear distinction between ester and ether bonds. An ether bond is noted with an O- as for example PC O-34:1.

1.4 Aim of this Work

Aim of this PhD thesis is the development of a FIA-FTMS method to quantify lipid species in biological samples. The instrument of interest is a Q Exactive Orbitrap high resolution mass spectrometer (with a resolution of 140,000 at m/z 200) equipped with a heated electro-spray-ionization source coupled to a conventional LC isocratic pump system. The method development includes lipid extraction, instrumental method, and data processing in an untargeted approach.

Data deconvolution comprises the development of an isotope correction algorithm to correct for the abundance of the monoisotopic peak (type I effect) and for the overlap of the second isotope peak of a species with the monoisotopic peak of a species with one less double bond (type II effect), as well as the correction of species-specific response effects observed for cholesteryl esters.

Furthermore, the method should be applicable to biological samples of clinical and scientific studies. Therefore, lipid species quantification should be accurate and reproducible allowing high throughput of samples.

2 Materials and Methods

2.1 Chemicals

Chloroform, 2-propanol, and hexane were purchased from Roth (Karlsruhe, Germany), methanol from Merck (Darmstadt, Germany), and 2,2,4-trimethylpentane from Honeywell (Seelze, Germany). All solvents were HPLC grade. Water (aqua ad iniectionem) for lipid extraction was purchased from B. Braun (Melsungen, Germany). Ammonium formate, CE, FC, and PC standards were purchased from Sigma-Aldrich (Taufkirchen, Germany). [25,26,26,26,27,27,27-D₇]-cholesterol was obtained from Cambridge Isotope Laboratories (Andover, MA, U.S.A.) with isotope purity higher than 98%. All CE standards have been dissolved in hexane/2-propanol (1:1 v/v), cholesterol and D₇-cholesterol were dissolved in chloroform/methanol (9:1 v/v) with 1 g/L butylated hydroxytoluene. The concentrations of the dissolved CE standards were determined by gas chromatography mass spectrometry (GC-MS) using a certified fatty acid methyl ester (FAME) mix (Supelco 37 component FAME mix) from Sigma-Aldrich (Taufkirchen, Germany) as described previously (Ecker, Scherer, Schmitz, & Liebisch, 2012). TG and DG standards were purchased from Larodan (Solna, Sweden) and dissolved in 2,2,4-trimethylpentane/2-propanol (3:1 v/v). Cardiolipin (CL), Cer, HexCer, LPC, LPE, PE, PG, PI, PS, and SM standards were purchased from Avanti (Alabaster, Alabama, USA) and dissolved in chloroform. Acetyl chloride of the highest analytical grade available was purchased from Fluka (Buchs, Switzerland).

2.2 Internal Standards

Quantification of lipid species was performed by addition of non-endogenous internal standards. The composition of pre-built IS mixtures for analysis of plasma and serum samples, and cell and tissue samples is listed in Table 2.1. The spike volume added for plasma/serum samples and cell/tissue samples was 25 µL and 50 µL, respectively.

2.3 Laboratory Equipment

Table 2.1 Composition of internal standard mixtures added to plasma and serum samples or cell and tissue samples.

Species	MW	Plasma/Serum IS		Cell/Tissue IS	
Unit	[g/mol]	[ng/spike]	[nmol/spike]	[ng/spike]	[nmol/spike]
CE 17:0	638.60	2500	3.91	500	0.78
CE 22:0	708.68	2500	3.53	500	0.71
Cer 32:1;2	509.48	12.5	0.025	50	0.10
Cer 35:1;2	551.53	12.5	0.023	50	0.091
CL 56:0	1240.85			100	0.081
DG 28:0	512.44	300	0.59	250	0.49
DG 40:0	680.63	300	0.44	250	0.37
D ₇ FC	393.40	2500	6.35	3750	9.53
HexCer 30:1;2	643.50	20	0.031	60	0.093
HexCer 35:1;2	713.58	20	0.028	60	0.084
LPC 13:0	453.29	375	0.83	50	0.11
LPC 19:0	537.38	375	0.70	50	0.093
LPE 13:0	411.24	25	0.06	50	0.12
PC 28:0	677.50	875	1.29	1250	1.85
PC 44:0	901.75	1250	1.39	1250	1.39
PE 28:0	635.45	100	0.16	500	0.79
PE 40:0	803.64	100	0.12	500	0.62
PG 28:0	666.45			125	0.19
PG 40:0	834.63			125	0.15
PI 34:0	838.56	125	0.15	250	0.30
PS 28:0	679.44	75	0.11	750	1.10
PS 40:0	847.63	75	0.088	750	0.88
SM 30:1;2	646.50	250	0.39	500	0.77
TG 51:0	848.78	1250	1.47	900	1.06
TG 57:0	932.88	1250	1.34	900	0.96

2.3 Laboratory Equipment

2.3.1 Laboratory at the University Hospital Regensburg

Centrifuge Megafuge 1.0R..... Heraeus (Hanau, Germany)

Glass Centrifuge Tubes Hecht-Assistant (Sondheim, Germany)

Filtration Milli-Q UF Plus Merck Millipore (Darmstadt, Germany)

GCMS-QP2010 Shimadzu (Kyoto, Japan)

2.3 Laboratory Equipment

GentleMACS Dissociator	Miltenyi Biotec (Bergisch Gladbach, Germany)
GentleMACS 10 mL Tubes	Miltenyi Biotec (Bergisch Gladbach, Germany)
PAL autosampler.....	CTC Analytics (Zwingen, Switzerland)
Pyrex Culture Tubes	SciLabware Ltd (Riverside, UK)
Q-Exactive Orbitrap.....	Thermo Fisher Scientific (Bremen, Germany)
Quattro Ultima MS.....	Micromass Communications Inc (Manchester, UK)
Sample Vials (1.5 mL volume)	VWR (Darmstadt, Germany)
Screw Caps (PTFE naturelle).....	VWR (Darmstadt, Germany)
Screw Caps (PTFE, Sil, PTFE)	VWR (Darmstadt, Germany)
Siemens Dimension Vista	Siemens Health Care GmbH (Erlangen, Germany)
SpeedVac	Christ (Osterode, Germany)
Tecan Genesis RSP 150.....	Tecan Group Ltd (Männedorf, Switzerland)
UltiMate 3000 isocratic pump	Thermo Fisher Scientific (Waltham, MA, USA)
Ultrasonic Desintegrator.....	B. Braun Melsungen (Melsungen, Germany)
Ultrasonicbath Sonorex.....	Bandelin (Berlin, Germany)
Vortex Genie 2	Bender & Hobein (Zurich, Switzerland)

2.3.2 Mass Spectrometry at the University of Southern Denmark

The analysis of CE response was additionally performed on an Orbitrap Fusion Tribrid from Thermo Fisher Scientific (San Jose, CA, USA) equipped with a TriVersa NanoMate from Advion Biosciences (Ithaca, NY, USA). The experiments were performed in collaboration with Prof. Christer Ejlsing at the University of Southern Denmark in Odense.

2.4 Biological Samples

Human plasma and serum samples were collected from residual patient material after clinical routine diagnostics.

Primary human skin fibroblasts were cultured in Dulbecco's Modified Eagle Medium (DMEM) supplemented with L-glutamine, nonessential amino acids, and 10% fetal calf serum at 5% CO₂ in a humidified incubator at 37°C as described previously (Drobnik et al., 1999).

Murine liver samples were collected from residual material analyzed for various scientific studies. The different liver samples were either solitary homogenized or pooled homogenates in MeOH:H₂O (1:1 v/v).

2.5 Sample Preparation

2.5.1 Tissue Homogenization

Organic tissues were weighed and cut into 50-300 mg pieces. MeOH:H₂O (1:1 v/v) was added to achieve a concentration of 50 mg/mL. The tissue was processed 1-3 times in the GentleMACS Dissociator with the pre-installed "protein_01" program (90 seconds per cycle). All tissues and samples were stored at -80°C.

2.5.2 Lipid Extraction

Internal standards (see 2.2 *Internal Standards*) were added to a glass centrifuge tube and the solvent was removed by vacuum centrifugation prior to lipid extraction. A sample amount of 10 µL serum, 10 µL plasma, cell homogenates containing 100 µg of protein or tissue homogenates containing a wet weight of 2 mg were subjected to lipid extraction. The samples were extracted according to the procedure described by Bligh and Dyer (Bligh & Dyer, 1959). An amount of 800 µL H₂O (adjusted for aqueous samples) and 3 mL B&D solution (MeOH/CHCl₃ 2:1 v/v) were added. The mixture was vortexed for 5 sec and incubated for 1 h at room temperature. Subsequently, 1 mL H₂O and 1 mL CHCl₃ was added, mixed and centrifuged for 10 min at 4,000 rpm (17,860 g). An amount of 500 µL of the separated chloroform phase was transferred into a

1.5 mL glass sample vial by a pipetting robot (Tecan Genesis RSP) and vacuum dried. The residues were dissolved in 1.2 mL of 7.5 mM ammonium formate in chloroform/methanol/2-propanol (1:2:4 v/v/v).

2.6 Lipid Species Quantification by FIA-FTMS

Lipid species quantification was performed by direct flow injection on a hybrid quadrupole-Orbitrap mass spectrometer (Q Exactive) equipped with a heated electro-spray-ionization source coupled to an UltiMate 3000 isocratic LC pump.

2.6.1 FIA-FTMS

The ion source was operated using the following settings: spray voltage of 3.5 kV (positive ion mode) and 2.5 kV (negative ion mode), S-lens RF level of 50, capillary temperature of 250 °C, aux gas heater temperature of 100 °C, and settings of 15 and 5 for sheath gas and aux gas, respectively. All data were acquired in profile mode. Amounts of 50 µL of the reconstituted sample extracts were injected by a PAL autosampler equipped with an isocratic LC pump. Chloroform/methanol/2-propanol (1:2:4 v/v/v) was delivered at an initial flow rate of 100 µL/min until 0.25 min, followed by 10 µL/min for sample analysis until 2.6 min and a wash out with 300 µL/min until 3.1 min. All FTMS data were recorded with a maximum injection time (IT) of 200 ms, an automated gain control (AGC) of 1×10^6 , three microscans, and a target resolution of 140,000 at m/z 200. MS/MS was applied for quantification of free cholesterol (FC) using an isolation window of 1 Da with normalized collision energy of 10%, an IT of 100 ms, an AGC of 1×10^5 , and a target resolution of 140,000 at m/z 200.

2.6.2 Lipid Class Determination

The list of lipid classes determined by FIA-FTMS is shown in Table 2.2. Positive ion mode data were analyzed for 0.7 min resulting in 31 averaged scans (three microscans). FC was analyzed for 0.4 min in positive ion mode by multiplexing (MSX) ammoniated precursor ions of cholesterol (m/z 404.39) and the corresponding internal standard D₇-cholesterol (m/z 411.43). Negative ion mode data were acquired in two scan events, m/z 400-650 and m/z 520-960. The

lower mass range was analyzed for 0.55 min (22 averaged scans) and the higher mass range for 0.6 min (25 averaged scans).

Table 2.2 Lipid classes determined by FIA-FTMS.

Lipid Class	Lipid Category	Experiment	Ion Mode	Adduct	Mass Range [<i>m/z</i>]
CE	ST	FTMS	positive	[M + NH ₄] ⁺	500-1000
Cer	SP	FTMS	negative	[M + HCOO] ⁻	520-960
DG	GL	FTMS	positive	[M + NH ₄] ⁺	500-1000
FC	ST	MSX/FTMS	positive	[M + NH ₄] ⁺	404.39 / 411.43
HexCer	SP	FTMS	negative	[M + HCOO] ⁻	520-960
LPA	GP	FTMS	negative	[M - H] ⁻	400-650
LPC	GP	FTMS	negative	[M + HCOO] ⁻	400-650
LPC O-	GP	FTMS	negative	[M + HCOO] ⁻	400-650
LPE	GP	FTMS	negative	[M - H] ⁻	400-650
LPE O-	GP	FTMS	negative	[M - H] ⁻	400-650
PC	GP	FTMS	negative	[M + HCOO] ⁻	520-960
PC O-	GP	FTMS	negative	[M + HCOO] ⁻	520-960
PE	GP	FTMS	negative	[M - H] ⁻	520-960
PE O-	GP	FTMS	negative	[M - H] ⁻	520-960
PG	GP	FTMS	negative	[M - H] ⁻	520-960
PI	GP	FTMS	negative	[M - H] ⁻	520-960
PS	GP	FTMS	negative	[M - H] ⁻	520-960
SM	SP	FTMS	negative	[M + HCOO] ⁻	520-960
TG	GL	FTMS	positive	[M + NH ₄] ⁺	500-1000

2.6.3 Data Processing and Quantification

2.6.3.1 Calculation of Isotopic Probabilities

The calculation of accurate masses and probabilities of isotopic peaks was performed with emass (Rockwood & Haimi, 2006). The atomic isotope probabilities have been adapted to the International Union of Pure and Applied Chemistry (Rosman & Taylor, 1998). The import of lipid species, sum formula and adduct was supported by self-programmed Microsoft Excel 2010 Macros.

2.6.3.2 Peak Assignment and Offset Correction

The peak assignment and offset correction of data recorded on the Q Exactive Orbitrap was performed in two steps with the ALEX software (Husen et al., 2013). In a first step, the output (.raw) files were converted into txt-files omitting the first 14 and last 26 scans. Afterwards, the peak information in the txt-files was screened for possible lipid species in an untargeted approach, including the

information of isotopic peaks. The offset correction of FTMS experiments was performed by averaging the mass deviation of three internal standards of each ion mode and mass range (Table 2.3), with a tolerance of $\Delta m/z$ 0.01. The offset correction of the MSX/FTMS experiment was performed with the protonated cholestadiene fragment of D₇-FC with m/z 376.3955. The actual lipid species assignment and intensity picking was performed with a tolerance of $\Delta m/z$ 0.0045 after offset correction. The area for the assigned peak was determined from baseline to baseline, independent of the selected m/z -tolerance.

Table 2.3 Internal standards used for offset correction of FTMS experiments.

Species	Adduct	m/z
positive ion mode m/z 500-1000		
CE 17:0	$[M + NH_4]^+$	656.6340
TG 51:0	$[M + NH_4]^+$	866.8171
PC 44:0	$[M + H]^+$	902.7572
negative ion mode m/z 400-650		
LPE 13:0	$[M - H]^-$	410.2313
LPC 13:0	$[M + HCOO]^-$	498.2837
LPC 19:0	$[M + HCOO]^-$	582.3776
negative ion mode m/z 520-960		
Cer 35:1;2	$[M + HCOO]^-$	596.526
PE 28:0	$[M - H]^-$	634.4453
PC 28:0	$[M + HCOO]^-$	722.4978

2.6.3.3 Isotope Correction

The isotope correction was performed by self-programmed Macros in Microsoft Excel 2010. The Macros corrected for the abundance of the monoisotopic peak (type I effect (Han & Gross, 2001)). The type II effect derives from the overlap of the second isotope peak of a species with the monoisotopic peak of a species with one less double bond (DB) (Ejsing et al., 2006). This isotope effect was not corrected for species with $m/z < 600$ or $m/z > 800$. Species with m/z 600-800 were corrected by multiplying species intensity with an intensity/area correction factor (I/A correction). The calculated I/A for a given m/z was determined with the following exponential decaying function:

$$\frac{I}{A}(\text{calcd}) = 5.212 * e^{\frac{4169}{(m/z+678.4)}}$$

2.6 Lipid Species Quantification by FIA-FTMS

The I/A correction factor for constellations where the measured I/A of the second isotope of the species with one additional DB (Species+1DB M+2) is smaller or even than the I/A of the monoisotopic species with one less DB (Species+0DB M+0) was calculated:

$$\frac{I}{A} \text{ Correction factor} = \frac{\frac{I}{A}(\text{calcd})}{\frac{I}{A}(M + 0 \text{ measured})}$$

For constellations where the measured I/A (Species+1DB M+2) > I/A (Species+0DB M+0), the I/A (measured) was calculated with the average of the monoisotopic species and the second isotope:

$$\frac{I}{A} \text{ Correction factor} = \frac{\frac{I}{A}(\text{calcd}) * 2}{\frac{I}{A}(M + 0 \text{ measured}) + \frac{I}{A}(M + 2 \text{ measured})}$$

Limitation was a false picked intensity of the monoisotopic species (see 3.1 *Isotope Correction Algorithm for FIA-FTMS*). The correction was only applied for a target resolution of 140,000 at m/z 200. Data recorded at lower resolutions were corrected for the type II effect by a stepwise correction based on theoretical isotope distributions (Haimi, Uphoff, Hermansson, & Somerharju, 2006; Han & Gross, 2005; Liebisch et al., 2004).

2.6.3.4 Sodium Correction

The sodium correction was applied for species analyzed as protonated adduct. These adducts are overlapping with the sodium adduct of a species of the same lipid class with two carbon atoms less and three DB less (e.g. PC 36:4 $[M+H]^+$ and PC 34:1 $[M+Na]^+$ with a $\Delta m/z$ of 0.00248). The fraction of sodium adduct within a sample was determined by averaging the intensity ratio of $[M+Na]^+/[M+H]^+$ of both internal standards of the corresponding lipid class. The ratio was used to calculate the intensity of sodium adduct of the overlapping species and subsequently subtracted from the protonated species.

2.6.3.5 Quantification

The quantification was performed with non-endogenous internal standards (Table 2.1) by multiplication of the spiked IS amount with the analyte-to-IS ratio of the intensities after isotope correction.

2.6.3.6 Cholesteryl Ester Response Correction

The CE response correction was performed by multiplying calculated species specific response factors on the quantified CE species concentration (Horing, Ejsing, Hermansson, & Liebisch, 2019). The response factors were calculated with the following equations (C is the number of carbon atoms of the acyl chain; DB is the number of double bonds of the acyl chain; A is the matrix factor):

$$response(calcd) = [0.049 * C + 0.57 * DB] * A$$

$$response\ factor = \frac{1}{response(calcd)}$$

The matrix factor was 0.95 for saturated species, 0.91 for monounsaturated species and 0.89 for polyunsaturated species (see 3.2.2 *Analytical Response of Cholesteryl Esters quantified by FIA-ESI-FTMS*).

2.6.3.7 Background Correction

The background correction was performed with three internal standard blanks analyzed within the same batch. The concentration of lipid species detected in the IS blanks were averaged and subtracted from the sample.

2.6.4 Method Validation

The validation of FIA-FTMS included intraday and day-to-day reproducibility, determination of limits of quantification (LOQ), and evaluation of the dynamic range of quantification.

To evaluate the intraday reproducibility, the samples were extracted five times and subjected to quantitative FIA-FTMS (MSX/FTMS for FC). The experiment was repeated on four different days separated evenly within a four month period to evaluate the day-to-day reproducibility. The coefficients of variation (CV)

2.6 Lipid Species Quantification by FIA-FTMS

were determined for human plasma, human fibroblast cells, and murine liver samples.

The LOQ were determined functionally as previously described for LC-MS/HRMS methods (Liebisch & Matysik, 2015; Schott et al., 2018). Non-endogenous internal standard species pairs were analyzed by FIA-FTMS (CE 17:0 and CE 22:0, DG 28:0 and DG 40:0, PC 28:0 and PC 44:0, TG 51:0 and TG 57:0). CE 17:0, DG 28:0, PC 28:0, and TG 51:0 were used as internal standards for quantification and CE 22:0, DG 40:0, PC 44:0, and TG 57:0 were spiked with decreasing concentrations. The concentrations of the titrated species are indicated in the corresponding figures. The results were fitted by a power function. The LOQ was defined as concentration where either the CV reached 20% or the accuracy left the range of 80-120%. The LOQ were determined in human plasma and for CE additionally in human skin fibroblast cells. The LOQ of free cholesterol (MSX/FTMS) were determined by titration of the synthetic D₇-FC standard using the endogenous amount of FC as internal standard for quantification.

The evaluation of the dynamic range of quantification was performed by spike experiments of the synthetic standards LPE 18:1, LPC 18:1, DG 36:1, CE 18:1, Cer 42:2;2, SM 36:2;2, PC 36:2 and TG 54:1. The measured concentration was plotted against the spiked in concentration and was fitted by a linear function. The experiment was performed without matrix, with human plasma, human skin fibroblast cells, and murine liver samples. The highest spike concentration (in vial) was 0.68 pmol/μL for LPE 18:1, 5.37 pmol/μL for LPC 18:1, 6.16 pmol/μL for DG 36:1, 7.94 pmol/μL for CE 18:1, 0.36 pmol/μL for Cer 42:2;2, 3.4 pmol/μL for SM 36:2;2, 3.3 pmol/μL for PC 36:2, and 4.75 pmol/μL for TG 54:1. The concentration of the infusate was calculated by dividing the amount added to the extraction in nmol by the dilution of 5.598 during extraction.

2.7 Instrument Response of Cholesteryl Esters

2.7.1 Preparation of Standard Mixtures and Matrix Spikes

For determination of instrument response a mixture of CE species was prepared composed of a homologous series of five saturated species varying in chain length (CE 10:0, CE 14:0, CE 16:0, CE 18:0, and CE 22:0), three monounsaturated species (CE 16:1, CE 18:1, and CE 24:1), and two polyunsaturated species (CE 18:2 and CE 18:3) to obtain a homologous series varying in the number of DB (CE 18:0-CE 18:3). CE 17:0 was used as internal standard for quantification (3.18 nmol, corresponding to 0.57 pmol/ μ L in-vial concentration). The concentration of stock solutions was determined by GC-MS of fatty acid methyl esters as described previously (Ecker et al., 2012). The CE mixture was measured in concentration range 1.6-22.8 pmol/ μ L total CE. The highest level had the following concentrations [pmol/ μ L]: CE 10:0 = 3.2, CE 14:0 = 2.87, CE 16:0 = 2.43, CE 16:1 = 3.08, CE 18:0 = 2.36, CE 18:1 = 2.39, CE 18:2 = 0.85, CE 18:3 = 0.95, CE 22:0 = 2.13, and CE 24:1 = 2.11. The species were dissolved in hexane/2-propanol (1:1 v/v).

The TG mixture with a total TG concentration of 5.4 pmol/ μ L was composed of [pmol/ μ L]: TG 42:0 = 1.23, TG 48:0 = 1.11, TG 51:0 = 1.05, TG 54:3 = 1.02, and TG 57:0 = 0.96.

The PC mixture with a total PC concentration of 5.8 pmol/ μ L was composed of [pmol/ μ L]: PC 28:0 = 1.32, PC 34:0 = 1.18, PC 34:2 = 1.18, PC 36:4 = 1.14, and PC 44:0 = 0.98.

2.7.2 FIA-FTMS using a Q Exactive Orbitrap

Lipid quantification was performed on a Q Exactive Orbitrap equipped with a heated electrospray ionization source coupled to a conventional isocratic pump. The parameters of the FIA-FTMS method are described under 2.6.1 *FIA-FTMS*. For determination of in-source fragmentation, the mass range was set to m/z 350-760 in positive ion mode.

2.7.3 Nano-ESI-FIA-FTMS using an Orbitrap Fusion

The measurements on an Orbitrap Fusion were performed in the laboratory of Prof. C. Ejlsing at the University of Southern Denmark in Odense. Samples were

infused with the chip-based robotic nanoflow ion source TriVersa NanoMate at a flow rate of 200 nL/min into an Orbitrap Fusion Tribrid with a resolution of 450,000 at m/z 200. Full scan FTMS data were acquired in positive ion mode for 1 min with a scan range of m/z 470-1030 using profile mode, a max IT of 100 ms, AGC of 1×10^5 , three microscans, and a target resolution setting of 450,000.

2.7.4 Data Processing and Determination of Response

The peak assignment and offset correction was performed as described earlier (2.6.3.2 *Peak Assignment and Offset Correction*). Detected species were corrected for the abundance of the monoisotopic peak (type I effect (Han & Gross, 2001)) and for the type II effect by a stepwise correction based on theoretical isotope distributions (Haimi et al., 2006; Han & Gross, 2005; Liebisch et al., 2004). Species quantification was performed after isotope correction as described in 2.6.3.5 *Quantification*.

The instrument response was defined as molar ratio:

$$response = \frac{n(detected)[mol]}{n(expected)[mol]}$$

2.8 Evaluation of Isotope Correction Algorithm

2.8.1 Preparation of Standard Mixtures and Matrix Spikes

Two standard mixtures were prepared. The mixture “M0” contained saturated species of different lipid classes and was composed of: LPE 18:0 (0.018 pmol/ μ L), LPC 18:0 (0.18 pmol/ μ L), DG 36:0 (0.18 pmol/ μ L), CE 18:0 (0.18 pmol/ μ L), SM 36:1;2 (0.18 pmol/ μ L), Cer 42:1;2 (0.018 pmol/ μ L), and TG 54:0 (0.18 pmol/ μ L). The mixture “M1” was composed of the corresponding species of the same lipid class with exactly one additional DB: LPE 18:1 (0.018 pmol/ μ L), LPC 18:1 (0.18 pmol/ μ L), DG 36:1 (0.18 pmol/ μ L), CE 18:1 (0.18 pmol/ μ L), SM 36:2;2 (0.18 pmol/ μ L), Cer 42:2;2 (0.018 pmol/ μ L), and TG 54:1 (0.18 pmol/ μ L).

2.8 Evaluation of Isotope Correction Algorithm

A volume of 25 μL of both mixtures subjected to lipid extraction, corresponding to 0.018 pmol/ μL (0.1 nmol added to lipid extraction) LPE and Cer, and 0.18 pmol/ μL (1 nmol added to lipid extraction) LPC, DG, CE, SM and TG, was defined as ratio M1:M0 = 1:1. Samples were analyzed with a constant amount of the M0 mixture and variable amounts of the M1 mixture. Samples with a M1:M0 ratio ranging from 0:1 up to 25:1 were analyzed. The concentration of the infusate was calculated by dividing the amount added to the extraction in nmol by the dilution of 5.598 during extraction. The serum/plasma IS was added to the extraction for quantification (Table 2.1).

2.8.2 FIA-FTMS using a Q Exactive Orbitrap

The isotope correction experiments were performed on a Q Exactive Orbitrap equipped with a heated electrospray ionization source coupled to a conventional isocratic pump. The parameters of the instrumental method are described under 2.6.1 *FIA-FTMS*.

2.8.3 Data Processing

The peak assignment and offset correction was performed as described earlier (2.6.3.2 *Peak Assignment and Offset Correction*). Detected species were corrected for the abundance of the monoisotopic peak (type I effect (Han & Gross, 2001)). For the type II isotope effect, three different correction algorithms were compared. The “corrected” values were corrected for the type II effect by a stepwise correction based on theoretical isotope distributions (Haimi et al., 2006; Han & Gross, 2005; Liebisch et al., 2004). The “uncorrected” data were not corrected for the type II effect. The “I/A corrected” values were corrected by multiplying species intensity with an intensity/area correction factor as described in 2.6.3.3 *Isotope Correction*. Species quantification was performed after isotope correction as described in 2.6.3.5 *Quantification*.

3 Results and Discussion

3.1 Isotope Correction Algorithm for FIA-FTMS

The most frequent occurring isotopic overlap in lipidomics spectra is the overlap of a monoisotopic species (Species+0DB M+0 – in the following referred to as M+0) with the second isotope of a species of the same lipid class and same number of C-atoms with one additional double bond (Species+1DB M+2 – in the following referred to as M+2), which we will referred to as double bond ambiguity (DBA) (Bielow et al., 2017). The peak shape and apex position of the species affected by DBA are depending on the instrument resolution, the abundance of both species, and the isotopic fidelity (Almeida, Pauling, Sokol, Hannibal-Bach, & Ejsing, 2015; Bielow et al., 2017; Kaufmann & Walker, 2012). To correct for this effect, we analyzed samples with a constant amount of the M0-mixture (saturated species) with variable amounts of the M1-mixture (species with one additional DB), as it is described in the experimental section (2.8 *Evaluation of Isotope Correction Algorithm*).

3.1.1 Peak Picking and Constellations

The first important step for the development of an isotope correction algorithm is the intensity picking. For peak assignment, we applied a m/z -tolerance of ± 0.0045 after lock-mass correction. The selected tolerance accounts for half the mass difference of the double bond overlap ($\Delta m/z$ 0.00894) resulting from incorporation of two ^{13}C -atoms into the specie with one additional double bond. This represents the most frequent M+2 isotope overlap due to the high natural abundance of ^{13}C with 1.07%. Using this setting, the ALEX software picks the intensity either at the apex, or, if not present within the m/z -tolerance, at m/z (expected) ± 0.0045 . The following peak constellations could be differentiated (illustrated in Figure 3.1).

First Case: The intensity of M+0 is picked at the apex within the selected m/z -tolerance and the intensity of M+2 is picked at m/z (expected) $+0.0045$.

Second Case: Both intensities are picked at the apex within the corresponding m/z -tolerance. Peaks of both species are partially or completely separated.

3.1 Isotope Correction Algorithm for FIA-FTMS

Third Case: The intensity of M+0 is picked at m/z (expected) -0.0045 and the intensity of M+2 is picked at the apex within the m/z -tolerance.

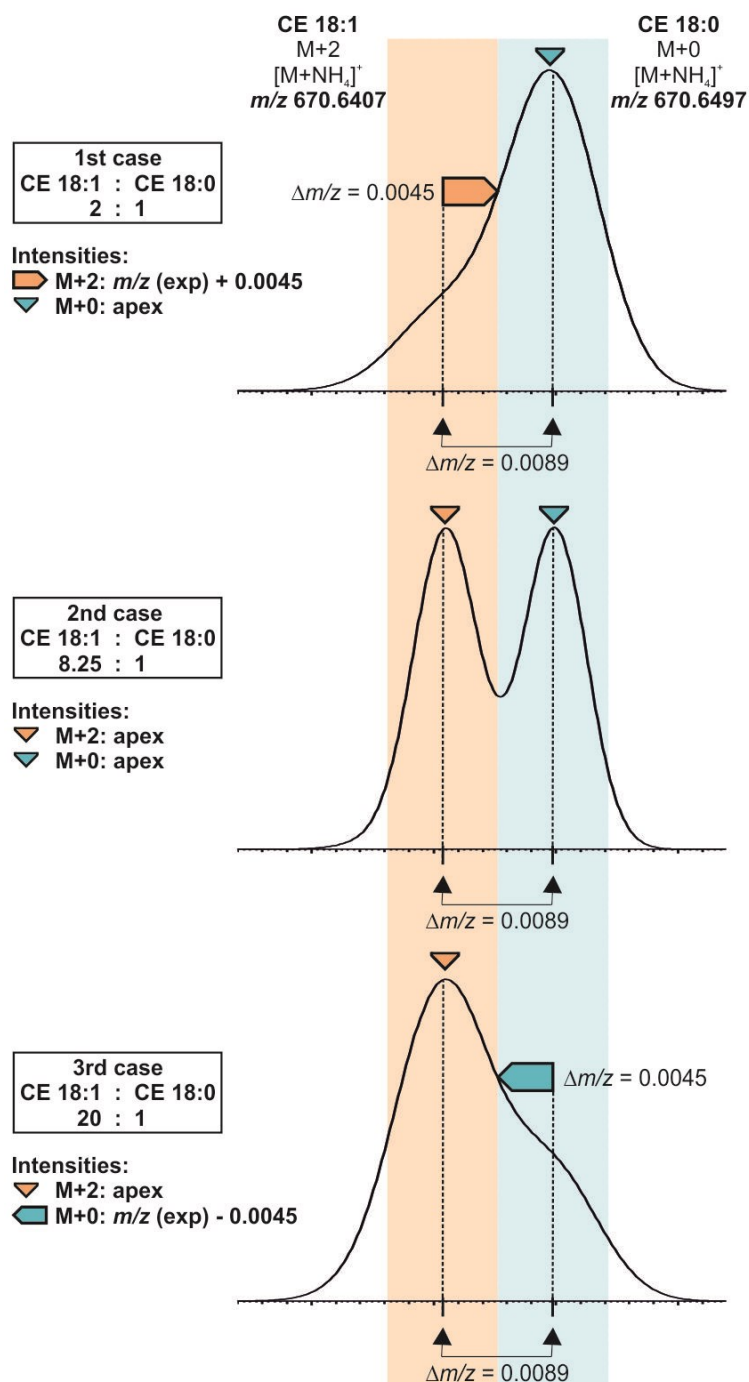


Figure 3.1 Peak picking and constellations. Peak constellation and picking of intensity illustrated for CE 18:1 M+2 and CE 18:0 M+0. The intensities are picked either at the apex (triangles) or at peak flank at m/z (expected) ± 0.0045 . The m/z -tolerance of ± 0.0045 for intensity picking of CE 18:1 M+2 and CE 18:0 M+0 is displayed in orange and blue, respectively. The spike ratio of the monoisotopic species is indicated in the figure legend. A target resolution of $R=100,000$ was chosen for the simulation.

3.1 Isotope Correction Algorithm for FIA-FTMS

The peak constellation and the respective case for peak picking are depending on the following factors: 1) the intensity ratio of both peaks (modified here by the spike amount of the M1-mix), 2) the fractional abundance of the M+2 isotope, and 3) the mass resolution. The fractional abundance of M+2 and mass resolution increase and decrease with m/z , respectively. Therefore, spectra of specie-pairs with DBA were evaluated for different lipid classes (each separated by approximately m/z 100) at different spike ratios of the M1/M0-mixture (Figure 3.2). The spectra were recorded at a target resolution of 140,000 at m/z 200. Of note, the resolution of Orbitrap instruments decreases with increasing m/z following a square root function. At higher m/z mass resolution is not sufficient to separate isobaric peaks at any of the tested spike ratios (see TG 54:1 M+2 and TG 54:0 M+0). With increasing spike amounts of TG 54:1, the peak maximum of TG 54:0 M+0 shifted towards the expected mass of TG 54:1 M+2 at m/z 908.8550. Analogously, the peak constellation changed from first case to third case. A third case was already assigned at spike ratio M1/M0 of 5:1 due to the high abundance of 21.1% for the M+2 isotopic peak of TG 54:1.

At lower m/z (LPC and CE) M+2 and M+0 peaks were at least partially separated, when the peak ratio allowed the detection of both isobaric peaks. When one of the isobaric peaks significantly prevailed, both peaks could not be resolved. However, for the resulting unresolved peak, the apex did not shift in m/z . For species with $m/z < 600$ we could only detect first and second cases, for species with $m/z > 800$ we could only detect first and third cases, and within the m/z -range 600-800 we could assign all three cases. This fits very well to our expectation because with a mass resolution setting of 140,000 FWHM (full width at half maximum) (at m/z 200) a peak width of 0.00894 Da at half height (corresponding to the mass difference of DBA) should be observed for peaks around m/z 678. This calculation is based on the square root function for mass resolution of Orbitrap analyzers (Makarov et al., 2006).

Interestingly, for lipid species which center around m/z 678 peak resolutions were observed which exceed the expected resolution (non-spiked sample) upon appearance of M+2 isobaric peaks as for example for CE 18:0 from expected 82,600 up to 105,400 and SM 36:1;2 from expected 76,900 up to 106,700 (Figure 3.2). While the resolution of LPE and LPC was not influenced by

3.1 Isotope Correction Algorithm for FIA-FTMS

addition of M+2, the resolution of TG 54:0 decreased slightly due to peak broadening.

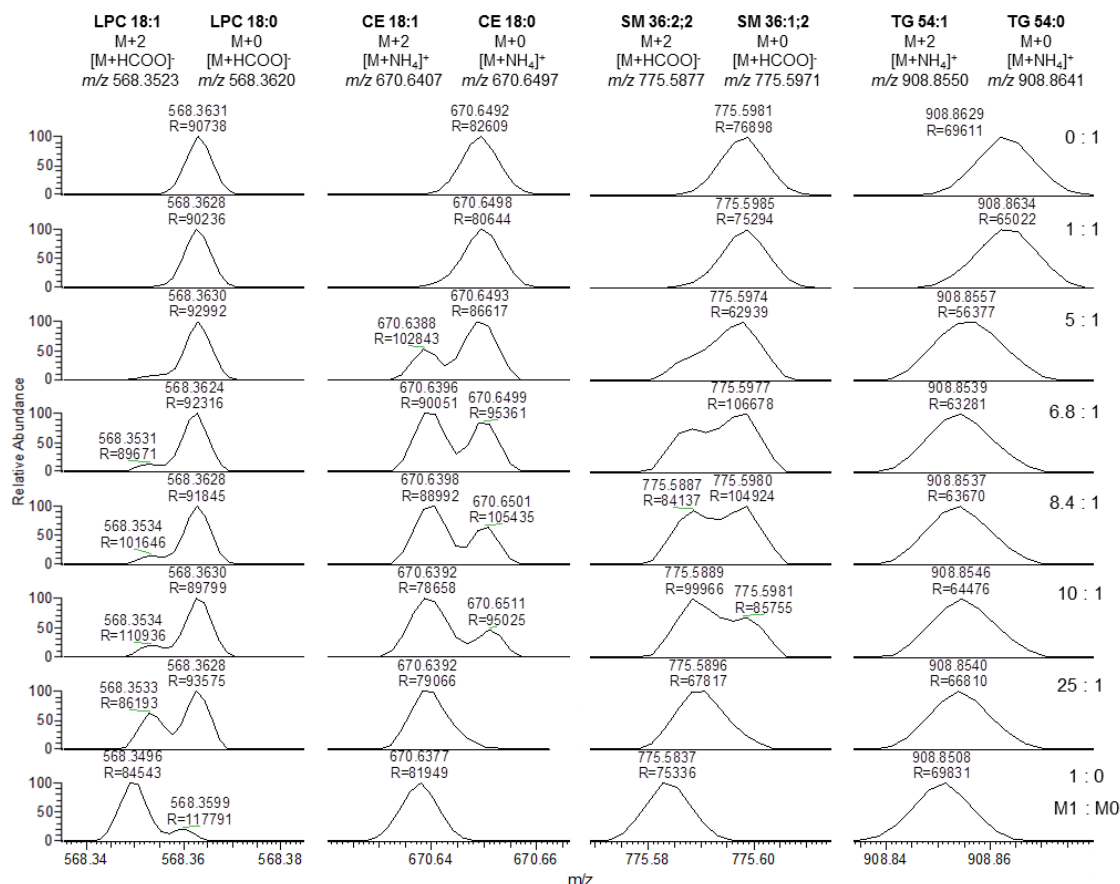


Figure 3.2 Mass spectra of the DB overlap of selected specie-pairs recorded at R=140,000 at m/z 200 on a Q Exactive. The figure illustrates changes of peak shape and shifting maxima induced by increasing abundance of the second isotope of the Species+1DB. Of note, spectra shown have not been offset corrected at this point.

3.1.2 Intensity/Area Ratio

Shotgun lipidomic data are commonly based on the analysis of peak intensities. An advantage of the ALEX software (Husen et al., 2013) is the possibility to obtain the information of peak areas. The peak area is determined from baseline to baseline and therefore independent of the selected m/z -tolerance. By recording both parameters, we noticed several advantages using intensity/area ratios. The experimentally determined I/A ratios of various species are displayed in Figure 3.3 for m/z range 400-1000. For these data, lipid species were selected that were not affected by DBA or other potential isobaric overlaps. Positive/negative ion mode, various target ions and ion abundances as well as sample matrixes were considered. Despite these vast

differences, the I/A ratio was only influenced by the physical mass to charge attribute. The m/z dependency of I/A ratios could be described by an exponential decaying function, which is correlating with the m/z dependent resolution of Orbitrap instruments.

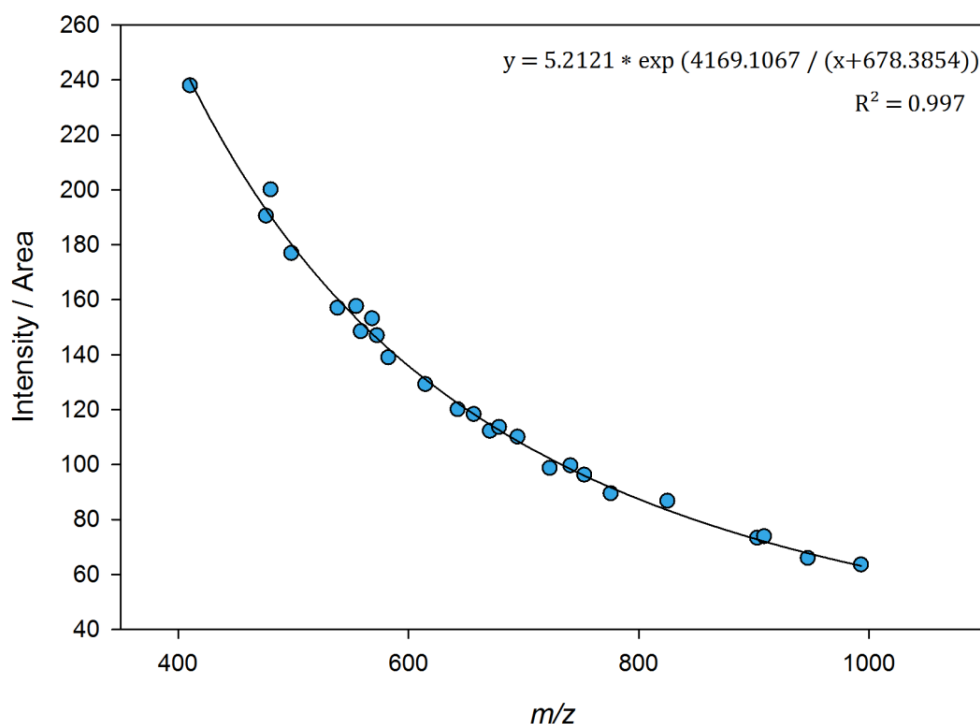


Figure 3.3 Determination of I/A ratios in m/z range 400-1000 recorded on a Q Exactive at $R=140,000$ at m/z 200. The I/A ratios were determined for the following overlap-free lipid species (in ascending m/z): LPE 13:0, LPE 18:2, LPE 18:0, LPC 13:0, LPC 16:1, Cer 32:1;2, CE 10:0, LPC 18:0, TG 30:0, LPC 19:0, CE 14:0, DG 36:0, TG 36:0, CE 18:0, PC 28:0 $[M+H]^+$, Cer 42:1;2, PC 28:0 $[M+HCOO]^-$, TG 42:0, CE 24:1, SM 36:1;2, TG 48:0, PC 44:0 $[M+H]^+$, TG 54:0, PC 44:0 $[M+HCOO]^-$, and TG 60:0.

Furthermore, the I/A ratios were highly reproducible for isolated peaks at a given target resolution. A reduction of the selected target resolution decreased the I/A ratios as expected, half resolution resulted in half I/A ratios. This reproducibility allows the detection of peak impurities. Partially overlapping species or contaminations decrease the I/A ratio significantly due to an increased peak area including both peaks (resulting from baseline to baseline determination of peak areas) but only the intensity of one of the peaks. In contrast, peak intensities of near-isobaric interferences led to peak coalescence induced losses of peak intensity. This phenomenon will be explained in detail in the next chapter.

3.1.3 Comparison of Isotope Correction Algorithms

Several software tools have been developed to process lipidomic data (LipidQA (Song, Hsu, Ladenson, & Turk, 2007), LIMSA (Haimi et al., 2006), FAAT (Leavell & Leary, 2006), LipID (Hubner, Crone, & Lindner, 2009), LipidSearch (Houjou, Yamatani, Imagawa, Shimizu, & Taguchi, 2005), LipidView (Ejsing et al., 2006), LipidInspector (Schwudke et al., 2006), LipidXplorer (Herzog et al., 2012)). Some of the mentioned algorithms contain a built-in isotope correction. Nevertheless, software is typically optimized to support a certain instrument or application. Therefore, we decided to perform data processing, including isotope correction, with self-programmed Excel Macros in an automated way. To evaluate the accuracy of isotope correction, we analyzed samples with a constant spike of the M0-mixture against increasing spike amounts of the M1-mixture and compared the three isotope correction algorithms “corrected”, “uncorrected” and “I/A corrected” as described in the materials and method section (*2.8 Evaluation of Isotope Correction Algorithm*).

The analysis of LPE, LPC, DG, CE, Cer, SM, and TG (in ascending m/z order) is shown in Figure 3.4, Figure 3.5, Figure 3.6, Figure 3.7, Figure 3.8, Figure 3.9, and Figure 3.10, respectively. Of note, all data were corrected for the type I isotope effect (Han & Gross, 2001) independent of the applied isotope correction algorithm. Additionally, species quantification of all cases was performed with the picked intensity of the quantified, monoisotopic species.

3.1 Isotope Correction Algorithm for FIA-FTMS

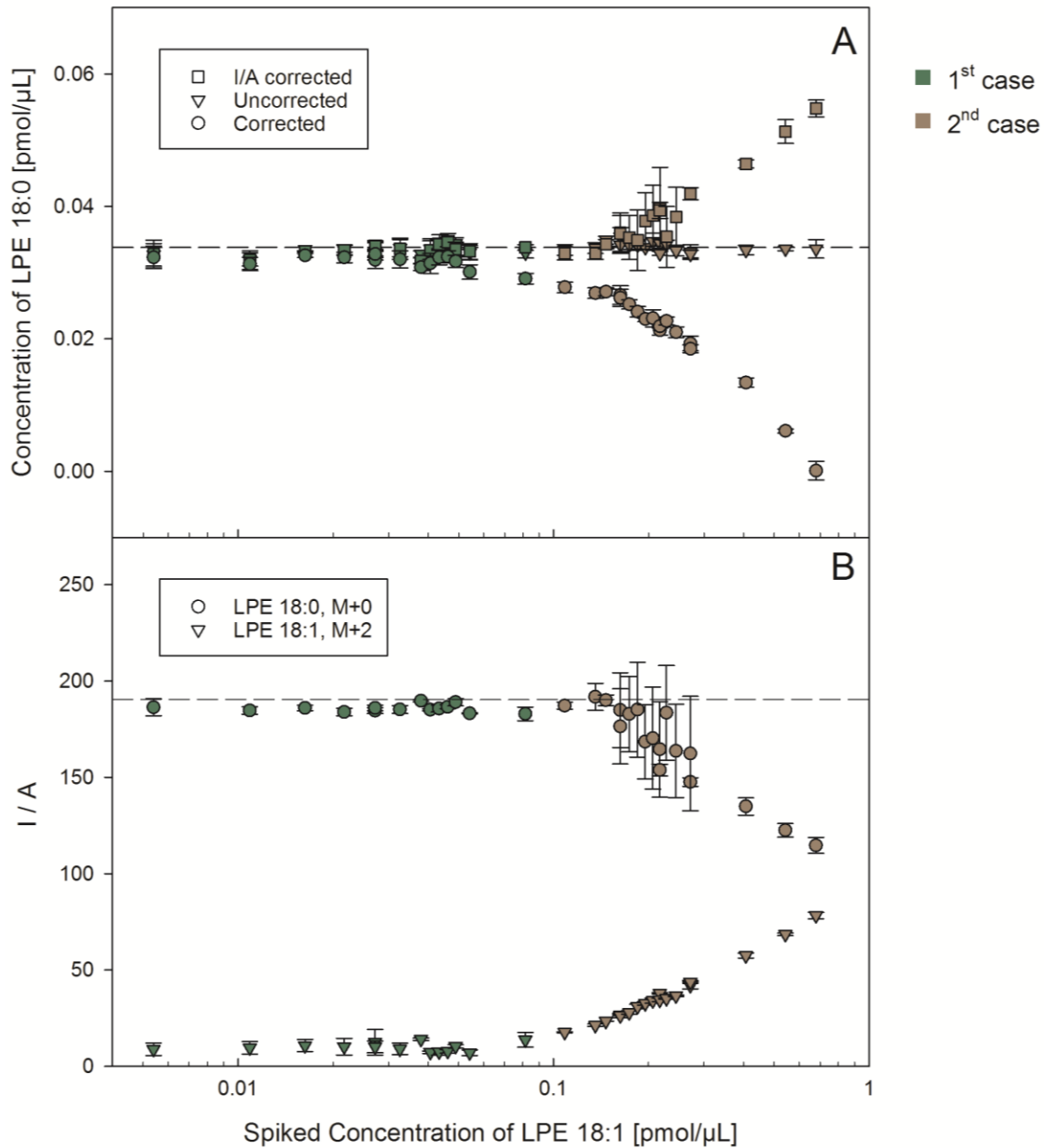


Figure 3.4 Quantification of LPE 18:0 at increasing concentrations of LPE 18:1 at target resolution of 140,000 at m/z 200. Panel A shows the quantification of isotope type II corrected (circles), uncorrected (triangles), and I/A corrected (squares) data. The dashed line indicates the spiked amount of LPE 18:0. Panel B displays the intensity/area ratio of LPE 18:0 and the second isotope of LPE 18:1. The dashed line indicates the calculated I/A of m/z 480.3096 (calculated with the exponential function, Figure 3.3). The color code describes the case of peak assignment. Each point represents the average of $n = 3$ technical replicates \pm SD.

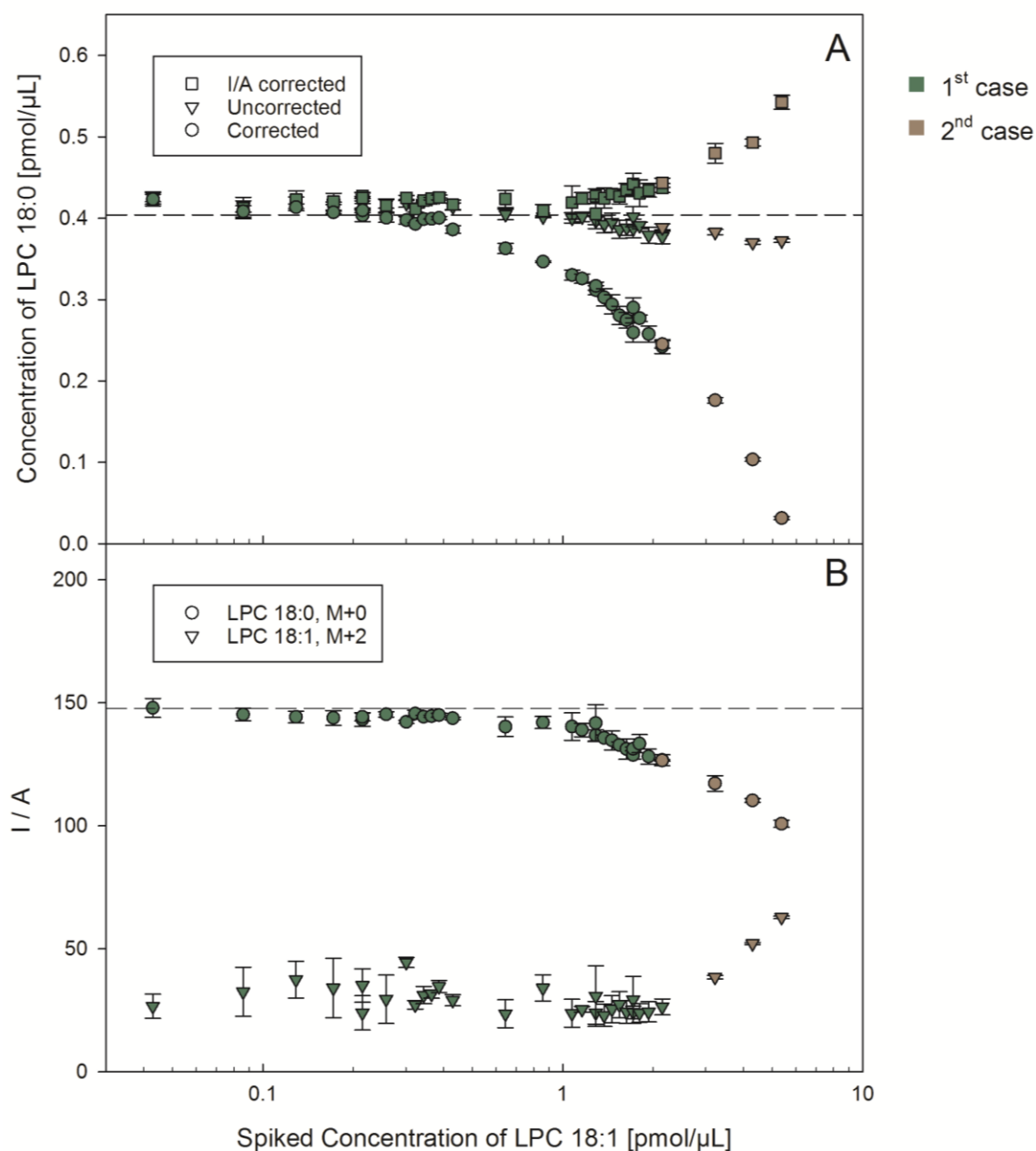


Figure 3.5 Quantification of LPC 18:0 at increasing concentrations of LPC 18:1 at target resolution of 140,000 at m/z 200. Panel A shows the quantification of isotope type II corrected (circles), uncorrected (triangles), and I/A corrected (squares) data. The dashed line indicates the spiked amount of LPC 18:0. Panel B displays the intensity/area ratio of LPC 18:0 and the second isotope of LPC 18:1. The dashed line indicates the calculated I/A of m/z 568.362 (calculated with the exponential function, Figure 3.3). The color code describes the case of peak assignment. Each point represents the average of $n = 3$ technical replicates \pm SD.

3.1 Isotope Correction Algorithm for FIA-FTMS

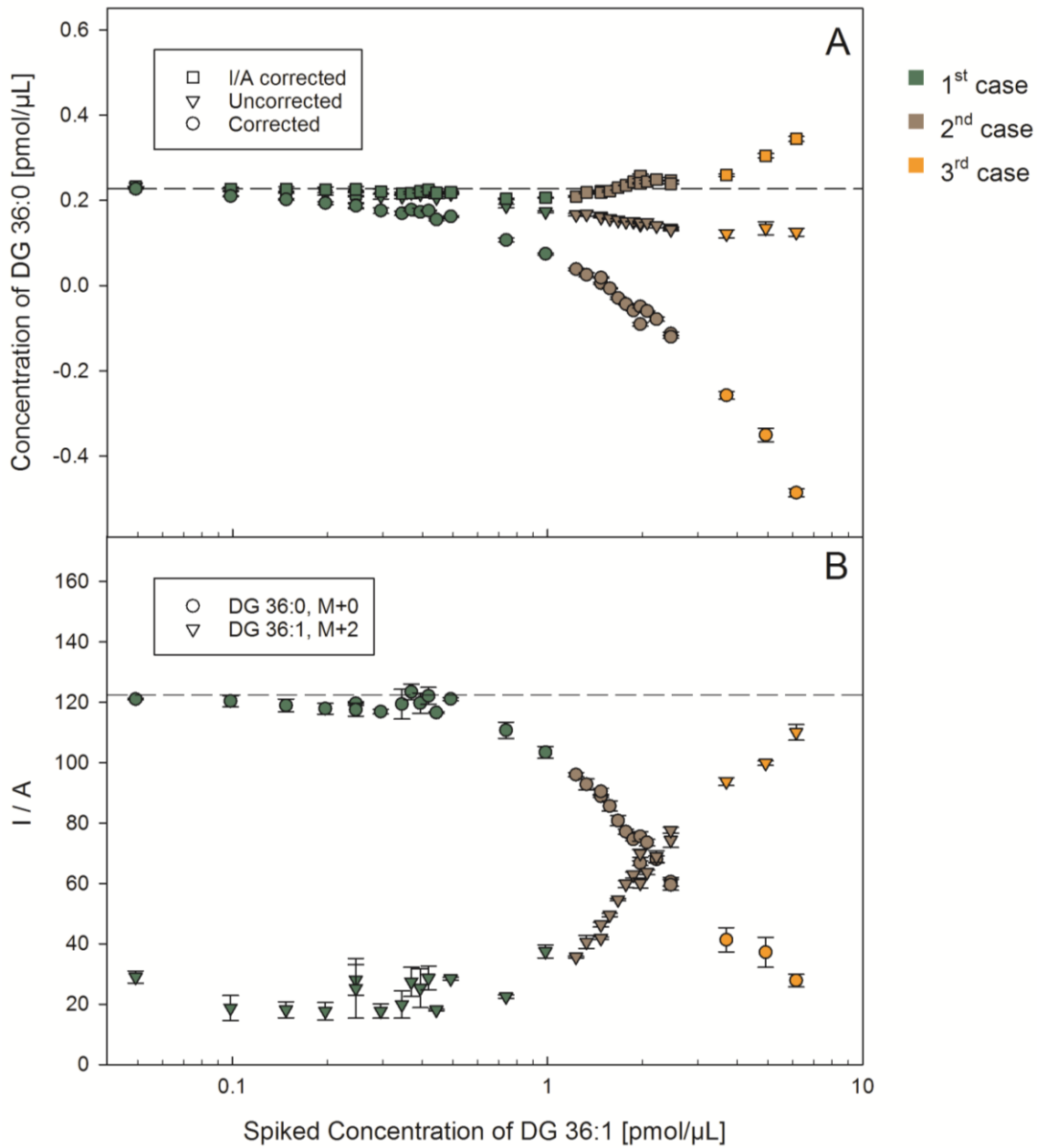


Figure 3.6 Quantification of DG 36:0 at increasing concentrations of DG 36:1 at target resolution of 140,000 at m/z 200. Panel A shows the quantification of isotope type II corrected (circles), uncorrected (triangles), and I/A corrected (squares) data. The dashed line indicates the spiked amount of DG 36:0. Panel B displays the intensity/area ratio of DG 36:0 and the second isotope of DG 36:1. The dashed line indicates the calculated I/A of m/z 642.6031 (calculated with the exponential function, Figure 3.3). The color code describes the case of peak assignment. Each point represents the average of $n = 3$ technical replicates \pm SD.

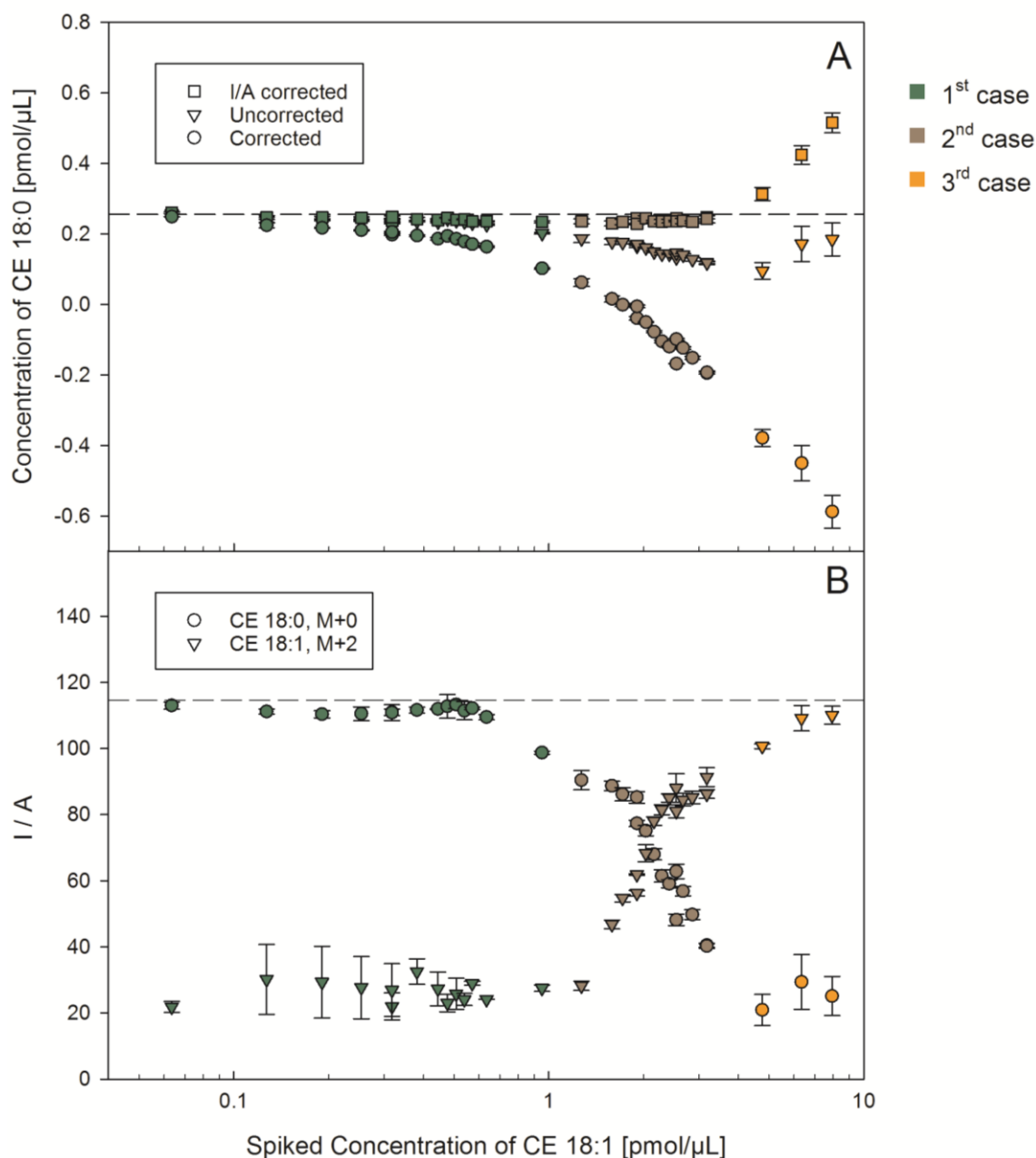


Figure 3.7 Quantification of CE 18:0 at increasing concentrations of CE 18:1 at target resolution of 140,000 at m/z 200. Panel A shows the quantification of isotope type II corrected (circles), uncorrected (triangles), and I/A corrected (squares) data. The dashed line indicates the spiked amount of CE 18:0. Panel B displays the intensity/area ratio of CE 18:0 and the second isotope of CE 18:1. The dashed line indicates the calculated I/A of m/z 670.6497 (calculated with the exponential function, Figure 3.3). The color code describes the case of peak assignment. Each point represents the average of $n = 3$ technical replicates \pm SD.

3.1 Isotope Correction Algorithm for FIA-FTMS

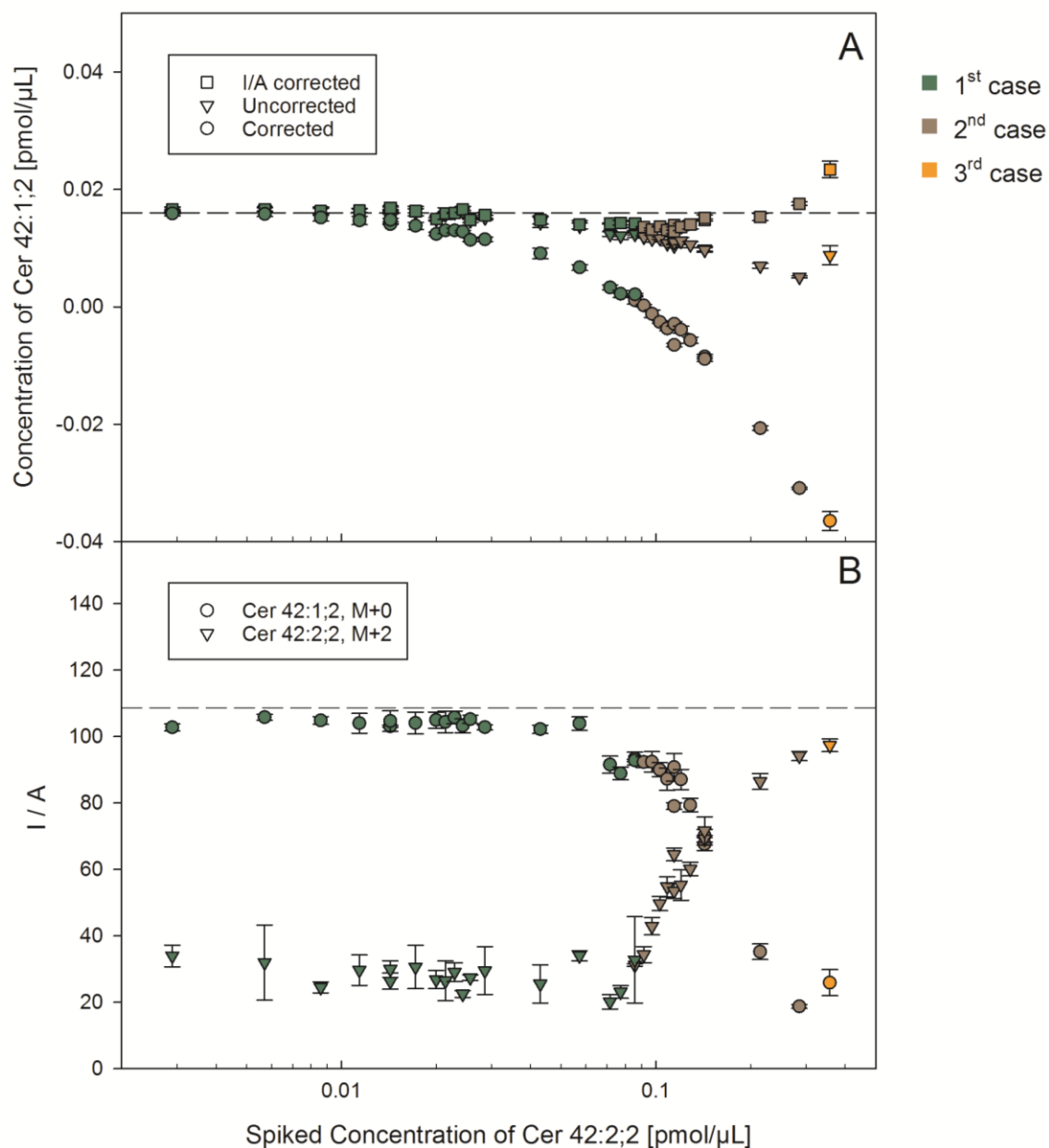


Figure 3.8 Quantification of Cer 42:1;2 at increasing concentrations of Cer 42:2;2 at target resolution of 140,000 at m/z 200. Panel A shows the quantification of isotope type II corrected (circles), uncorrected (triangles), and I/A corrected (squares) data. The dashed line indicates the spiked amount of Cer 42:1;2. Panel B displays the intensity/area ratio of Cer 42:1;2 and the second isotope of Cer 42:2;2. The dashed line indicates the calculated I/A of m/z 694.6355 (calculated with the exponential function, Figure 3.3). The color code describes the case of peak assignment. Each point represents the average of $n = 3$ technical replicates \pm SD.

3.1 Isotope Correction Algorithm for FIA-FTMS

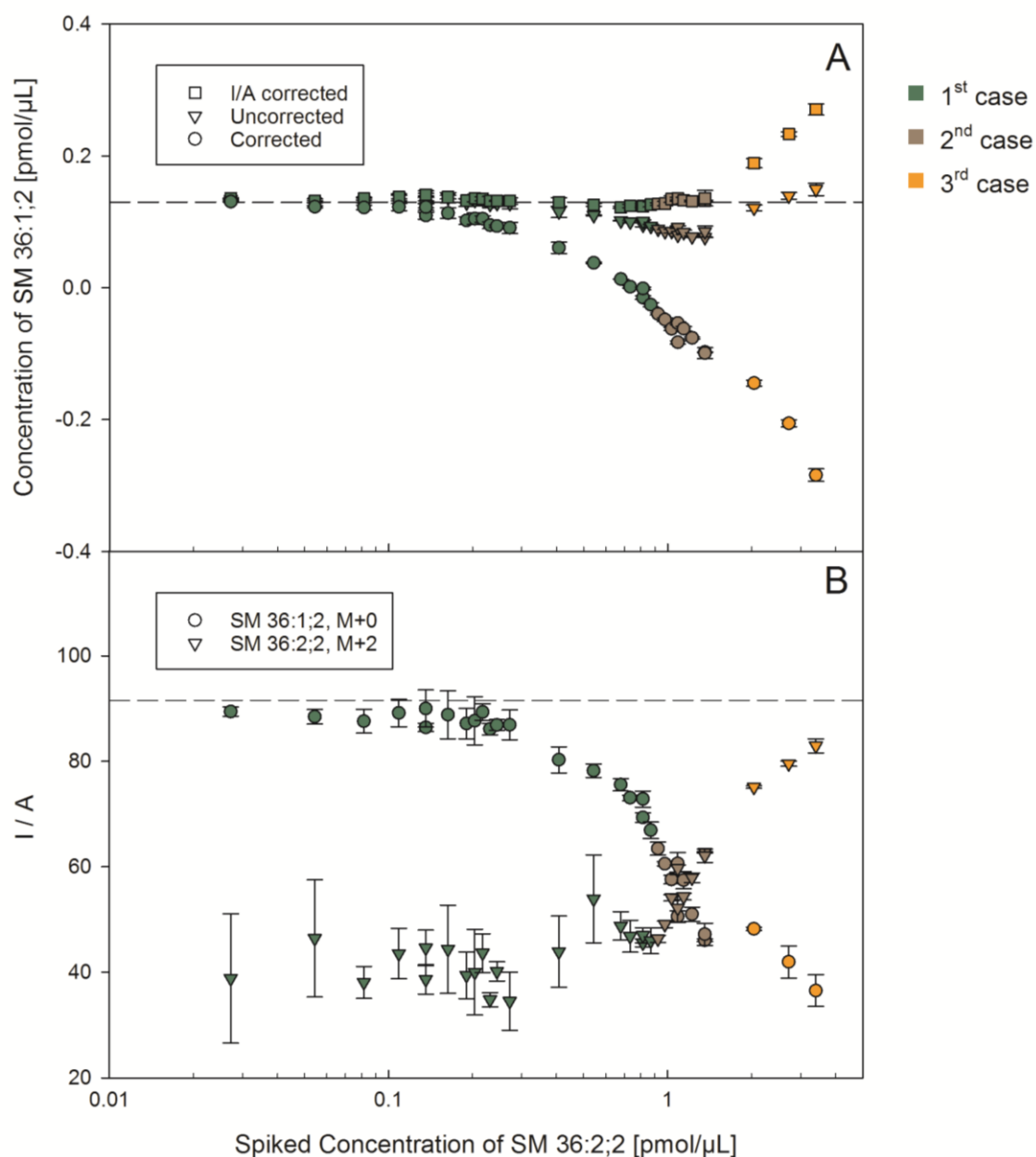


Figure 3.9 Quantification of SM 36:1;2 at increasing concentrations of SM 36:2;2 at target resolution of 140,000 at m/z 200. Panel A shows the quantification of isotope type II corrected (circles), uncorrected (triangles), and I/A corrected (squares) data. The dashed line indicates the spiked amount of SM 36:1;2. Panel B displays the intensity/area ratio of SM 36:1;2 and the second isotope of SM 36:2;2. The dashed line indicates the calculated I/A of m/z 775.5971 (calculated with the exponential function, Figure 3.3). The color code describes the case of peak assignment. Each point represents the average of $n = 3$ technical replicates \pm SD.

3.1 Isotope Correction Algorithm for FIA-FTMS

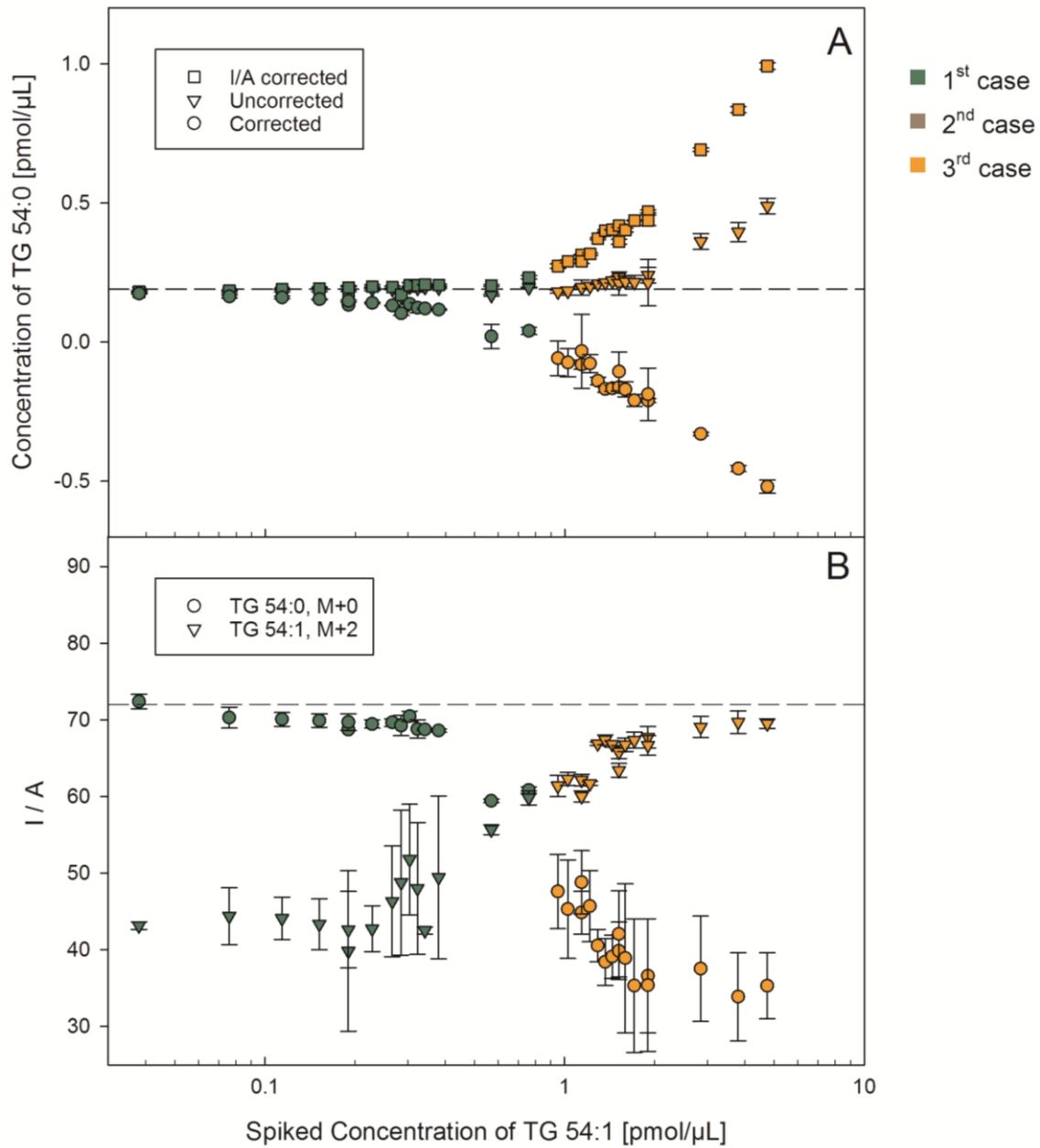


Figure 3.10 Quantification of TG 54:0 at increasing concentrations of TG 54:1 at target resolution of 140,000 at m/z 200. Panel A shows the quantification of isotope type II corrected (circles), uncorrected (triangles), and I/A corrected (squares) data. The dashed line indicates the spiked amount of TG 54:0. Panel B displays the intensity/area ratio of TG 54:0 and the second isotope of TG 54:1. The dashed line indicates the calculated I/A of m/z 908.8641 (calculated with the exponential function, Figure 3.3). The color code describes the case of peak assignment. Each point represents the average of $n = 3$ technical replicates \pm SD.

3.1.3.1 Type II Correction of Isotopic Overlap

First thing to notice, the “corrected” values of all species pairs were remarkably overcorrected at higher spike amounts of the species with one additional double bond. For species at low m/z , we expect that application of type II correction results in too low concentrations because mass resolution is sufficient to separate M+2 and M+0 isobaric peaks. Thus, intensities of M+0 are picked at the apex and should not be influenced by the M+2 peak. Similarly, we expect that for slightly higher m/z despite mass separation is not sufficient to clearly separate M+2 and M+0 (e.g. SM 36:1;2 with m/z 775.5971; Figure 3.2). Unexpectedly, even for completely overlapping species, as observed for TG (Figure 3.2), application of type II correction resulted in significant overcorrection at higher intensities of M+2. This indicates that the intensities of the M+0 and M+2 are not behaving additively. Of note, the applied correction algorithm based on theoretical isotope distributions is commonly used for other systems (Haimi et al., 2006; Han & Gross, 2005; Liebisch et al., 2004).

3.1.3.2 Concentrations without Type II Correction

To further understand the previously mentioned phenomenon, we evaluated concentrations without application of isotope type II correction. The “uncorrected” concentrations fitted mostly very well to the target concentrations. Especially LPE 18:0 (m/z 480.3096, Figure 3.4), LPC 18:0 (m/z 568.362, Figure 3.5), and TG 54:0 (m/z 908.8641, Figure 3.10) showed accurate values with a low deviation to the target concentration up to high spike amounts of the M1-mixture. Although, for the third case the intensity for M+0 is not picked at the apex but from the peak flank, concentrations of TG 54:0 were in good alignment with the target concentration. However, we would not recommend using concentrations calculated this way since shifts in m/z and/or peak shape will change resulting concentrations substantially.

For DG 36:0 (m/z 642.6031, Figure 3.6), CE 18:0 (m/z 670.6497, Figure 3.7), Cer 42:1;2 (m/z 694.6355, Figure 3.8), and SM 36:1;2 (m/z 775.5971, Figure 3.9) the uncorrected quantification matched the target values very well for a first case. Concentrations calculated for second case were below target concentrations even though peaks were partially separated and increased values could be expected due to the partial peak overlap.

3.1.3.3 Peak Coalescence in FTMS

We did not expect that both, type II isotope correction of overlapping peaks (e.g. for TG 54:0) results in significantly too low concentrations, and uncorrected concentrations of partially overlapping peaks fit very well to target concentrations. A potential explanation for these observations could be destructive (and/or constructive) interference of ions described for iontrap instruments using FTMS (Fourier-Transform mass spectrometry) (Aizikov, Mathur, & O'Connor, 2009; Huang, Tiedemann, Land, McIver, & Hemminger, 1994; Nakata, Hart, & Peterson, 2010). This effect occurs when two near-isobaric ion populations oscillate initially with slightly different frequencies and these populations start to coalesce after a number of oscillations. However, the individual ion frequency is not detectable anymore and a coupled oscillating frequency will be measured instead. The number of oscillations leading to peak coalescence of two ion populations is abundance dependent. It is described that destructive interferences can result in a distorted relative isotopic abundance (RIA) and is depending on the mass resolution (Almeida et al., 2015; Kaufmann & Walker, 2012). This may explain the shift of the m/z of unresolved ions towards the m/z of the dominating ion. Moreover, it provides a potential explanation why the intensity of these overlapping peaks seems to represent only the intensity of the dominating ion and not as expected the sum of both ions. Instead of an increased intensity some peaks appear broader.

3.1.3.4 The “I/A Correction”

We aimed to get more accurate concentrations for peaks affected by peak coalescence induced losses of intensity which center around m/z 678. As these peaks appear to experience a change in resolution, the idea was to use an intensity and area based type of correction, which was termed in the following as I/A correction. The following formulas were developed empirically to achieve the most accurate concentrations.

For samples with higher abundance of the monoisotopic species $M+0$ (up to the point of intersection of I/A ratios) the correction factor was calculated with the following equation based on the measured and the expected I/A:

3.1 Isotope Correction Algorithm for FIA-FTMS

$$\frac{I}{A} \text{ Correction factor } (M + 0) = \frac{\frac{I}{A}(\text{calcd})}{\frac{I}{A}(M + 0 \text{ measured})}$$

When the M+2 ion is dominating over the M+0, the I/A measured of both species (M+0 and M+2) was applied for concentration correction:

$$\frac{I}{A} \text{ Correction factor}(M + 0) = \frac{\frac{I}{A}(\text{calcd}) * 2}{\frac{I}{A}(M + 0 \text{ measured}) + \frac{I}{A}(M + 2 \text{ measured})}$$

The application of this correction reduced the deviation of quantification of DG 36:0 (m/z 642.6031, Figure 3.6), CE 18:0 (m/z 670.6497, Figure 3.7), Cer 42:1;2 (m/z 694.6355, Figure 3.8), and SM 36:1;2 (m/z 775.5971, Figure 3.9) to a minimum. I/A correction practically only affects concentrations when the measured I/A deviates from the expected (=calculated). Such deviations occur with increasing intensities of M+2 ions for coalescent peaks. For case one and two constellations, the I/A correction appears to result in more accurate concentrations. Obviously, correction is also accurate for constellations with a dominating M+2 ion when I/A of both ions M+0 and M+2 were used for correction. As discussed above we would not recommend using results from a third case constellation because the intensity for M+0 is not picked at the apex but from the peak flank. When mass resolution is sufficient to separate isobaric peaks as for the tested LPE and LPC species, uncorrected concentrations are more accurate than I/A corrected. Therefore, we would recommend applying the I/A correction only for coalescent peaks, which is in our setting a mass range of about m/z 600-800.

3.1.4 Resolution dependent Isotope Correction

As demonstrated earlier, quantification of data corrected for the type II effect was too low for all analyzed m/z at a resolution setting of 140,000 at m/z 200, most likely due to peak coalescence of near-isobaric M+0 and M+2 ions. Since peak coalescence was described as a mass resolution dependent phenomenon, M1/M0-mixtures were also analyzed at resolutions settings of 70,000 and 35,000 at m/z 200. Our expectation was that for lower mass resolution the overlapping peaks represent the intensities of both M+0 and M+2 ions which afford type II isotopic correction to achieve accurate concentrations. The quantification of LPE 18:0, LPC 18:0, DG 36:0, and CE 18:0 is shown in Figure 3.11 and the quantification of the higher m/z species Cer 42:1;2, SM 36:1;2, and TG 54:0 is displayed in Figure 3.12. In contrast to the above-described evaluation, here, for third case constellations (orange color) the intensity was picked at the apex of the M+2 ion to base the evaluation on the presumably more correct coalescent ion intensity picked in the M+2 mass window. As expected, a decrease in mass resolution resulted in more accurate (type II corrected) concentrations for all analyzed lipid species. That lyso-species require lower mass resolution to converge to target concentrations fits also very well to a resolution-dependent peak coalescence model. Even third case assignments using the intensity from the apex of the M+2 peak followed the expectations. However, here one should keep in mind that the parameters for peak picking were not adapted to lower resolutions settings.

3.1 Isotope Correction Algorithm for FIA-FTMS

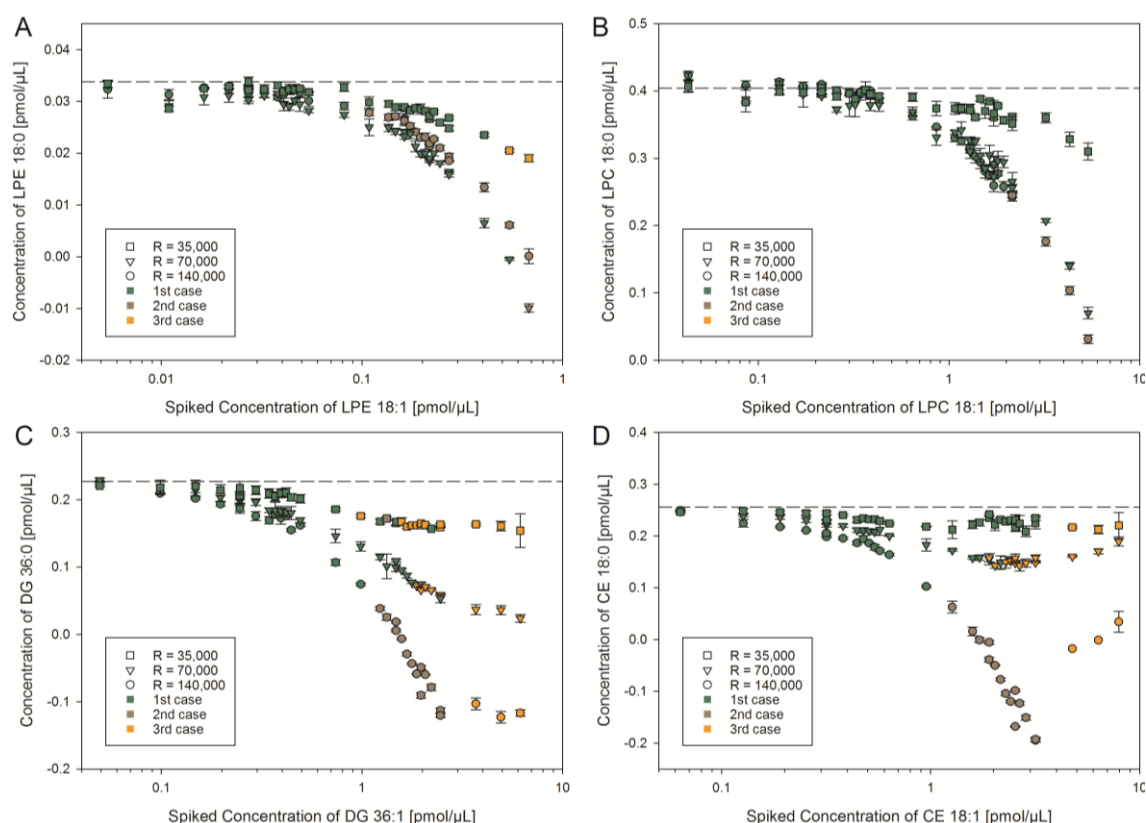


Figure 3.11 Quantification of (A) LPE 18:0 m/z 480.3096, (B) LPC 18:0 m/z 568.362, (C) DG 36:0 m/z 642.6031, and (D) CE 18:0 m/z 670.6497 at increasing spike amounts of the corresponding species+1DB recorded on a Q Exactive at resolution settings of 140,000, 70,000, and 35,000 (m/z 200). All data were corrected for the type II effect (“corrected”). The dashed line indicates the target value of the saturated species. Third case constellations used the apex intensity of the M+2. Each point represents the average of $n = 3$ technical replicates \pm SD.

3.1 Isotope Correction Algorithm for FIA-FTMS

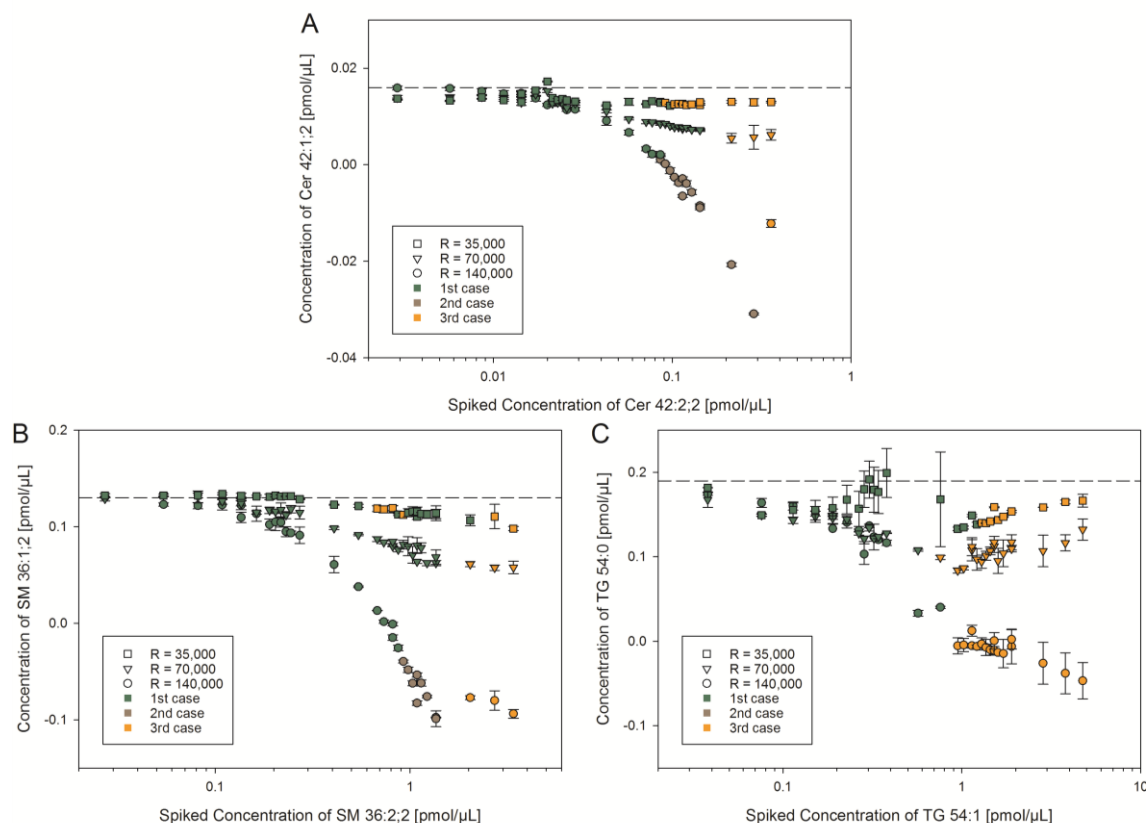


Figure 3.12 Quantification of (A) Cer 42:1;2 m/z 694.6355, (B) SM 36:1;2 m/z 775.5971, and (C) TG 54:0 m/z 908.8641 at increasing spike amounts of the corresponding species+1DB recorded on a Q Exactive at resolution settings of 140,000, 70,000, and 35,000 (m/z 200). All data were corrected for the type II effect (“corrected”). The dashed line indicates the target value of the saturated species. Third case constellations used the apex intensity of the M+2. Each point represents the average of $n = 3$ technical replicates \pm SD.

3.1.5 Influence of Sample Matrix

FIA-FTMS should be applicable for quantification of samples used in basic science as well as in clinical studies. The analyzed samples usually contain plenty of various analytes that may influence lipid species quantification. To verify the presented isotope correction and quantification in biological samples, the M1/M0 spike experiment was performed in human plasma, murine liver, and human skin fibroblast samples. The basal concentration of lipid species present in the different matrices was determined by three technical replicates (CV's < 3% for all species). Additionally, PC 36:2 was added to the M1-mixture and PC 36:1 to the M0-mixture providing a further species pair at m/z 832.6073 (PC 36:1 analyzed as $[M+HCOO]^-$).

The analysis of LPE 18:0, LPC 18:0, DG 36:0, CE 18:0, Cer 42:1;2, SM 36:1;2, PC 36:1, and TG 54:0 are shown in Figure 3.13, Figure 3.14, Figure 3.15, Figure 3.16, Figure 3.17, Figure 3.18, Figure 3.19, and Figure 3.20, respectively. In general, data evaluation of murine liver (panel B), human plasma (panel C), and human skin fibroblast samples (panel D) matched very well the results obtained for the synthetic standard samples (panel A) for the corresponding type of isotope correction. This is independent of basal amounts already present in the matrices for the M+0 and/or M+2 species. For example, the basal concentration of SM 36:1;2 determined by FTMS in human plasma was 0.033 ± 0.001 pmol/ μ L. The I/A corrected values were in good agreement with the target value of SM 36:1;2 (dotted line) representing the sum of the spiked amount (0.13 pmol/ μ L) and the basal concentration (Figure 3.18C). Furthermore, similar trends of I/A ratios were observed in the synthetic standard and matrix samples. However, some exceptions are apparent from the figures that should be mentioned in detail.

First, LPE 18:0 quantification in murine liver samples (Figure 3.13B) showed almost identical values for all applied isotope corrections (corrected, uncorrected, and I/A corrected) and these values were also matching with the target value of LPE 18:0 representing the sum of spiked amount (0.034 pmol/ μ L) and basal concentration (0.59 pmol/ μ L). The high amount of LPE 18:0 compared to the low amount of LPE 18:1 M+2 (highest spike of LPE 18:1 was 0.54 pmol/ μ L, with an isotopic fractional abundance of 4.69%) led

3.1 Isotope Correction Algorithm for FIA-FTMS

to first case constellations with negligible influence of the second isotope on LPE 18:0 quantification. Noticeably, the measured and calculated I/A ratios of LPE 18:0 M+0 were almost identical leading to an I/A correction factor of about 1 and virtually no correction.

Second, the I/A corrected values of DG 36:0 in human plasma (Figure 3.15C) were ~4-fold higher than the target value (0.22 pmol/μL). The I/A ratio of DG 36:0 used for response factor calculation was ~one fourth of the I/A (calcd) with 122.4. As already mentioned, the peak area used for calculation of I/A ratios includes all peaks that are not baseline resolved to the species of interest. In this case, a contamination located at the shoulder (to lower m/z) of the second isotope of DG 36:1 elevated the peak area significantly resulting in an inaccurate I/A correction. Considering an automated quantification, our data processing Macro will recognize these implausible I/A ratios and label the results accordingly. For such species the use the uncorrected concentrations is recommended.

Third exception is shown by the quantification of CE 18:0 in human plasma (Figure 3.16C). The lipid profile of human plasma is well characterized and cholesteryl esters are one of the main lipid classes (Bowden et al., 2017; Sales et al., 2016). The FTMS determined concentration of CE 18:1 in the used plasma was 1.62 ± 0.02 pmol/μL. CE 18:1 has a fractional abundance of 12.68% for the second isotope. Hence, the increased abundance of CE 18:1 M+2 led to a shift to higher ratios of CE 18:1 M+2/CE 18:0 for each individual sample in comparison to the matrix free sample. Therefore, we could not detect a first case constellation for the investigated spike range. However, I/A corrected concentrations of CE 18:0 matched very well the target value similar as demonstrated for matrix free, liver, and cell samples.

The analysis of PC 36:1 m/z 832.6073 in murine liver, human plasma, and human skin fibroblast cells is shown in Figure 3.19. As described above for other lipid classes, the “corrected” values were significantly overcorrected due to peak coalescence. Most accurate concentrations were achieved without further correction, similar to that shown for the quantification of TG 54:0 at m/z

3.1 Isotope Correction Algorithm for FIA-FTMS

908.8641 (Figure 3.20). Again concentrations calculated from third case constellations are not reliable.

3.1 Isotope Correction Algorithm for FIA-FTMS

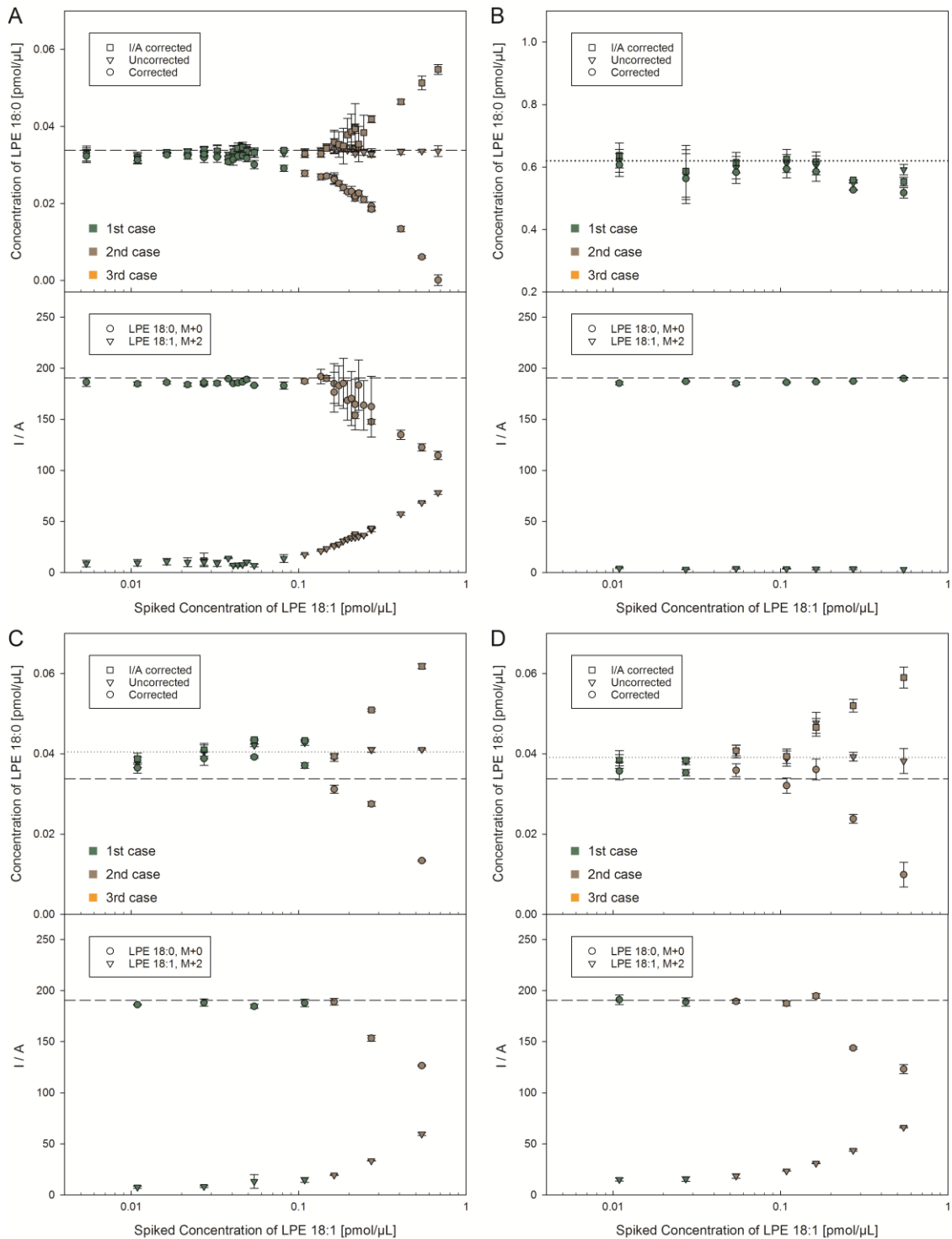


Figure 3.13 Quantification of LPE 18:0 m/z 480.3096 at increasing spike amounts of LPE 18:1 m/z 478.2939 recorded (A) without matrix and spiked on (B) murine liver, (C) human plasma, and (D) human skin fibroblast samples using a mass resolution setting of 140,000 at m/z 200. The dashed line in the upper panel indicates the spiked amount of LPE 18:0 and in the lower panel the I/A (calcd) of m/z 480.3096. The dotted line (upper panel) represents the target concentration of LPE 18:0 (spiked-in and basal sample amount). Each point represents the average of $n = 3$ technical replicates \pm SD.

3.1 Isotope Correction Algorithm for FIA-FTMS

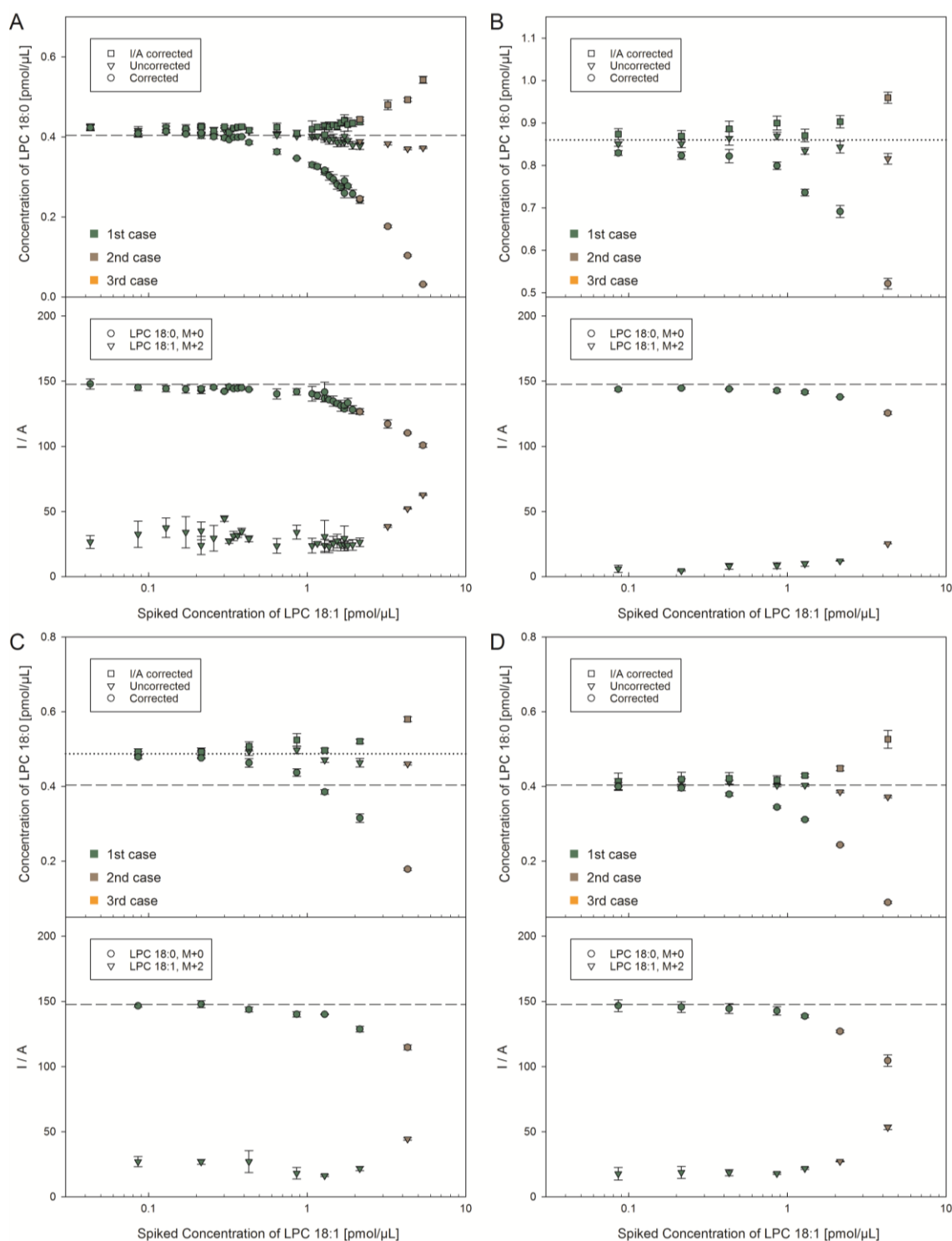


Figure 3.14 Quantification of LPC 18:0 m/z 568.362 at increasing spike amounts of LPC 18:1 m/z 566.3463 recorded (A) without matrix and spiked on (B) murine liver, (C) human plasma, and (D) human skin fibroblast samples using a mass resolution setting of 140,000 at m/z 200. The dashed line in the upper panel indicates the spiked amount of LPC 18:0 and in the lower panel the I/A (calcd) of m/z 568.362. The dotted line (upper panel) represents the target concentration of LPC 18:0 (spiked-in and basal sample amount). Each point represents the average of $n = 3$ technical replicates \pm SD.

3.1 Isotope Correction Algorithm for FIA-FTMS

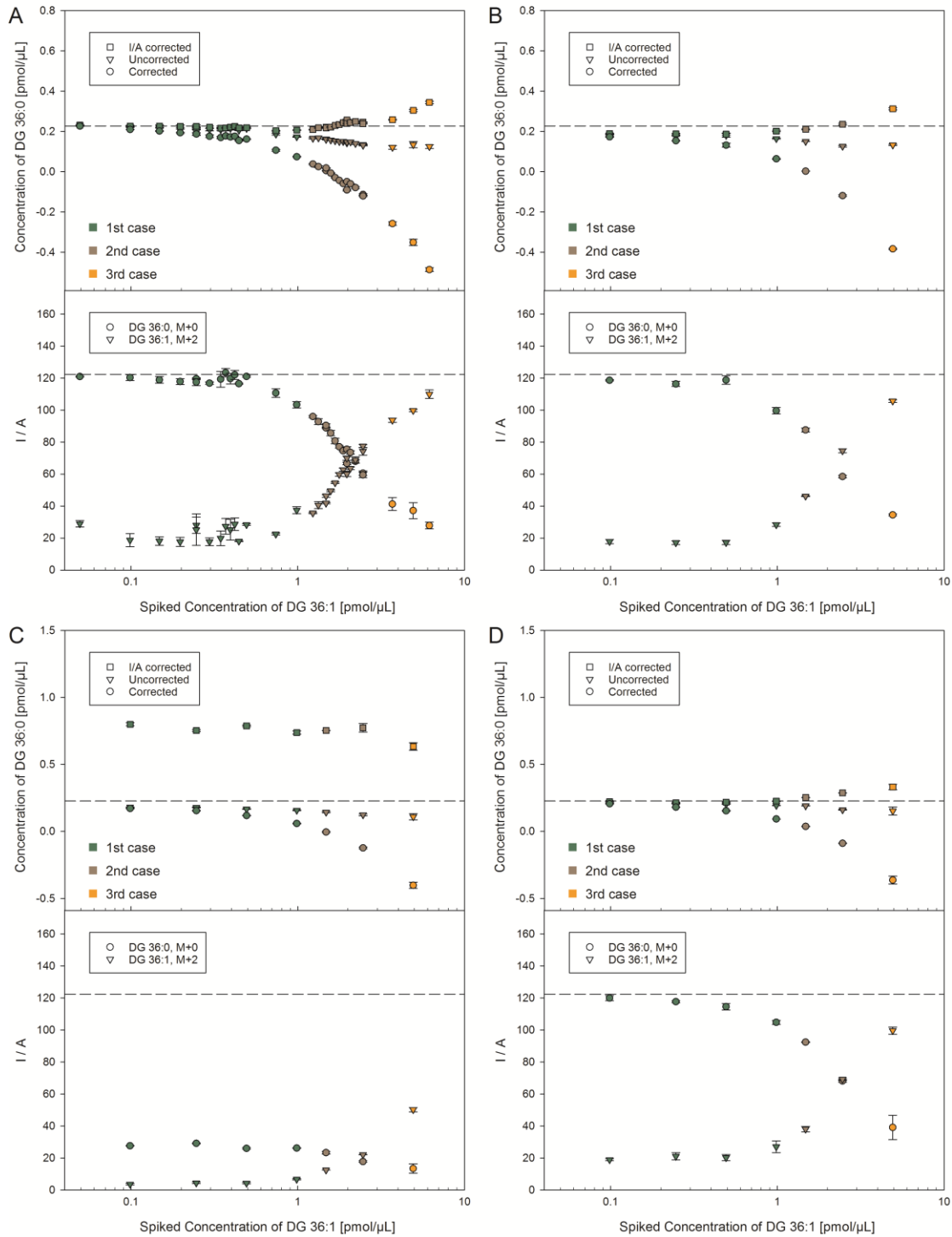


Figure 3.15 Quantification of DG 36:0 m/z 642.6031 at increasing spike amounts of DG 36:1 m/z 640.5875 recorded (A) without matrix and spiked on (B) murine liver, (C) human plasma, and (D) human skin fibroblast samples using a mass resolution setting of 140,000 at m/z 200. The dashed line in the upper panel indicates the spiked amount of DG 36:0 and in the lower panel the I/A (calcd) of m/z 642.6031. The dotted line (upper panel) represents the target concentration of DG 36:0 (spiked-in and basal sample amount). Each point represents the average of $n = 3$ technical replicates \pm SD.

3.1 Isotope Correction Algorithm for FIA-FTMS

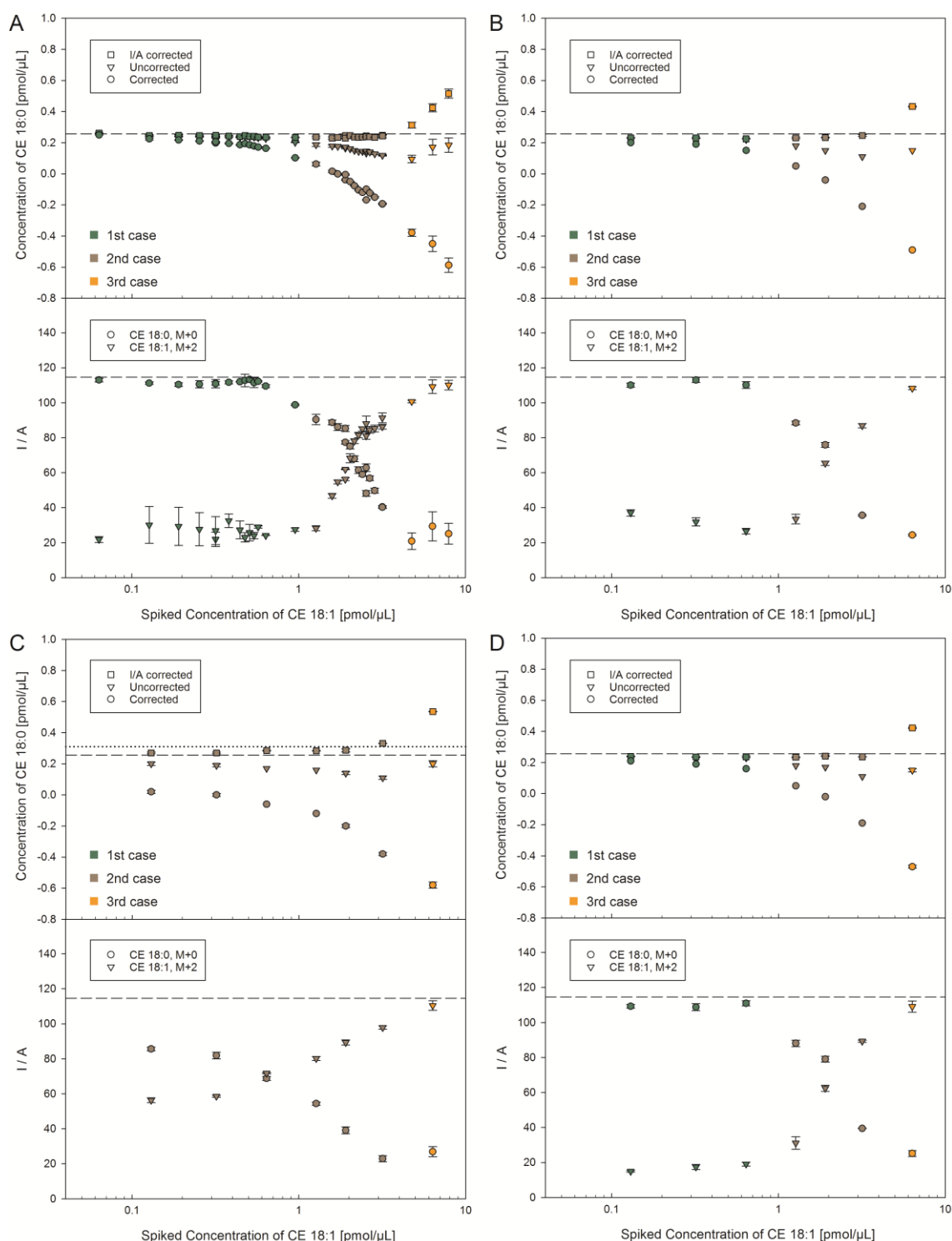


Figure 3.16 Quantification of CE 18:0 m/z 670.6497 at increasing spike amounts of CE 18:1 m/z 668.6340 recorded (A) without matrix and spiked on (B) murine liver, (C) human plasma, and (D) human skin fibroblast samples using a mass resolution setting of 140,000 at m/z 200. The dashed line in the upper panel indicates the spiked amount of CE 18:0 and in the lower panel the I/A (calcd) of m/z 670.6497. The dotted line (upper panel) represents the target concentration of CE 18:0 (spiked-in and basal sample amount). Each point represents the average of $n = 3$ technical replicates \pm SD.

3.1 Isotope Correction Algorithm for FIA-FTMS

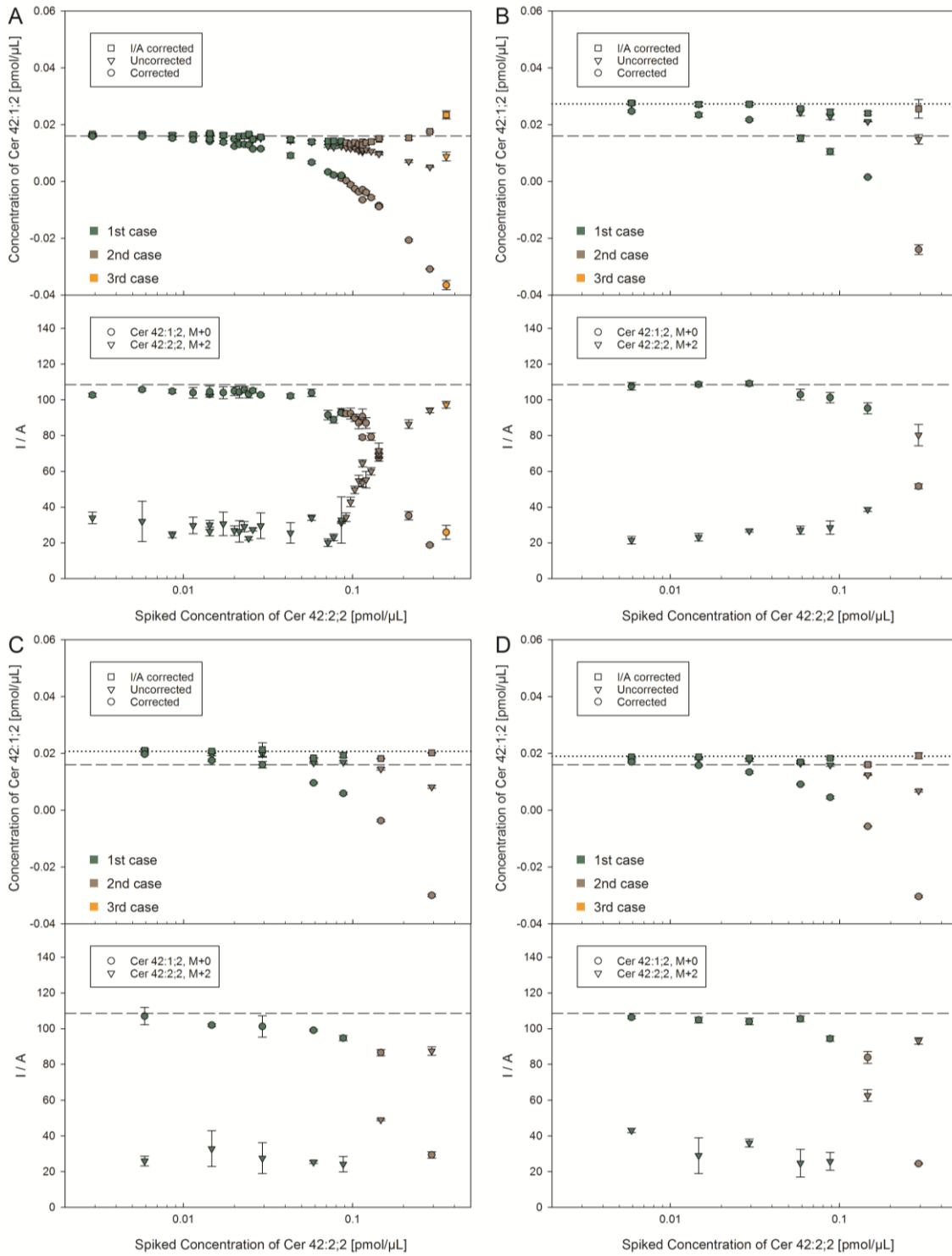


Figure 3.17 Quantification of Cer 42:1;2 m/z 694.6355 at increasing spike amounts of Cer 42:2;2 m/z 692.6199 recorded (A) without matrix and spiked on (B) murine liver, (C) human plasma, and (D) human skin fibroblast samples using a mass resolution setting of 140,000 at m/z 200. The dashed line in the upper panel indicates the spiked amount of Cer 42:1;2 and in the lower panel the I/A (calcd) of m/z 694.6355. The dotted line (upper panel) represents the target concentration of Cer 42:1;2 (spiked-in and basal sample amount). Each point represents the average of $n = 3$ technical replicates \pm SD.

3.1 Isotope Correction Algorithm for FIA-FTMS

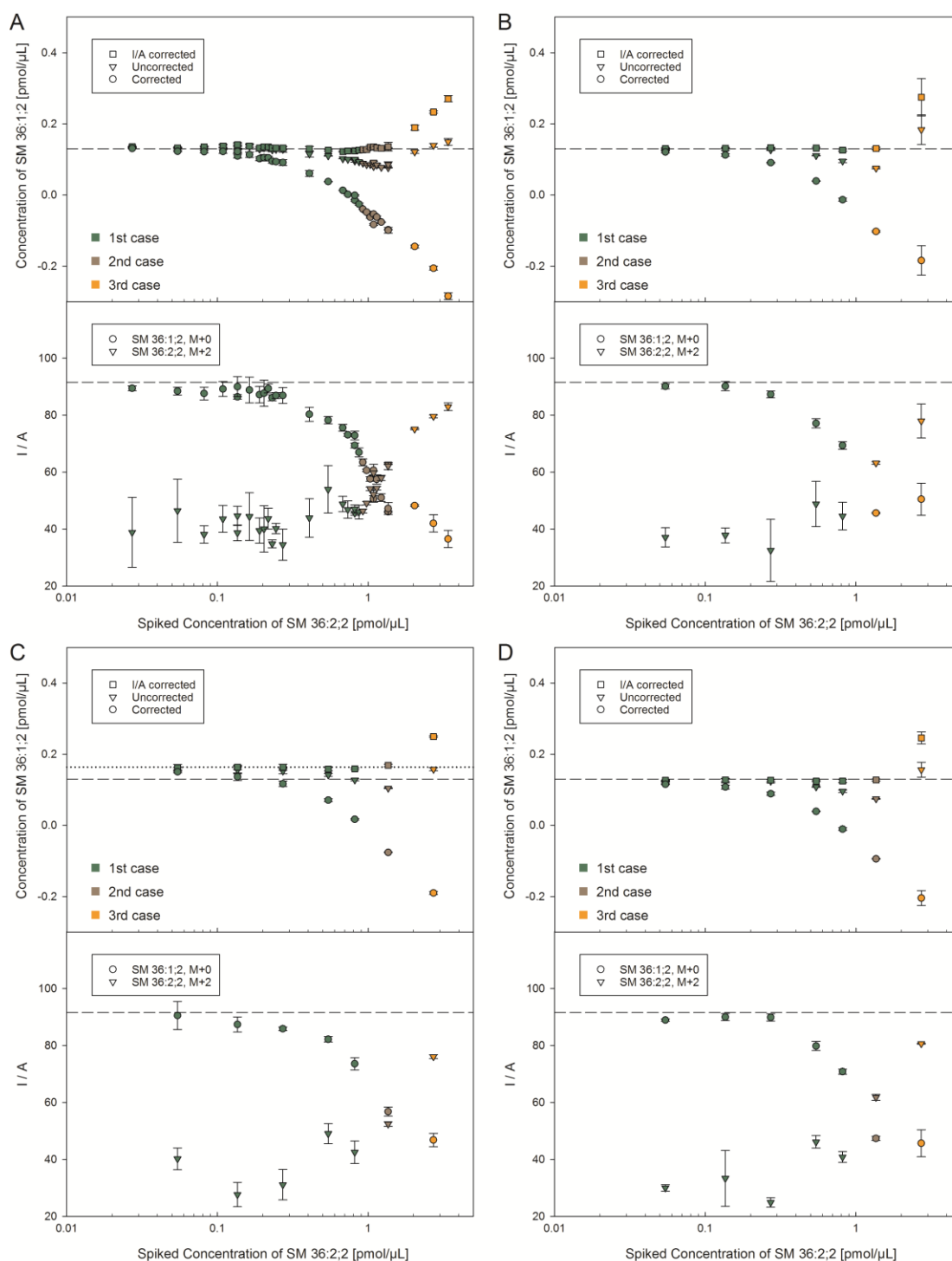


Figure 3.18 Quantification of SM 36:1;2 m/z 775.5971 at increasing spike amounts of SM 36:2;2 m/z 773.5814 recorded (A) without matrix and spiked on (B) murine liver, (C) human plasma, and (D) human skin fibroblast samples using a mass resolution setting of 140,000 at m/z 200. The dashed line in the upper panel indicates the spiked amount of SM 36:1;2 and in the lower panel the I/A (calcd) of m/z 775.5971. The dotted line (upper panel) represents the target concentration of SM 36:1;2 (spiked-in and basal sample amount). Each point represents the average of $n = 3$ technical replicates \pm SD.

3.1 Isotope Correction Algorithm for FIA-FTMS

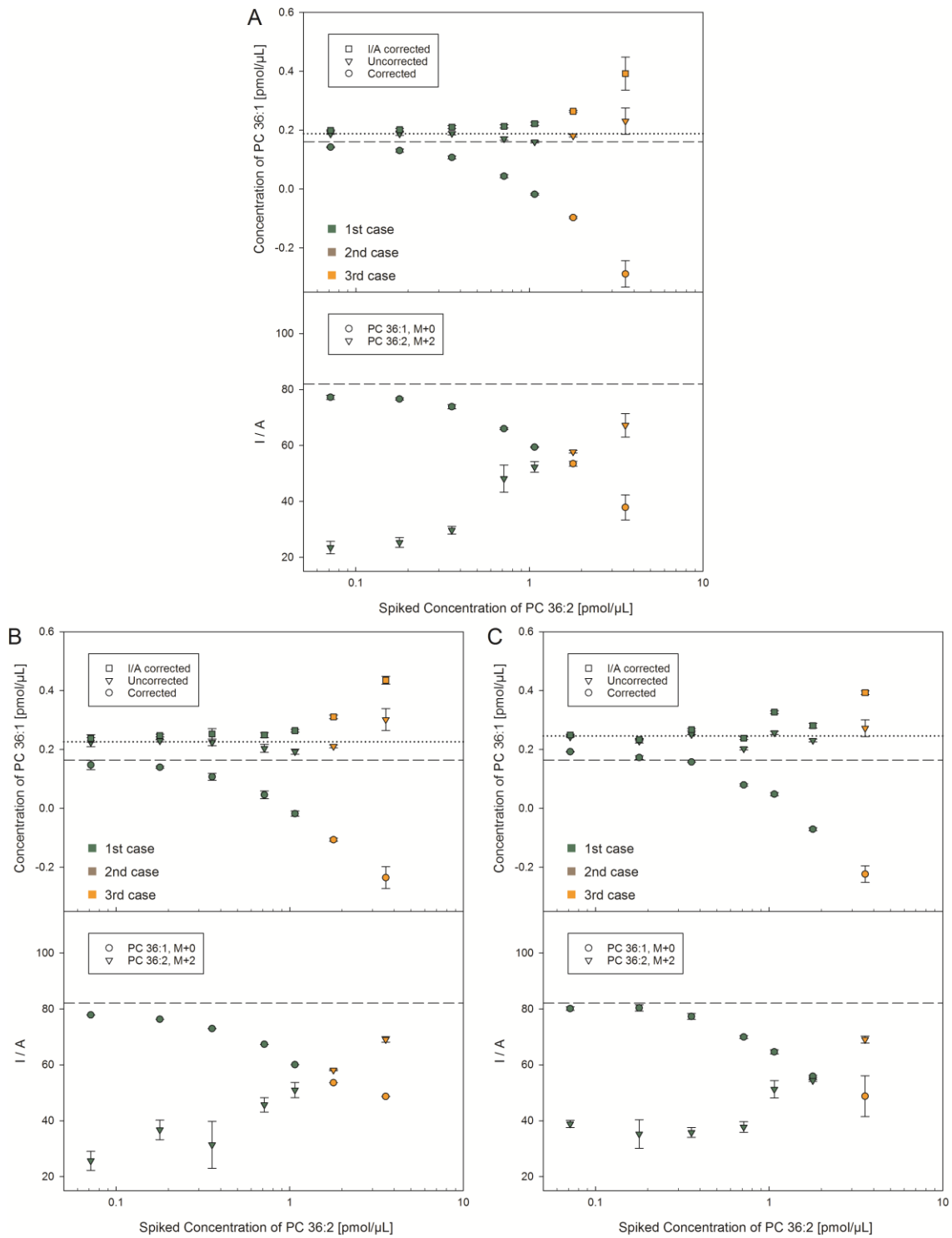


Figure 3.19 Quantification of PC 36:1 m/z 832.6073 at increasing spike amounts of PC 36:2 m/z 830.5917 spiked on (A) murine liver, (B) human plasma, and (C) human skin fibroblast samples using a mass resolution setting of 140,000 at m/z 200. The dashed line in the upper panel indicates the spiked amount of PC 36:1 and in the lower panel the I/A (calcd) of m/z 832.6073. The dotted line (upper panel) represents the target concentration of PC 36:1 (spiked-in and basal sample amount). Each point represents the average of $n = 3$ technical replicates \pm SD.

3.1 Isotope Correction Algorithm for FIA-FTMS

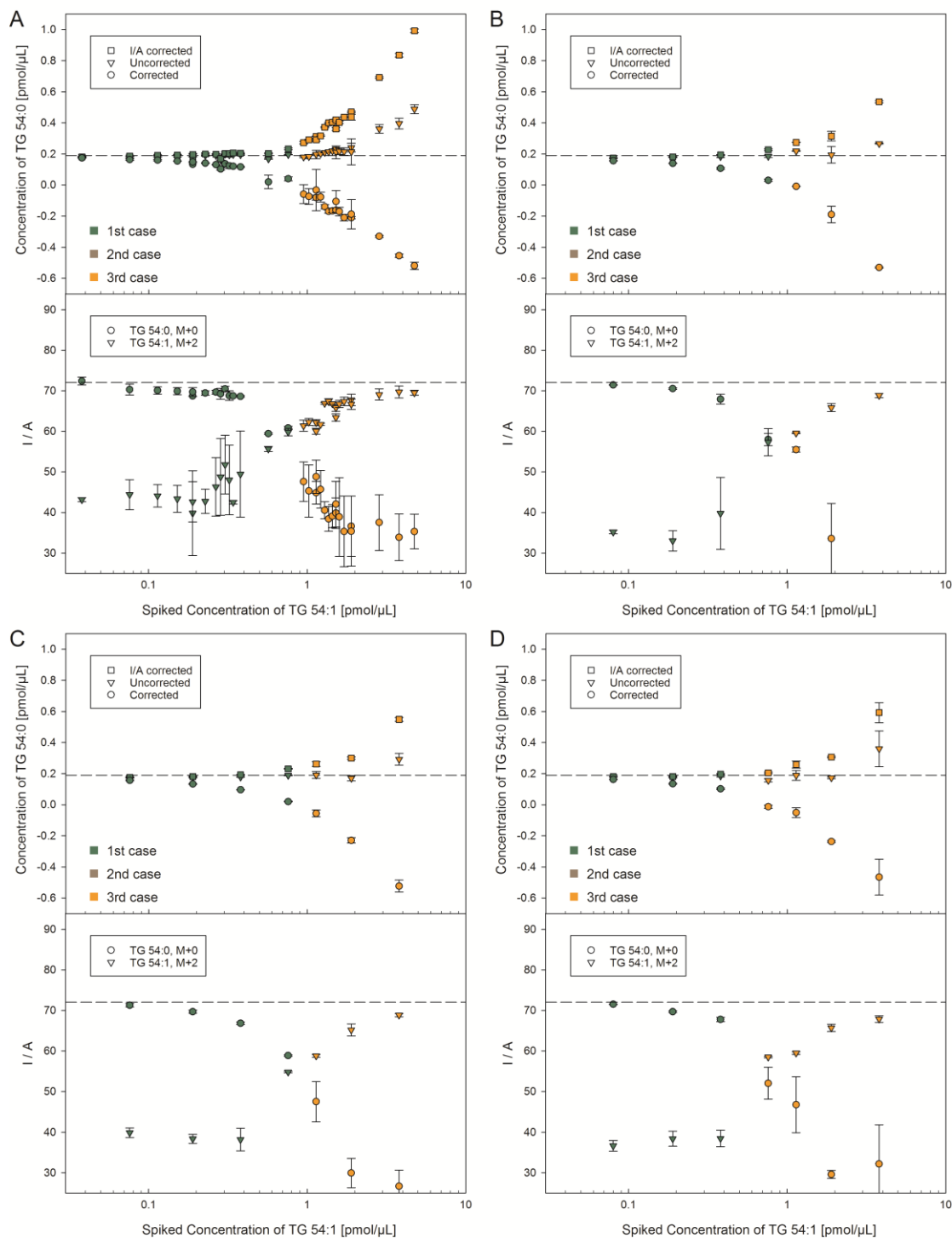


Figure 3.20 Quantification of TG 54:0 m/z 908.8641 at increasing spike amounts of TG 54:1 m/z 906.8484 recorded (A) without matrix and spiked on (B) murine liver, (C) human plasma, and (D) human skin fibroblast samples using a mass resolution setting of 140,000 at m/z 200. The dashed line in the upper panel indicates the spiked amount of TG 54:0 and in the lower panel the I/A (calcd) of m/z 908.8641. The dotted line (upper panel) represents the target concentration of TG 54:0 (spiked-in and basal sample amount). Each point represents the average of $n = 3$ technical replicates \pm SD.

3.1.6 Summary of Isotope Correction Algorithm for FIA-FTMS

The lipidomic analysis of biological samples by FIA-FTMS using our platform typically comprises lipid classes in mass range of m/z 400-1000 (listed in Table 2.2). A series of spike experiments revealed that intensities of near-isobaric species may behave not additive, most likely due to peak coalescence, a phenomenon occurring in iontrap FTMS. This effect is mass resolution depended. Since reduction of mass resolution will result in a potential risk of isobaric overlap of analytes, the performance of isotopic correction algorithms was evaluated at the highest mass resolution setting of 140,000 (at m/z 200). This mass resolution is sufficient to resolve isobaric peaks resulting from DBA up to m/z 600 without peak coalescence affecting their intensities. Therefore, as expected, no further correction of isotopic overlap is necessary below m/z 600. The evaluated lipid species demonstrated that peak coalescence occurs within a mass range of approximately m/z 600-800 resulting in decreased concentrations. These concentrations could be corrected by I/A correction introduced here to get closer to target concentrations. An unexpected finding was that the peaks in range of m/z 800-1000, which include unresolved isobaric peaks from DBA, need no type II isotope correction to match target concentrations (illustrated in Figure 3.21); instead this correction may result in significant overcorrection. Importantly, only intensities picked in first and second case constellations should be considered as accurate but not those from a third case assignment.

3.1 Isotope Correction Algorithm for FIA-FTMS

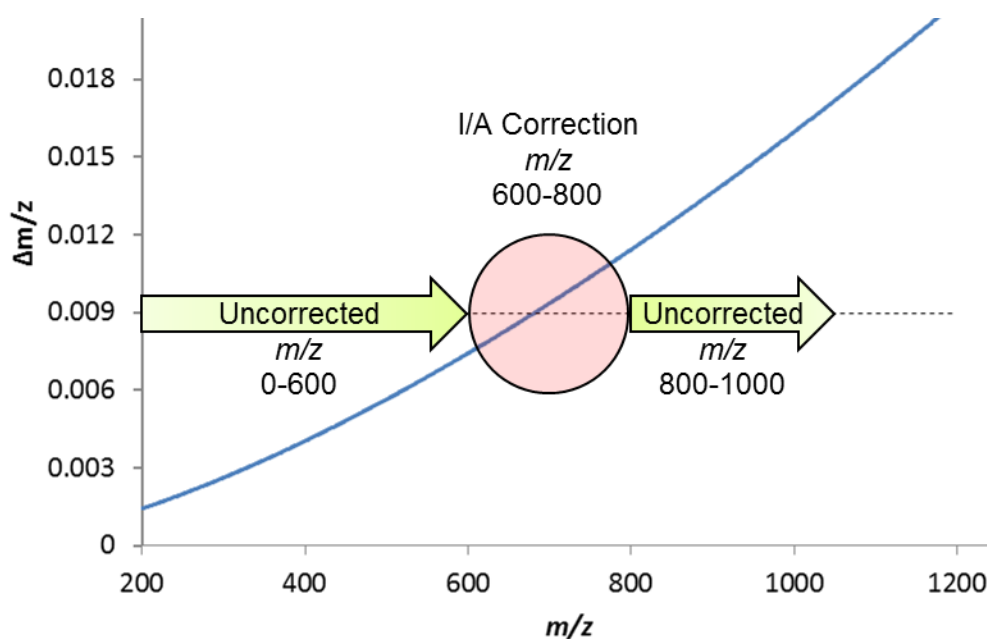


Figure 3.21 Resolvable $\Delta m/z$ considering a $1 \times \text{FWHM}$ separation of two equal abundant species using a mass resolution setting of 140,000 (at m/z 200). The dashed line indicates the DBA difference of $\Delta m/z$ 0.00894. In the mass range type II isotopic correction is not necessary for $m/z < 600$ and 800-1000. I/A correction improves the accuracy in mass range m/z 600-800.

3.2 Quantification of Cholesterol and Cholesteryl Ester

Quantification of FC and CE in biological samples like serum or lipoprotein fractions (Wiesner, Leidl, Boettcher, Schmitz, & Liebisch, 2009) needs to be accurate and reproducible to translate lipidomic tools finally to clinical applications (Burla et al., 2018; Holcapek, Liebisch, & Ekroos, 2018). The following chapters provide detailed insight in the quantification of FC by FIA-MSX/FTMS and CE by FIA-FTMS.

The annotation of FC and CE is based on the fact that cholesterol represents by far the most abundant sterol with 27 carbons and 1 DB (ST 27:1) in the investigated mammalian samples (Liebisch et al., 2013). In rare diseases of the cholesterol biosynthesis pathway like lathosterolosis the cholesterol isomers lathosterol and zymostenol may be present at higher level. In that case their identification needs chromatographic separation (Krakowiak et al., 2003).

3.2.1 Quantification of Free Cholesterol by FIA-MSX/FTMS

Direct quantification of FC was recently described using a chip-based direct infusion nano-ESI-MSX-FTMS/MS-based approach for human and murine plasma samples (Gallego, Hojlund, & Ejning, 2017). Here, we evaluated whether direct quantification of FC is also feasible using FIA-ESI-MSX/FTMS with a quadrupole-Orbitrap instrument in human serum, human fibroblast cells and murine liver samples. As described by Gallego et al. (Gallego et al., 2017) ammoniated FC and CE undergo in-source fragmentation to yield a protonated cholestadiene fragment at m/z 369.3516. Therefore, the extent of in-source fragmentation was assessed in our setting by infusing neat analytical FC and CE 17:0 standards. The percentage of intact analyte was calculated out of the added intensities of the ammoniated species and the protonated cholestadiene fragment. The experiment revealed significant differences in their susceptibility to in-source fragmentation: 27% of FC and 74% of CE 17:0 are unimpaired.

To achieve accurate FC quantification, we took advantage from multiplexing (MSX) of analyte and internal standard pairs in PRM (Gallego et al., 2017; Liebisch & Matysik, 2015; Matysik & Liebisch, 2017; Schott et al., 2018). In an initial experiment, FC concentrations of human serum samples were determined by MSX/FTMS at mass resolution settings of 17,500 at m/z 200, and then

3.2 Quantification of Cholesterol and Cholesteryl Ester

compared to our previously established method using FIA-MS/MS and an acetyl chloride derivatization on a triple quadrupole mass spectrometer (Liebisch et al., 2006). FC concentrations determined by these methods did not sufficiently correlate, with markedly higher values observed by the MSX/FTMS method. Mass resolution of the method was increased, to evaluate whether an isobaric interference is present. Product ion spectra at increased mass resolution revealed an isobaric fragment ion at m/z 369.337 (Figure 3.22), which most likely derives from monoacylglycerol MG 20:0. FTMS analysis confirmed matching ions at m/z 404.3734 $[M+NH_4]^+$ in positive and m/z 431.3378 $[M+HCOO]^-$ in negative ion mode. In order to ensure an unambiguous differentiation of cholestadiene and the isobaric interference (mass difference of 0.015 Da), we chose a mass resolution setting of 140,000 at m/z 200 providing baseline separation of both peaks.

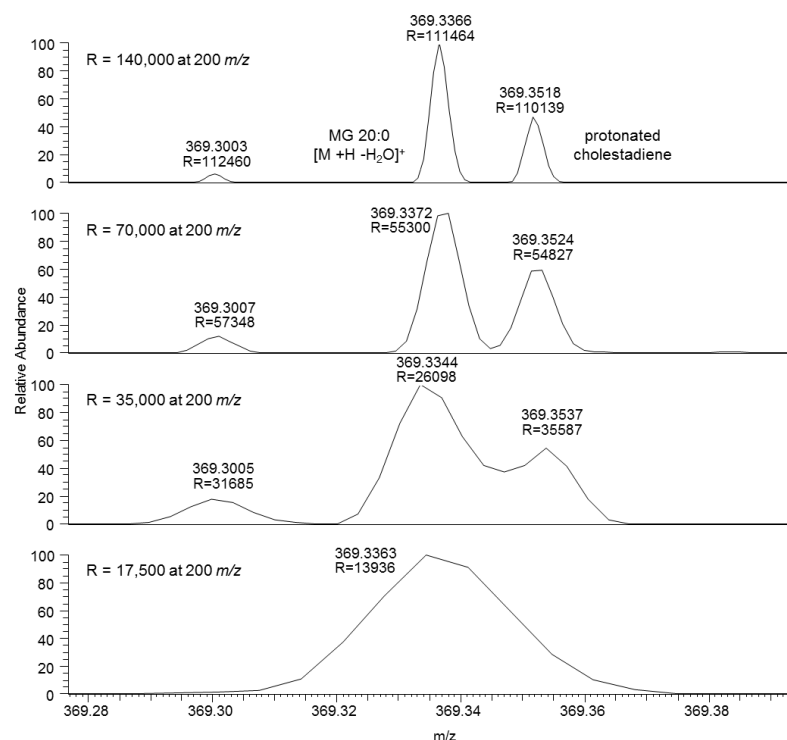


Figure 3.22 MSX/FTMS spectra of FC $[M+NH_4]^+$ in human serum recorded at different resolutions. A series of spectra recorded in positive ion mode at mass resolution settings of 17,500, 35,000, 70,000, and 140,000 (at m/z 200) reveals isobaric ions of protonated cholestadiene and MG 20:0 $[M+H-H_2O]^+$ ($\Delta m/z$ 0.015).

3.2 Quantification of Cholesterol and Cholesteryl Ester

Despite the poor ionization and low signal intensity of FC $[M+NH_4]^+$, we evaluated the accuracy of the high resolution MSX method. Therefore, we compared our acetyl chloride derivatization with direct MSX analysis in human serum, cultured cells, and murine liver samples. Of note, the derivatization increased the signal intensity of FC and D₇-FC by ~400 fold. Nevertheless, all analyzed samples were in good agreement with in average 3-6% higher concentrations for the derivatized samples (Table 3.1) indicating that the direct analysis performs as well as the acetyl chloride derivatization method.

Table 3.1 Comparison of FC analyzed directly or after performance of derivatization with acetyl chloride for human serum, cultured primary human fibroblast cells, and murine liver samples, measured by FIA-MSX/FTMS.

Serum [μM]			Cells [nmol/mg protein]		Liver [nmol/mg wet weight]	
Sample	Derivatization	Direct Analysis	Derivatization	Direct Analysis	Derivatization	Direct Analysis
1	951	834	53	50	4.3	4.1
2	1136	1076	62	61	4.6	4.1
3	1199	1092	56	55	4.5	4.4
4	1456	1284	71	69	4.6	4.2
5	1591	1595	48	50	6.4	6.0
6	1437	1380	43	44	3.4	3.4
7	1038	1065	54	54	3.6	3.6
8	1646	1568			4.3	4.4
9	888	873			2.6	2.8

3.2.2 Analytical Response of Cholesteryl Esters quantified by FIA-ESI-FTMS

Cholesterol is mainly stored or transported as CE, which is one of the most abundant lipid classes in human plasma (Burla et al., 2018; Sales et al., 2016). In laboratory testing, the amount of cholesterol is determined as total cholesterol (TC equals esterified and non-esterified) with enzymatic tests certified for clinical diagnostic. In an initial experiment, we compared TC concentrations of 18 human serum samples determined by MSX/FTMS for FC and FTMS for CE with the enzymatically determined values (mean TC concentration was 5.17 ± 2.56 mM). MS and enzymatically derived TC concentrations showed a good correlation but MS values were about 50% higher (Figure 3.23). Since previous studies indicated that lipid species

response may be influenced by length and unsaturation degree of the acyl chains (Brugger, Erben, Sandhoff, Wieland, & Lehmann, 1997; Cullen et al., 1997; Hutchins, Barkley, & Murphy, 2008; Koivusalo, Haimi, Heikinheimo, Kostinen, & Somerharju, 2001; Liebisch et al., 2006), we investigated the analytical response of CE species in detail.

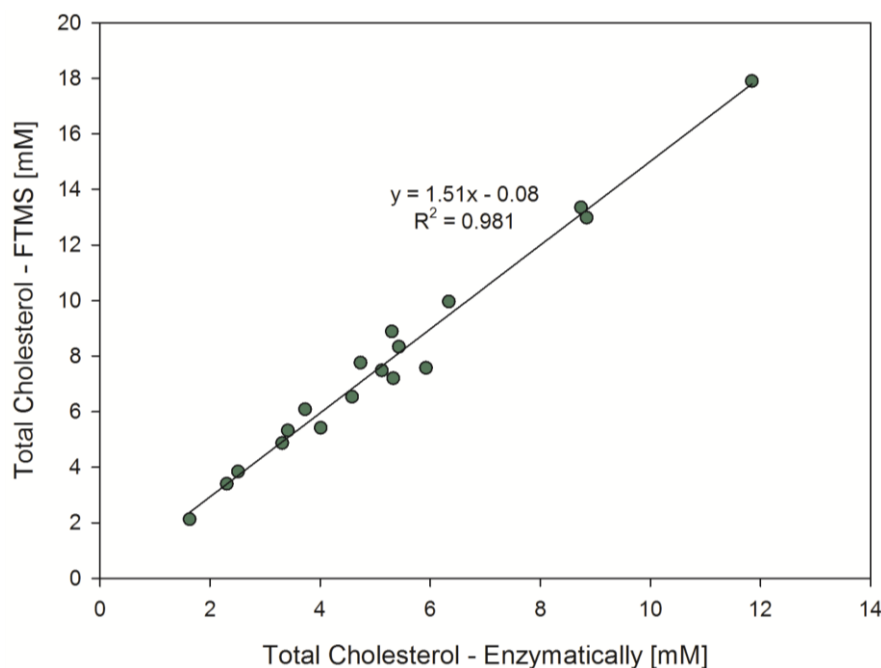


Figure 3.23 Correlation of total cholesterol determined enzymatically and by FIA-FTMS and FIA-MSX/FTMS. A total of n=18 human serum samples were analyzed.

3.2.2.1 Effect of Acyl Chain Composition and Ionization Adduct

To study these effects, a standard mixture containing five saturated and five unsaturated CE species was compiled, analyzed by FTMS, and their response determined as specified in the experimental section (2.7 *Instrument Response of Cholesteryl Esters*). Two things are apparent from analysis of NH_4 -adducts – the instrument response of saturated and monounsaturated species increases linearly with the acyl chain length (Figure 3.24A). Notably, however, the acyl chain unsaturation has a significantly higher influence on the response, which also increases systematically with double-bond count (Figure 3.24A, inset).

3.2 Quantification of Cholesterol and Cholesteryl Ester

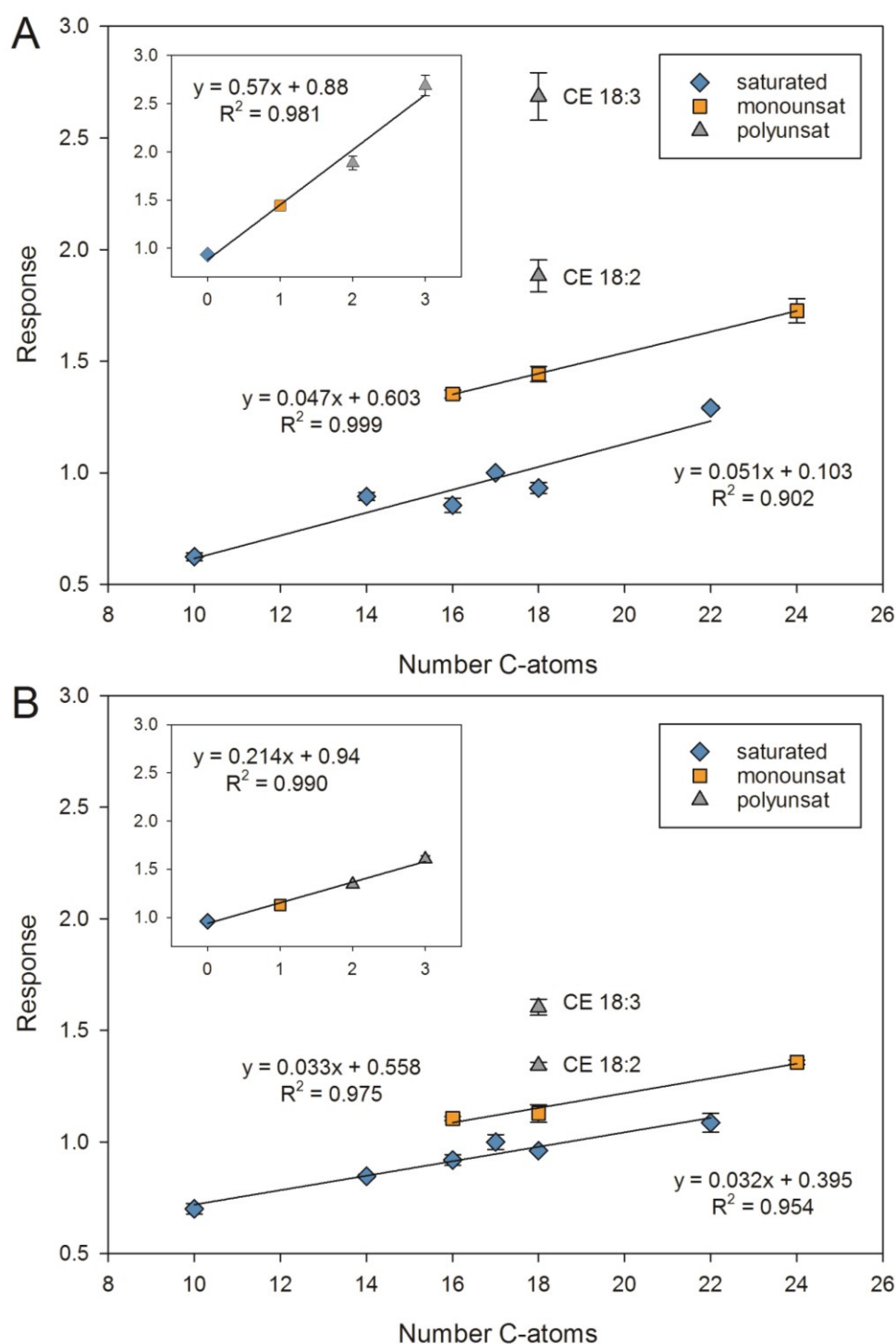


Figure 3.24 Effect of acyl chain length and degree of unsaturation on CE species response. The figure shows the determined response of (A) NH₄⁺-adducts and (B) Na⁺-adducts. The response of saturated (blue), monounsaturated (orange), and polyunsaturated (grey) species is plotted against the acyl chain length. Total CE concentration is 9.41 pmol/μL. The inset displays the response of C18-CE species plotted against the number of double bonds. The response was calculated as the molar ratio of detected to expected quantities. Displayed are mean ± SD of three independent experiments.

3.2 Quantification of Cholesterol and Cholesteryl Ester

On the basis of these data, we expect a linear dependency for increasing acyl chain lengths for each series of polyenoic CE species, with a slope similar to that of the saturated and monounsaturated species. Due to a limited number of polyunsaturated CE species commercially available we could not test their response in detail. The chosen TC concentration of 9.41 pmol/ μ L (in vial) is corresponding to 5.44 mM (comparable to serum concentrations), and resembles the mean TC concentration of the 18 human serum samples determined enzymatically with 5.17 ± 2.56 mM.

Considerable use has been made of the positive charged ammonium adduct for analysis of CE (Liebisch et al., 2006). To gain further information on CE response behavior, corresponding response experiments have been performed with the alkali metal ion adduct $[M+Na]^+$ (Figure 3.24B). The trends observed are similar; however, the impact of acyl chain length and DB number on the species specific response is lower. The response increases for the NH_4 -adduct with a linear slope of 0.57 and for the Na-adduct with 0.214.

Collisional activation of $[M+NH_4]^+$ results in the formation of the characteristic cholestadiene ion of m/z 369. This product ion is the result of an initial hydrogen rearrangement, so that the resulting carbon-centered cationic site, following the loss of H_2O and NH_3 , can be delocalized over the adjacent double bond (Murphy, 2015). As already mentioned, it has been shown that CE species $[M+NH_4]^+$ undergo in-source fragmentation producing the specific fragment ion of m/z 369 during electrospray. Therefore, we asked whether the observed response effect may be caused by in-source fragmentation during electrospray ionization. Individual CE species were analyzed by FTMS, and the percentage of intact ions was calculated out of the added intensities of precursor $[M+NH_4]^+$ and the protonated cholestadiene fragment (Figure 3.25). The figure demonstrates that species stability increases with the acyl chain length as well as with the degree of unsaturation. The similarity to the observed response effects (Figure 3.24) indicates that the in-source fragmentation is a main cause for response differences of CE species. The presence of double bonds in the acyl chain substantially decreases the susceptibility of $[CE+NH_4]^+$ ions to undergo in-source fragmentation, signifying a pronounced charge stabilizing

effect. Analogous explanation can be applied for the stabilization effect induced by chain length, although to a slightly lower extent compared to DB.

Sodiated ions $[M+Na]^+$ displayed different fragmentation characteristics compared to ammoniated (CE 17:0 and CE 22:0 product ion spectra of $[M+NH_4]^+$ and $[M+Na]^+$ are displayed in Figure 3.26). While at 20% HCD ammoniated precursor ions $[M+NH_4]^+$ are completely fragmented to cholestadiene ions of m/z 369, $[M+Na]^+$ ions did only partially fragment as CE 17:0 and CE 22:0 at m/z 661.589 and 731.668 represent the most intense ions, respectively. Moreover, sodiated ions form the acyl chain fragments at m/z 293.245 for fatty acid 17:0 and m/z 363.323 for fatty acid 22:0. This clearly indicates an increased stability of Na-adducts that might be related also to their less pronounced response effects (Figure 3.24).

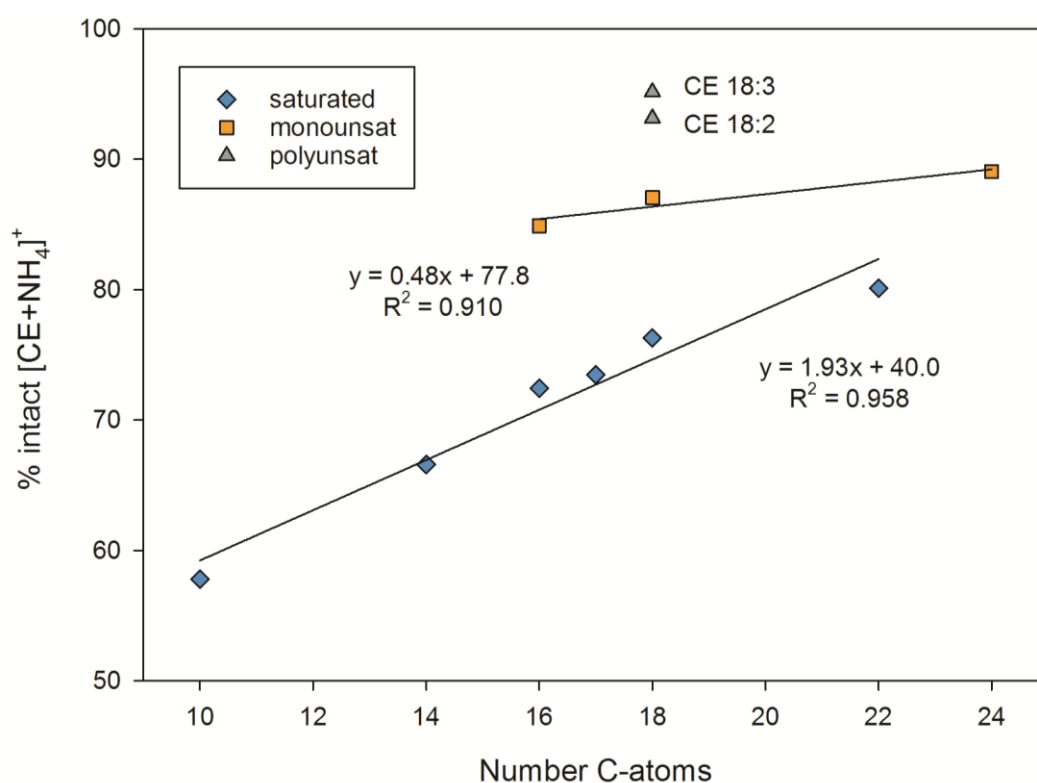


Figure 3.25 In-source fragmentation of CE species. Each CE species was analyzed separately by FIA-FTMS. Displayed is the percentage of intact precursor $[M+NH_4]^+$ against the number of carbons of the acyl chain.

3.2 Quantification of Cholesterol and Cholesteryl Ester

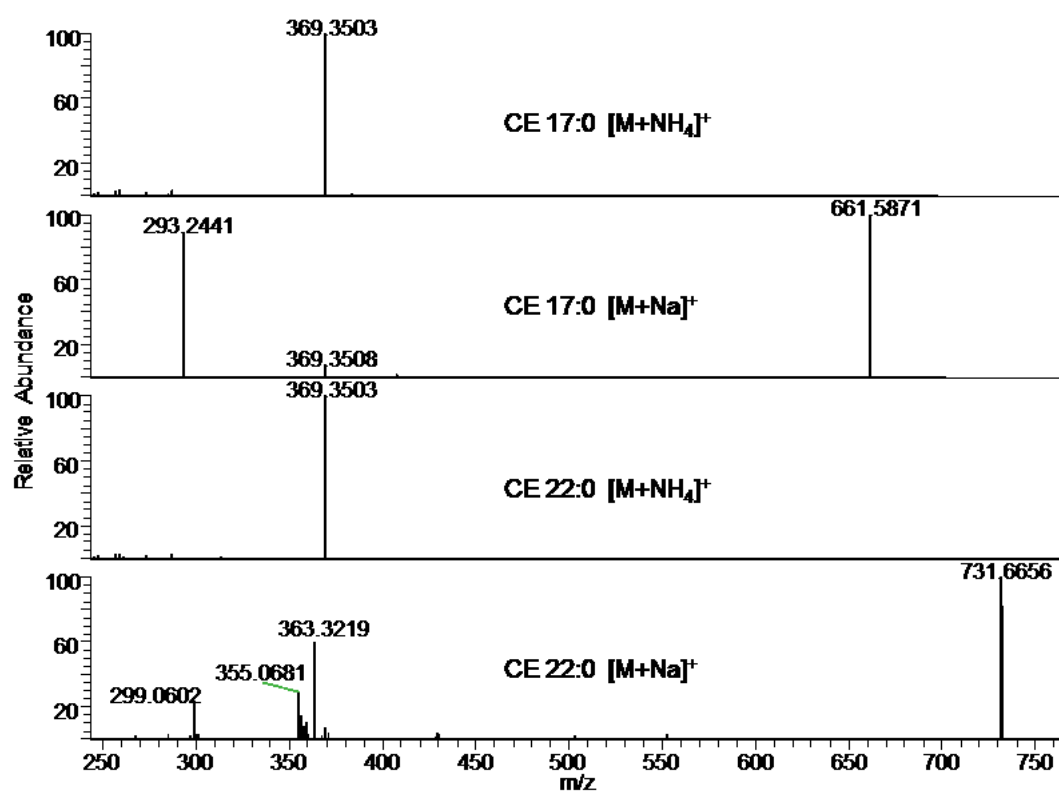


Figure 3.26 Comparison of FTMS/MS spectra of CE 17:0 and CE 22:0 analyzed as $[M+NH_4]^+$ and $[M+Na]^+$. Spectra have been recorded at 20% HCD in positive ion mode.

3.2.2.2 Effect of Total CE Concentration

Previous mass spectrometric studies indicate that lipid concentration of the infusate may influence analytical response (Koivusalo et al., 2001; Yang & Han, 2011). To investigate the influence of CE concentration on the response, the mixture of CE standards was measured at 11 concentrations ranging from ~1.7 to 23.6 pmol/ μ L in the infusate. While the response of saturated and monounsaturated CE species remained constant within the concentration range of interest, a pronounced increase was observed for polyunsaturated species, in particular for CE 18:3 (Figure 3.27). This indicates that at high sample concentrations the polyunsaturated CE species are markedly overrepresented. Of note, the concentrations applied here fit very well to previously described recommendations for lipid concentrations of infusates in shotgun mass spectrometry (Koivusalo et al., 2001; Yang & Han, 2011).

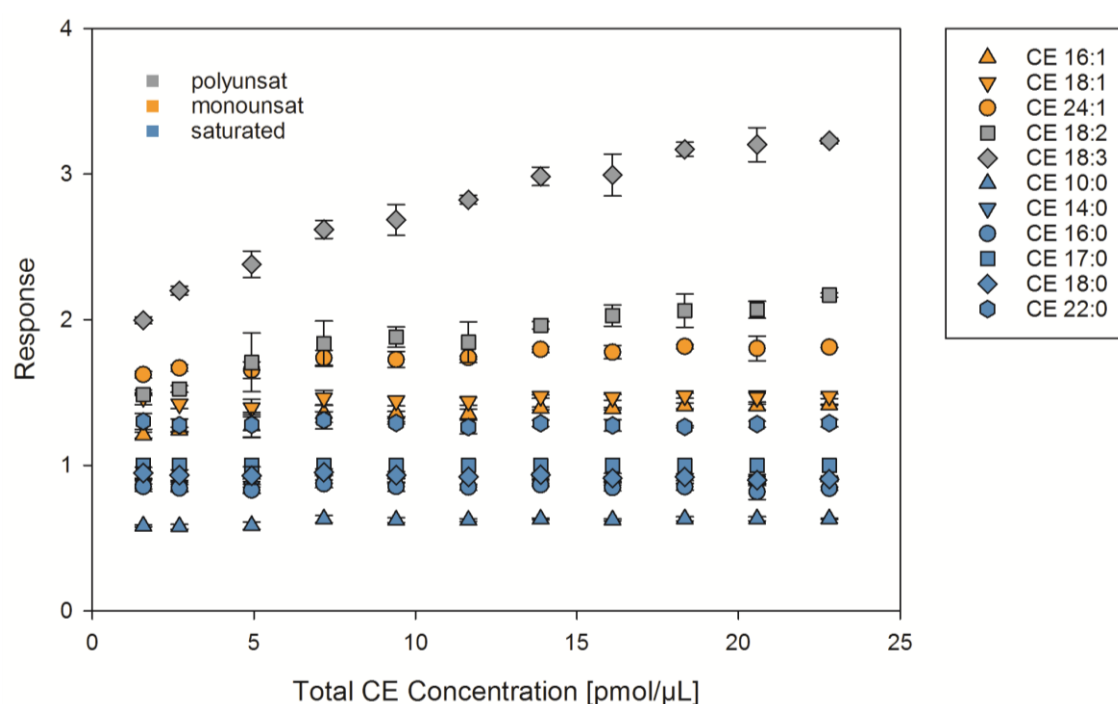


Figure 3.27 Effect of total CE concentration on CE species response. CE species are plotted against the total CE concentration of the injected standard mix. Displayed are mean \pm SD of three independent experiments.

To check if this effect also derives from different in-source species stability, we monitored the amount of in-source fragmentation of C18-CE species in a dilution series within a spike range of approximate 1000-folds of magnitude (Figure 3.28). Nonetheless, concentration had only negligible effects on the

3.2 Quantification of Cholesterol and Cholesteryl Ester

susceptibility to undergo in-source fragmentation. Hence, a potential explanation could be that aggregation of highly hydrophobic CE at higher concentrations results in less efficient ionization. Notably, the introduction of double bonds influences species polarity/polarity-distribution, as well as the acyl chain structure. Here, it has to be considered that the response was calculated using the CE 17:0 as internal standard, which explains that relative response of saturated species is not influenced by concentration effects since they have a similar polarity and structure and aggregate in a similar way, accordingly. Unexpectedly, monounsaturated CE species seem to behave like saturated species in this respect. Polyunsaturated CE species, however, appear to be less susceptible to aggregation resulting in an increased relative response due to enhanced aggregation of the saturated internal standard. To accurately compensate for this effect, spike-in of unsaturated CE internal standards could be advantageous.

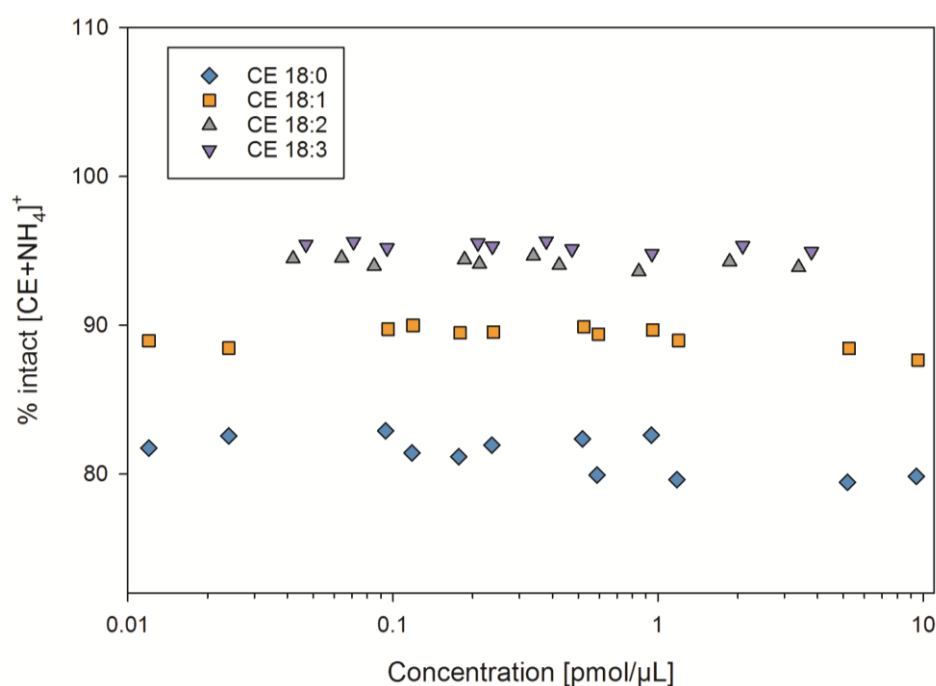


Figure 3.28 Effect of concentration on the in-source fragmentation. Each C18-CE species was analyzed separately by FIA-FTMS. Displayed is the percentage of intact precursor $[M+NH_4]^+$ against the concentration in the infusate.

3.2.2.3 Influence of Sample Matrix

Typically, biological samples comprise a complex mixture of different lipid classes and species. Therefore, we asked how responses of CE lipids are influenced by addition of triacylglycerols (TG) and phosphatidylcholines (PC), representing the other main components of human serum. To a constant concentration of the CE standard mixture, we spiked in either a mix of different TG, PC, or both, in concentrations resembling the physiological range for these lipid classes, and analyzed those samples by FIA-FTMS. The composition and concentration of the defined mixtures is described in chapter 2.7.1 *Preparation of Standard Mixtures and Matrix Spikes*. Inclusion of TG and PC reduced the response of CE species to a similar extent and this effect was more pronounced for polyunsaturated species (Figure 3.29). Simultaneous addition of both, TG and PC, showed an additional response reduction, again more pronounced for polyunsaturated species. The response was reduced to 95% for CE 18:0, to 91% for CE 18:1, and to 89% for CE 18:2 and CE 18:3. The chain length had only a neglectable influence on the response reduction (data not shown).

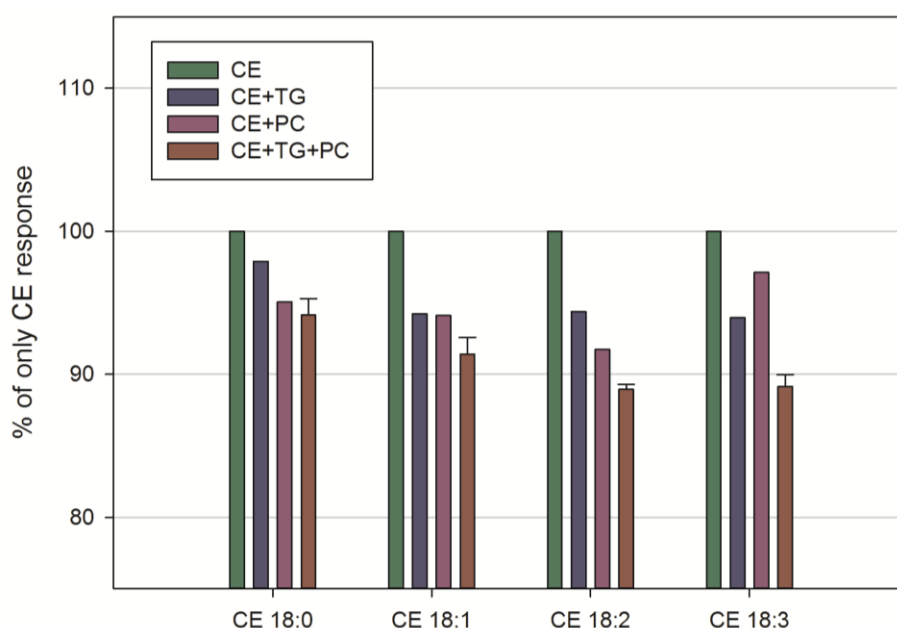


Figure 3.29 Response changes induced by addition of TG and/or PC. The responses of the C18-CE species of the CE mixture with a total cholesterol concentration of 9.41 pmol/μL were analyzed in the presence of a PC mixture (total PC concentration of 5.8 pmol/μL), TG mixture (total TG concentration of 5.4 pmol/μL), and both lipid class mixtures together. Addition of TG and PC shows mean ± SD of two technical replicates.

3.2 Quantification of Cholesterol and Cholesteryl Ester

We checked for the in-source fragmentation of C18-CE species in presence of TG and/or PC but could not detect any changes (Figure 3.30). Potentially, the presence of other lipid classes influences aggregation of CE species.

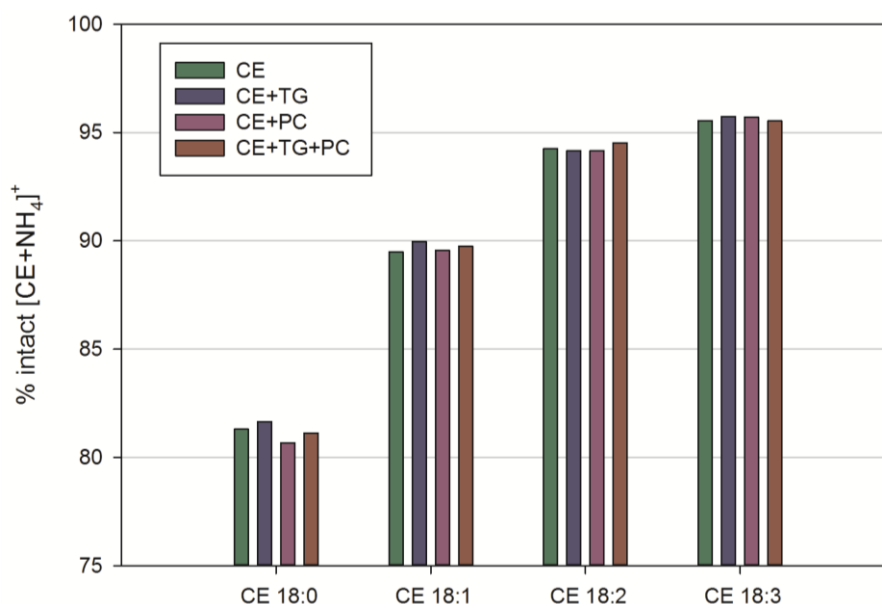


Figure 3.30 Influence of TG and/or PC on the in-source fragmentation. Each C18-CE species was analyzed separately by FIA-FTMS.

3.2.2.4 Quantification of CE Species in a Dilution Series of Human Serum

To further understand the influence of sample concentration on CE species response, we selected three patient serum samples differing in their TC and total TG concentrations: patient #1 with high TC (8.74 mM) and low TG (1.48 mM), patient #2 with high TC (8.84 mM) and high TG (3.66 mM), and patient #3 with low TC (4.58 mM) and low TG (2.09 mM). The reference levels were determined by enzymatic testing. The samples were extracted, diluted sequentially (by a factor of two) up to a 132-fold dilution, and finally analyzed by FIA-FTMS and FIA-MSX/FTMS. The dilution effect was calculated from the non-diluted related to the mean concentration of 16-fold dilution. Total CE concentration decreased to 86% for both high TC samples and to 90% for the low TC sample (Table 3.2), and as expected, dilution effects were most pronounced for polyunsaturated (PUFA) CE species confirming our results obtained with synthetic standard mixtures. In addition, dilution effects for both

high TC samples (patient #1 and #2) were almost identical, even though their TG level is diverging. This argues for a minor influence of TG compared to TC concentration on CE species response (total lipid concentration vs lipid class concentration). Moreover, dilutions of more than 8-fold did not result in a further decrease of total CE and PUFA CE species concentrations. Saturated CE species and free cholesterol were not influenced by sample dilution, and monounsaturated (MUFA) CE species only slightly. However, in dilutions of 16-fold and higher signals of FC were below the LOD. Therefore, the FC concentration measured at 8-fold dilution was used to calculate TC for further dilution steps. Notably, also for most diluted samples total cholesterol concentrations determined by FTMS and MSX/FTMS were about 30% higher than those analyzed enzymatically. Hence, an accurate quantification of CE species by FTMS requires application of species-specific response factors even in diluted samples. Remarkably, when these samples were subjected to analysis of additional lipid classes, we observed that dilution of more than 4-fold reduced signals of some low-abundant lipid species below the limit of detection (LOD) due to a relative increase of ions of the chemical background. For example LPC 20:4 could be quantified up to 32-fold dilution with a CV of <13% and fell under the LOD after further dilution. Other examples were Cer 42:1;2, PE 34:1, PI 38:4 et cetera. Since those lipid species have been shown to be relevant in previous studies (Drobnik et al., 2003; Heimerl et al., 2014; Peng et al., 2018; Sigrüener et al., 2014), we chose to omit further sample dilution and to consider the concentration effect within the detected species-specific response.

3.2 Quantification of Cholesterol and Cholesteryl Ester

Table 3.2 Dilution effect on CE concentrations quantified in three human serum samples by FIA-FTMS. Each value represents n=3 technical replicates.

x-fold dilution			1	2	4	8	16	32	64	132	Dilution Effect
TC	#1	mM	13.7	13.3	12.8	12.4	12.2	12.1	12.3	12.4	89%
	#2	mM	13.9	13.3	12.9	12.8	12.3	12.4	12.3	12.5	89%
	#3	mM	6.9	6.9	6.6	6.5	6.4	6.4	6.5	6.5	92%
Total CE	#1	mM	11.1	10.7	10.1	9.8	9.5	9.5	9.7	9.7	86%
	#2	mM	11.5	10.9	10.6	10.4	9.9	10.0	9.9	10.2	86%
	#3	mM	5.5	5.4	5.1	5.1	4.9	4.9	5.0	5.1	90%
CE 22:6	#1	μM	117	107	97	89	86	82	83	83	74%
		% of total	1.1%	1.0%	1.0%	0.9%	0.9%	0.9%	0.9%	0.8%	
	#2	μM	109	100	95	85	81	79	78	78	74%
		% of total	0.9%	0.9%	0.9%	0.8%	0.8%	0.8%	0.8%	0.8%	
	#3	μM	74	70	63	61	59	59	58	59	80%
		% of total	1.4%	1.3%	1.2%	1.2%	1.2%	1.2%	1.2%	1.2%	
CE 20:5	#1	μM	260	243	218	206	194	193	202	201	74%
		% of total	2.4%	2.3%	2.1%	2.1%	2.0%	2.0%	2.1%	2.1%	
	#2	μM	160	144	135	129	118	119	118	121	74%
		% of total	1.4%	1.3%	1.3%	1.2%	1.2%	1.2%	1.2%	1.2%	
	#3	μM	84	82	74	71	68	67	70	69	81%
		% of total	1.5%	1.5%	1.4%	1.4%	1.4%	1.4%	1.4%	1.3%	
CE 20:4	#1	mM	0.99	0.94	0.89	0.83	0.79	0.80	0.83	0.82	79%
		% of total	9.0%	8.8%	8.7%	8.5%	8.3%	8.5%	8.6%	8.5%	
	#2	mM	1.07	0.99	0.94	0.92	0.84	0.86	0.85	0.88	79%
		% of total	9.3%	9.0%	8.9%	8.8%	8.5%	8.6%	8.6%	8.6%	
	#3	mM	0.91	0.91	0.82	0.82	0.77	0.77	0.80	0.80	85%
		% of total	16.6%	16.8%	16.0%	16.1%	15.6%	15.6%	15.9%	15.7%	
CE 18:3	#1	μM	448	423	393	372	354	348	355	358	79%
		% of total	4.0%	4.0%	3.9%	3.8%	3.7%	3.7%	3.7%	3.7%	
	#2	μM	298	278	266	253	237	234	230	240	79%
		% of total	2.6%	2.5%	2.5%	2.4%	2.4%	2.3%	2.3%	2.4%	
	#3	μM	113	113	103	98	97	96	98	99	85%
		% of total	2.1%	2.1%	2.0%	1.9%	2.0%	1.9%	1.9%	2.0%	
CE 18:2	#1	mM	5.78	5.53	5.20	4.97	4.84	4.77	4.86	4.94	84%
		% of total	52.3%	51.8%	51.3%	50.8%	50.8%	50.5%	50.2%	50.7%	
	#2	mM	5.97	5.61	5.41	5.27	5.01	5.03	4.96	5.15	84%
		% of total	52.0%	51.5%	51.3%	50.6%	50.5%	50.4%	50.2%	50.6%	
	#3	mM	2.58	2.53	2.39	2.32	2.27	2.26	2.32	2.33	88%
		% of total	47.1%	46.5%	46.4%	45.8%	45.9%	45.9%	46.0%	45.8%	
CE 18:1	#1	mM	1.94	1.92	1.86	1.84	1.82	1.81	1.83	1.81	94%
		% of total	17.5%	18.0%	18.3%	18.8%	19.1%	19.1%	18.9%	18.6%	
	#2	mM	2.14	2.08	2.03	2.07	2.00	2.02	1.98	2.00	93%
		% of total	18.6%	19.1%	19.2%	19.8%	20.2%	20.2%	20.1%	19.6%	
	#3	mM	0.91	0.92	0.91	0.91	0.89	0.88	0.88	0.88	98%
		% of total	16.7%	17.0%	17.6%	18.0%	18.1%	17.9%	17.4%	17.3%	
CE 16:0	#1	mM	0.78	0.78	0.77	0.77	0.76	0.78	0.81	0.82	97%
		% of total	7.1%	7.3%	7.6%	7.9%	8.0%	8.2%	8.4%	8.4%	
	#2	mM	0.94	0.91	0.90	0.93	0.90	0.91	0.92	0.95	96%
		% of total	8.2%	8.3%	8.5%	9.0%	9.0%	9.1%	9.3%	9.3%	
	#3	mM	0.46	0.46	0.46	0.46	0.46	0.47	0.48	0.50	101%
		% of total	8.4%	8.5%	8.9%	9.1%	9.4%	9.5%	9.5%	9.9%	

3.2.2.5 Model Compilation for calculating Species-specific Responses

The experimentally gathered information about CE response behavior including acyl chain composition, in-source fragmentation, sample concentration, and addition of TG and PC have been used to compile a model to calculate species-specific response factors for biological samples, especially adapted for serum and plasma samples. First, the number of carbon atoms of the acyl chain increased the response linearly and the slope of that increase seems to be independent of the number of DB. Therefore, we used the mean of the regression line slopes of saturated and MUFA CE species to include the linear carbon dependency in our model (C is the number of carbons):

$$response(calcd) = 0.049 * C$$

Second, we demonstrated a linear relationship of response to the number of DB of the acyl chain (Figure 3.24A, inset). Chain length and DB dependency were compiled additively for response calculation (DB is the number of double bonds):

$$response(calcd) = 0.049 * C + 0.57 * DB$$

The fact that CE species response was influenced by the total CE concentration was included by analyzing the carbon and DB dependency at physiological TC concentrations of human serum samples. Third, species response was affected by the addition of other lipid components. This matrix factor was derived from changes in response upon addition of TG and PC (Figure 3.29). The determined factor was 0.95 for CE 18:0, 0.91 for CE 18:1, and 0.89 for CE 18:2 and CE 18:3. For response calculation, the factor of the species with the corresponding number of DB was applied. For species with a higher degree of unsaturation, the matrix factor of 0.89 was used since it reached saturation after two DB (A is the matrix factor):

$$response(calcd) = [0.049 * C + 0.57 * DB] * A$$

To simplify the application of response correction, the calculated response was converted into a factor, which seems to be more consistent with already published literature (Chen, Green, & Nichols, 2013; Han & Gross, 2001;

Koivusalo et al., 2001). Measured CE concentrations were multiplied by the calculated species-specific response factors:

$$response\ factor = \frac{1}{[0.049 * C + 0.57 * DB] * A}$$

3.2.2.6 Application of Response Correction on Human Serum Samples

The response calculation model was applied to calculate the species-specific response factors of CE determined in human serum samples (Table 3.3). These factors have been used to correct CE concentrations of the 18 human serum samples of our initially performed experiments (Figure 3.31). FTMS and MSX/FTMS derived TC concentrations were in good agreement after correction of the individual CE response arguing that accurate quantification of CE by FTMS needs implementation of CE species-specific response factors.

Table 3.3 Species-specific response factors of CE species determined for human serum/plasma samples.

Species	C-atoms (=C)	Double Bonds (=DB)	Matrix Factor (=A)	Response factor CE only ^a	Response factor ^b
CE 14:0	14	0	0.95	1.46	1.53
CE 15:0	15	0	0.95	1.36	1.43
CE 16:1	16	1	0.91	0.74	0.81
CE 16:0	16	0	0.95	1.27	1.34
CE 17:1	17	1	0.91	0.71	0.78
CE 18:3	18	3	0.89	0.39	0.43
CE 18:2	18	2	0.89	0.49	0.56
CE 18:1	18	1	0.91	0.69	0.75
CE 20:5	20	5	0.89	0.26	0.29
CE 20:4	20	4	0.89	0.31	0.34
CE 22:6	22	6	0.89	0.22	0.25
CE 22:4	22	4	0.89	0.30	0.33

^a Response factor = 1 / (0.049 * C + 0.57 * DB)

^b Response factor = 1 / [(0.049 * C + 0.57 * DB) * A]

3.2 Quantification of Cholesterol and Cholesteryl Ester

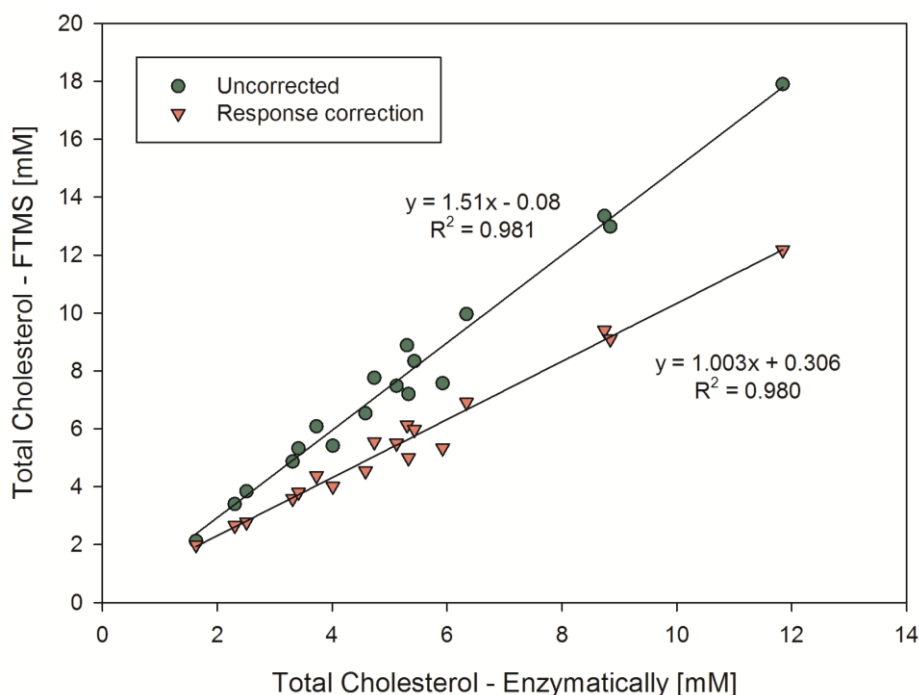


Figure 3.31 Correlation of total cholesterol determined enzymatically and by FIA-FTMS and FIA-MSX/FTMS. Response correction was applied for all detected CE species. A total of n=18 human serum samples were analyzed.

3.2.2.7 Response Comparison with Chip-based Infusion nano ESI-FTMS

The described response effects were observed using FIA with a conventional LC system coupled to a Q Exactive Orbitrap high resolution FTMS instrument. Another question was whether such response differences are limited to conventional ESI. Therefore, we analyzed the CE mixture samples as $[\text{CE}+\text{NH}_4]^+$ by chip-based nano-ESI coupled to an Orbitrap Fusion (Figure 3.32) in collaboration with Prof. Christer Ejlsing's labs. The linear increase of response with DB count matched very well the results obtained by conventional ESI (Figure 3.24A). The trend for the acyl chain length appears similar; however, it does not seem to follow a linear trend at higher carbon numbers. In addition, the response was increasing with the TC concentration and this effect was more pronounced for PUFA species (Figure 3.32B). The response of saturated species was not influenced within the TC concentration range. Possible explanation might be again lipid aggregation that results in less efficient ionization of highly hydrophobic CE species. The quantification was performed with the saturated internal standard CE 17:0 that should aggregate alike the

3.2 Quantification of Cholesterol and Cholesteryl Ester

analyzed saturated CE species. The concentration effect observed by nano-ESI resembles the data recorded with our conventional LC pump system (Figure 3.27), although the effect was slightly higher on our setup.

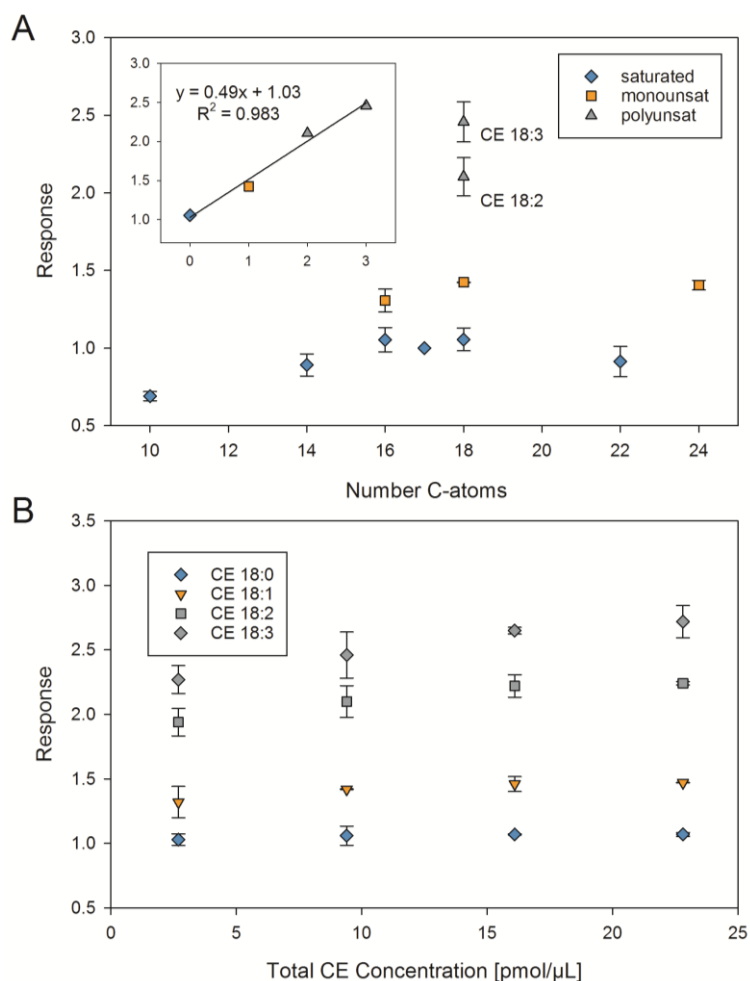


Figure 3.32 CE species response measured on an Orbitrap Fusion using nano-ESI. Panel A shows the effect of acyl chain length and degree of unsaturation (TC concentration was 9.41 pmol/μL). The insert illustrates the response of C18-CE species plotted against the number of double bonds. Panel B displays the effect of total CE concentration on C18-CE species response.

Nonetheless, the comparison of ESI and nano-ESI demonstrated that the marked effect of DB number is not limited to conventional ESI. Remarkably, the response trends observed for both ion sources were similar despite strongly disparate flow rates of 200 nL/min and 10 μL/min for nano-ESI and ESI, respectively. This indicates that the correction of response should be considered for different systems and that the mathematical model for calculation of CE species-specific response factors may be applicable in different

3.2 Quantification of Cholesterol and Cholesteryl Ester

instrument setups. However, such models should be adjusted and validated for the individual setup.

3.3 Method Validation

The biological samples have been measured and analyzed by FIA-FTMS as described in the experimental section (2.6 *Lipid Species Quantification by FIA-FTMS*).

3.3.1 Intraday and Day-to-Day Reproducibility

The reproducibility was determined for CE, FC (MSX/FTMS), DG, TG, Cer, LPC, LPE, PC, PC O-, PE, PE O-, PG, and PI (see Table 3.4 - Table 3.11). Intraday CV's were generally < 5% for all analyzed species. For day-to-day precision, the CV's were slightly higher, but for the majority of species still below 15%. These findings demonstrate that the workflow including extraction, FIA-FTMS analysis, and data evaluation delivers reproducible concentrations. Even the analysis of samples within a four-month time interval (day-to-day reproducibility) confirms the high reproducibility over time.

The mean concentrations determined for intraday and day-to-day precision matched very well for most lipid classes. However, concentrations of DG in the day-to-day experiments (Table 3.5) were slightly higher and those of TG (Table 3.6) slightly lower compared to the intraday concentrations. A possible explanation for this shift could be sample instability related to activity of lipases during freeze and thaw cycles. These enzymes may hydrolyze TG to DG that can be further degraded to MG.

Table 3.4 Coefficient of variation (CV) of intraday and day-to-day precision of CE species and FC determined in human serum, human fibroblast cell homogenates, and murine liver samples by FIA-FTMS and FIA-MSX/FTMS. CE species $[M+NH_4]^+$ have been corrected for their response.

Species	Human serum				Human fibroblast cells				Murine liver			
	Intraday precision		Day-to-day precision		Intraday precision		Day-to-day precision		Intraday precision		Day-to-day precision	
	Mean n=5 [nmol/mL]	CV	Mean n=5 [nmol/mL]	CV	Mean n=5 [nmol/mg protein]	CV	Mean n=5 [nmol/mg protein]	CV	Mean n=5 [nmol/mg wet weight]	CV	Mean n=5 [nmol/mg wet weight]	CV
CE 14:0	46	1%	48	8%								
CE 15:0	14	5%	14	8%								
CE 16:1	121	2%	125	6%	0.18	17%	0.19	15%				
CE 16:0	544	2%	570	8%	0.63	23%	0.64	24%	0.033	5%	0.032	9%
CE 17:1	18	3%	21	11%	0.14	3%	0.15	9%				
CE 18:3	61	2%	60	7%								
CE 18:2	1853	2%	1851	7%								
CE 18:1	681	1%	705	6%	1.4	6%	1.5	8%	0.025	6%	0.026	9%
CE 20:5	29	2%	28	9%								
CE 20:4	195	3%	186	9%								
CE 22:6	13	2%	11	12%								
CE 22:1					0.19	4%	0.21	1%				
FC	1121	3%	1179	11%	59	3%	57	9%	4.2	2%	4.1	11%

Table 3.5 CV of intraday and day-to-day precision of DG species determined as $[M+NH_4]^+$ in human serum, human fibroblast cell homogenates, and murine liver samples by FIA-FTMS.

Species	Human serum				Human fibroblast cells				Murine liver			
	Intraday precision		Day-to-day precision		Intraday precision		Day-to-day precision		Intraday precision		Day-to-day precision	
	Mean n=5 [nmol/mL]	CV	Mean n=5 [nmol/mL]	CV	Mean n=5 [nmol/mg protein]	CV	Mean n=5 [nmol/mg protein]	CV	Mean n=5 [nmol/mg wet weight]	CV	Mean n=5 [nmol/mg wet weight]	CV
DG 32:2					0.11	9%	0.12	12%	0.0085	12%	0.0083	16%
DG 32:1	1.9	16%	2.0	17%	0.46	5%	0.46	4%	0.089	4%	0.093	3%
DG 32:0									0.11	6%	0.11	12%
DG 34:2	4.1	6%	4.5	8%	0.55	3%	0.55	5%	0.13	1%	0.12	5%
DG 34:1	7.7	16%	8.0	11%	1.3	8%	1.2	7%	0.19	2%	0.20	3%
DG 36:4	5.2	27%	5.1	13%								
DG 36:3	7.4	4%	8.5	9%	0.21	9%	0.21	5%	0.035	4%	0.034	15%
DG 36:2	8.9	4%	10.1	10%	0.96	3%	1.0	3%	0.11	3%	0.11	4%
DG 36:1					0.56	11%	0.54	11%	0.038	2%	0.041	8%
DG 36:0					1.8	6%	1.8	3%				
DG 38:4									0.091	3%	0.080	13%
DG 38:3					0.16	5%	0.18	4%	0.013	7%	0.013	15%
DG 38:2					0.18	5%	0.20	7%				

Table 3.6 CV of intraday and day-to-day precision of TG species determined as $[M+NH_4]^+$ in human serum, human fibroblast cell homogenates, and murine liver samples by FIA-FTMS.

Species	Human serum				Human fibroblast cells				Murine liver			
	Intraday precision		Day-to-day precision		Intraday precision		Day-to-day precision		Intraday precision		Day-to-day precision	
	Mean n=5 [nmol/mL]	CV	Mean n=5 [nmol/mL]	CV	Mean n=5 [nmol/mg protein]	CV	Mean n=5 [nmol/mg protein]	CV	Mean n=5 [nmol/mg wet weight]	CV	Mean n=5 [nmol/mg wet weight]	CV
TG 40:3					0.14	6%	0.14	6%	0.015	5%	0.014	8%
TG 40:1	2.9	2%	2.9	4%					0.0067	7%	0.0063	3%
TG 40:0	4.7	3%	4.6	3%								
TG 42:2	2.0	3%	1.9	5%								
TG 42:1	5.8	4%	5.8	6%								
TG 42:0	8.1	1%	7.9	5%								
TG 44:3	1.4	3%	1.2	6%								
TG 44:2	5.3	2%	5.1	6%								
TG 44:1	13	2%	13	3%	0.16	4%	0.15	5%	0.0067	6%	0.0062	8%
TG 44:0	13	1%	12	7%	0.098	9%	0.10	10%	0.0060	5%	0.0059	13%
TG 45:1	2.2	5%	2.1	6%								
TG 46:3	3.4	5%	3.3	6%	0.091	5%	0.090	7%				
TG 46:2	12	3%	11	5%	0.31	3%	0.30	5%	0.019	5%	0.017	12%
TG 46:1	26	2%	25	8%	0.48	2%	0.46	5%	0.044	3%	0.041	5%
TG 46:0	20	2%	20	7%	0.23	5%	0.23	11%	0.037	2%	0.037	4%
TG 47:2	2.0	4%	1.8	4%								
TG 47:1	5.1	2%	4.9	6%								
TG 47:0	4.6	3%	4.4	6%								
TG 48:4	8.5	2%	8.2	8%	0.50	3%	0.49	9%	0.058	5%	0.055	10%
TG 48:3	13	2%	12	7%	0.31	3%	0.29	5%	0.021	3%	0.016	18%
TG 48:2	36	2%	36	5%	1.0	3%	1.0	4%	0.16	3%	0.14	11%
TG 48:1	60	2%	60	4%	1.2	2%	1.2	4%	0.23	3%	0.23	5%
TG 48:0	27	1%	27	7%	0.34	5%	0.34	7%	0.14	4%	0.14	4%

Species	Human serum				Human fibroblast cells				Murine liver			
	Intraday precision		Day-to-day precision		Intraday precision		Day-to-day precision		Intraday precision		Day-to-day precision	
	Mean n=5 [nmol/mL]	CV	Mean n=5 [nmol/mL]	CV	Mean n=5 [nmol/mg protein]	CV	Mean n=5 [nmol/mg protein]	CV	Mean n=5 [nmol/mg wet weight]	CV	Mean n=5 [nmol/mg wet weight]	CV
TG 49:2	6.6	2%	6.4	6%	0.13	5%	0.12	7%	0.012	4%	0.010	15%
TG 49:1	12	1%	11	6%	0.13	6%	0.13	7%	0.012	5%	0.011	6%
TG 49:0	3.6	3%	3.6	8%								
TG 50:5	4.1	2%	3.7	5%	0.10	2%	0.10	8%				
TG 50:4	16	2%	15	8%	0.16	3%	0.15	6%				
TG 50:3	55	2%	52	7%	1.2	2%	1.2	4%	0.25	3%	0.19	19%
TG 50:2	121	2%	117	8%	2.9	2%	2.8	4%	0.80	3%	0.68	10%
TG 50:1	112	2%	113	5%	1.9	2%	1.9	4%	0.57	3%	0.55	5%
TG 51:4	3.6	3%	3.4	4%								
TG 51:3	8.4	3%	8.1	4%	0.11	5%	0.11	5%	0.011	4%	0.0095	20%
TG 51:2	14	2%	14	6%	0.28	2%	0.27	6%	0.022	2%	0.020	10%
TG 51:1	8.6	2%	8.7	3%	0.14	3%	0.14	10%	0.011	4%	0.010	5%
TG 52:6	6.2	2%	5.5	11%								
TG 52:5	28	1%	26	8%	0.11	3%	0.11	6%				
TG 52:4	120	1%	112	7%	1.1	8%	1.2	12%	0.27	4%	0.17	31%
TG 52:3	283	1%	275	5%	3.2	2%	3.1	2%	0.85	3%	0.66	19%
TG 52:2	302	2%	300	6%	4.7	1%	4.6	2%	0.79	3%	0.72	8%
TG 52:1					1.1	2%	1.1	4%	0.15	3%	0.14	3%
TG 53:5	3.6	3%	3.5	6%								
TG 53:4	4.7	3%	4.4	6%								
TG 53:3	8.2	3%	8.0	3%	0.22	3%	0.22	4%				
TG 53:2	8.4	3%	8.2	8%	0.28	2%	0.28	3%	0.014	2%	0.012	13%
TG 53:1	2.5	3%	2.5	6%	0.073	5%	0.067	12%				

Species	Human serum				Human fibroblast cells				Murine liver			
	Intraday precision		Day-to-day precision		Intraday precision		Day-to-day precision		Intraday precision		Day-to-day precision	
	Mean n=5 [nmol/mL]	CV	Mean n=5 [nmol/mL]	CV	Mean n=5 [nmol/mg protein]	CV	Mean n=5 [nmol/mg protein]	CV	Mean n=5 [nmol/mg wet weight]	CV	Mean n=5 [nmol/mg wet weight]	CV
TG 54:7	8.6	1%	7.2	16%								
TG 54:6	28	2%	24	12%	0.14	4%	0.14	4%				
TG 54:5	54	2%	50	9%	0.32	2%	0.32	6%				
TG 54:4	75	2%	71	7%	1.09	2%	1.04	3%	0.11	3%	0.091	19%
TG 54:3	78	1%	75	8%	4.24	2%	4.09	6%	0.30	3%	0.24	12%
TG 54:2	30	2%	29	8%	2.15	2%	2.06	5%	0.14	3%	0.12	6%
TG 54:1	7.1	4%	6.6	9%								
TG 55:3					0.19	3%	0.19	3%				
TG 55:2					0.10	7%	0.10	10%				
TG 56:8	9.3	2%	7.7	20%								
TG 56:7	23	1%	19	17%								
TG 56:6	25	3%	22	10%	0.27	3%	0.27	3%				
TG 56:5	16	1%	15	11%	0.45	2%	0.43	2%				
TG 56:4	4.1	5%	3.5	17%	0.74	1%	0.72	6%				
TG 56:3					1.3	2%	1.3	3%				
TG 56:2	3.4	7%	2.7	20%	0.56	2%	0.56	4%				
TG 56:1					0.15	1%	0.14	6%				
TG 58:8	4.2	1%	3.2	19%								
TG 58:7	4.1	3%	3.1	18%								
TG 58:3					0.50	2%	0.49	5%				
TG 58:2					0.29	3%	0.29	5%				
TG 60:4					0.15	3%	0.15	8%				
TG 60:3					0.35	8%	0.33	12%				

Table 3.7 CV of intraday and day-to-day precision of Cer species determined as $[M+HCOO]^-$ in human serum, human fibroblast cell homogenates, and murine liver samples by FIA-FTMS.

Species	Human serum				Human fibroblast cells				Murine liver			
	Intraday precision		Day-to-day precision		Intraday precision		Day-to-day precision		Intraday precision		Day-to-day precision	
	Mean n=5 [nmol/mL]	CV	Mean n=5 [nmol/mL]	CV	Mean n=5 [nmol/mg protein]	CV	Mean n=5 [nmol/mg protein]	CV	Mean n=5 [nmol/mg wet weight]	CV	Mean n=5 [nmol/mg wet weight]	CV
Cer 34:1;2					0.23	2%	0.23	5%	25	4%	26	3%
Cer 36:1;2									4.3	6%	4.4	6%
Cer 38:1;2									3.1	5%	3.4	7%
Cer 40:2;2									4.3	5%	4.3	6%
Cer 40:1;2	0.92	4%	0.98	7%					7.9	3%	8.7	5%
Cer 41:1;2	0.91	4%	0.98	5%					2.8	9%	2.8	5%
Cer 42:2;2	1.7	6%	1.8	7%	0.32	3%	0.33	5%	33	5%	33	4%
Cer 42:1;2	2.7	5%	2.8	3%	0.20	6%	0.21	6%	26	4%	26	4%
Cer 44:2;2					0.048	7%	0.050	5%				

Table 3.8 CV of intraday and day-to-day precision of LPC species $[M+HCOO]^-$ and LPE species $[M-H]^-$ determined in human serum, human fibroblast cell homogenates (only LPC), and murine liver samples by FIA-FTMS.

Species	Human serum				Human fibroblast cells				Murine liver			
	Intraday precision		Day-to-day precision		Intraday precision		Day-to-day precision		Intraday precision		Day-to-day precision	
	Mean n=5 [nmol/mL]	CV	Mean n=5 [nmol/mL]	CV	Mean n=5 [nmol/mg protein]	CV	Mean n=5 [nmol/mg protein]	CV	Mean n=5 [nmol/mg wet weight]	CV	Mean n=5 [nmol/mg wet weight]	CV
LPC 16:1	3.4	2%	3.7	6%	1.4	3%	1.3	6%	0.16	2%	0.16	4%
LPC 16:0	157	2%	173	6%	0.84	3%	0.85	5%	1.39	3%	1.34	3%
LPC 17:0	3.0	2%	3.3	5%								
LPC 18:2	54	2%	55	4%	0.50	3%	0.52	5%	0.052	3%	0.047	9%
LPC 18:1	34	2%	36	5%	3.6	3%	3.6	7%	0.29	3%	0.28	3%
LPC 18:0	52	1%	57	7%					0.49	4%	0.49	3%
LPC 20:4	10	1%	11	3%								
LPC 20:3	2.9	4%	3.1	7%								
LPE 16:1	0.37	3%	0.38	6%					0.048	4%	0.048	5%
LPE 16:0									0.31	1%	0.29	6%
LPE 18:2									0.032	4%	0.031	8%
LPE 18:1	2.4	2%	2.4	4%					0.39	4%	0.36	9%
LPE 18:0	0.59	5%	0.60	9%					0.43	2%	0.40	7%
LPE 20:4	0.95	3%	0.90	2%								
LPE 22:6	0.55	8%	0.50	7%								

Table 3.9 CV of intraday and day-to-day precision of PC and PC O- species determined as $[M+HCOO]^-$ in human serum, human fibroblast cell homogenates, and murine liver samples by FIA-FTMS.

Species	Human serum				Human fibroblast cells				Murine liver			
	Intraday precision		Day-to-day precision		Intraday precision		Day-to-day precision		Intraday precision		Day-to-day precision	
	Mean n=5 [nmol/mL]	CV	Mean n=5 [nmol/mL]	CV	Mean n=5 [nmol/mg protein]	CV	Mean n=5 [nmol/mg protein]	CV	Mean n=5 [nmol/mg wet weight]	CV	Mean n=5 [nmol/mg wet weight]	CV
PC 30:0	3.0	3%	3.2	2%	4.1	2%	4.0	4%	0.62	2%	0.63	2%
PC 32:2	2.7	4%	2.8	5%	2.2	2%	2.2	6%	0.049	5%	0.045	4%
PC 32:1	13	4%	13	5%	14	2%	14	4%	1.9	2%	1.9	3%
PC 32:0	12	3%	12	6%	4.8	2%	4.9	4%	3.9	3%	3.9	4%
PC 33:1	3.5	3%	3.9	6%	1.0	3%	1.0	2%	0.026	5%	0.027	9%
PC 33:0					0.26	5%	0.26	7%	0.026	3%	0.024	16%
PC 34:4									0.015	4%	0.013	11%
PC 34:3	15	3%	15	4%	0.84	4%	0.81	6%	0.018	3%	0.016	11%
PC 34:2	458	2%	494	5%	11	2%	11	5%	0.59	2%	0.57	5%
PC 34:1	238	2%	241	6%	29	1%	29	5%	1.4	2%	1.5	4%
PC 35:5					4.2	3%	4.1	8%				
PC 35:4					1.8	4%	1.7	7%				
PC 35:2	9.9	2%	10.8	5%	0.80	5%	0.75	11%				
PC 35:1	4.3	5%	4.4	3%	0.82	1%	0.79	4%				
PC 36:5	24	1%	23	7%	0.29	2%	0.26	9%				
PC 36:4	195	2%	202	4%	0.88	1%	0.88	5%	0.074	3%	0.065	11%
PC 36:3	125	3%	125	6%	3.2	2%	3.1	5%	0.047	3%	0.042	7%
PC 36:2	251	1%	261	5%	15	1%	16	4%	0.24	2%	0.23	5%
PC 36:1	31	3%	34	5%	5.0	1%	5.1	5%	0.24	1%	0.23	6%
PC 37:2					0.37	2%	0.35	13%				
PC 38:6	67	3%	69	6%	0.34	2%	0.35	5%	0.013	6%	0.013	14%
PC 38:5	56	1%	54	7%	0.76	1%	0.73	6%				
PC 38:4	101	3%	105	4%	1.0	3%	1.0	7%	0.058	2%	0.050	10%

Species	Human serum				Human fibroblast cells				Murine liver			
	Intraday precision		Day-to-day precision		Intraday precision		Day-to-day precision		Intraday precision		Day-to-day precision	
	Mean n=5 [nmol/mL]	CV	Mean n=5 [nmol/mL]	CV	Mean n=5 [nmol/mg protein]	CV	Mean n=5 [nmol/mg protein]	CV	Mean n=5 [nmol/mg wet weight]	CV	Mean n=5 [nmol/mg wet weight]	CV
PC 38:3	31	1%	32	5%	1.2	2%	1.2	4%	0.024	2%	0.022	4%
PC 38:2					1.6	2%	1.6	4%	0.020	5%	0.018	4%
PC 38:1									0.013	3%	0.012	11%
PC 39:3	3.8	5%	3.8	2%	1.9	2%	2.0	6%	0.072	4%	0.068	17%
PC 40:7	4.3	3%	4.2	13%								
PC 40:6	22	2%	21	7%	0.28	1%	0.29	9%				
PC 40:5	10	4%	10	6%								
PC 40:4	2.8	5%	2.9	11%								
PC O-32:3					0.34	3%	0.34	7%				
PC O-32:2					0.25	6%	0.26	7%				
PC O-32:1					0.74	2%	0.77	5%	0.13	2%	0.13	4%
PC O-32:0					0.55	4%	0.54	7%	0.034	3%	0.034	4%
PC O-34:3	6.1	1%	6.5	5%								
PC O-34:2	5.3	5%	5.4	7%	0.54	2%	0.54	2%	0.022	3%	0.022	5%
PC O-34:1	3.2	2%	3.4	5%	1.3	3%	1.3	3%	0.036	3%	0.035	4%
PC O-36:5	8.6	2%	8.8	6%								
PC O-36:4	11	3%	11	5%								
PC O-36:3	3.3	3%	3.6	7%	0.27	5%	0.26	4%				
PC O-36:2					0.58	1%	0.57	4%				
PC O-36:1					0.47	3%	0.46	10%				
PC O-38:6	4.5	3%	4.6	8%								
PC O-38:5	11	3%	12	5%								
PC O-38:4	5.2	2%	5.3	6%								

Table 3.10 CV of intraday and day-to-day precision of PE and PE O- species determined as [M-H]⁻ in human serum, human fibroblast cell homogenates, and murine liver samples by FIA-FTMS.

Species	Human serum				Human fibroblast cells				Murine liver			
	Intraday precision		Day-to-day precision		Intraday precision		Day-to-day precision		Intraday precision		Day-to-day precision	
	Mean n=5 [nmol/mL]	CV	Mean n=5 [nmol/mL]	CV	Mean n=5 [nmol/mg protein]	CV	Mean n=5 [nmol/mg protein]	CV	Mean n=5 [nmol/mg wet weight]	CV	Mean n=5 [nmol/mg wet weight]	CV
PE 32:1					1.1	1%	1.1	3%	0.028	3%	0.029	4%
PE 34:2	2.8	1%	2.9	4%	3.8	1%	3.7	3%	0.067	4%	0.065	5%
PE 34:1					5.1	1%	5.1	5%	0.11	3%	0.11	4%
PE 36:4	3.8	5%	3.8	7%	0.68	2%	0.67	6%	0.046	4%	0.040	11%
PE 36:3	2.2	4%	2.2	11%	1.9	2%	1.9	4%				
PE 36:2	9.1	2%	9.0	5%	13	1%	13	3%	0.073	4%	0.071	4%
PE 36:1					5.0	1%	4.9	4%	0.069	6%	0.072	3%
PE 38:6	4.5	3%	4.7	6%	0.56	3%	0.57	3%	0.023	4%	0.020	15%
PE 38:5	2.8	5%	3.1	11%	2.1	2%	2.2	3%				
PE 38:4	9.6	2%	9.8	6%	3.6	1%	3.5	6%	0.12	4%	0.11	10%
PE 38:3					1.2	2%	1.2	6%				
PE 38:2					1.3	4%	1.3	3%				
PE 40:6	2.6	4%	3.0	6%	0.95	2%	0.99	3%	0.015	7%	0.014	19%
PE O-32:2									0.013	4%	0.012	7%
PE O-32:1									0.018	5%	0.020	12%
PE O-34:3					0.37	5%	0.37	5%	0.023	6%	0.022	7%
PE O-34:2					1.6	3%	1.6	6%	0.13	2%	0.13	4%
PE O-36:4					0.50	2%	0.51	7%				
PE O-36:3	2.5	2%	2.8	3%	0.81	2%	0.81	6%	0.036	5%	0.034	7%
PE O-36:2					1.1	2%	1.1	7%	0.054	3%	0.053	4%
PE O-38:6	7.2	2%	6.9	10%								
PE O-38:5	8.5	2%	8.5	6%	1.6	3%	1.6	4%	0.092	6%	0.081	12%
PE O-38:4					0.67	1%	0.68	7%				

Table 3.11 CV of intraday and day-to-day precision of PG and PI species determined as [M-H]⁺ in human serum, human fibroblast cell homogenates (only PI), and murine liver samples by FIA-FTMS.

Species	Human serum				Human fibroblast cells				Murine liver			
	Intraday precision		Day-to-day precision		Intraday precision		Day-to-day precision		Intraday precision		Day-to-day precision	
	Mean n=5 [nmol/mL]	CV	Mean n=5 [nmol/mL]	CV	Mean n=5 [nmol/mg protein]	CV	Mean n=5 [nmol/mg protein]	CV	Mean n=5 [nmol/mg wet weight]	CV	Mean n=5 [nmol/mg wet weight]	CV
PG 30:0									0.010	2%	0.010	6%
PG 32:1									0.056	2%	0.059	6%
PG 32:0									0.13	2%	0.14	4%
PG 34:2	0.18	5%	0.18	6%					0.089	2%	0.096	7%
PG 34:1	0.74	3%	0.74	2%					0.27	1%	0.30	9%
PG 36:2	0.84	2%	0.83	1%					0.017	3%	0.019	16%
PG 36:1	0.38	5%	0.41	4%					0.016	6%	0.018	13%
PG 38:7	1.3	6%	1.4	11%					0.078	9%	0.090	23%
PG 40:7	0.48	3%	0.51	6%								
PI 34:2					0.88	3%	0.84	4%				
PI 34:1	4.1	6%	4.0	9%	2.3	2%	2.2	6%	0.050	8%	0.051	26%
PI 36:4					0.28	4%	0.29	6%	0.029	5%	0.029	11%
PI 36:3					0.67	3%	0.69	2%				
PI 36:2	6.9	4%	7.0	5%	2.7	3%	2.9	2%	0.028	7%	0.030	12%
PI 36:1	3.1	4%	3.1	11%	3.5	4%	3.6	2%				
PI 38:4	32	4%	32	7%	4.7	4%	5.0	3%	0.34	5%	0.37	13%
PI 40:6					0.46	5%	0.47	4%				
PI 40:4					0.40	3%	0.41	4%				

3.3.2 Limits of Quantification

The LOQs were determined functionally as described in the experimental section (2.6.4 *Method Validation*) for the main lipid classes of human plasma. However, since it is known that sample matrix can have a substantial influence on the LOQ, it was also assessed for FC and CE in cultured human skin fibroblast cell matrix. The LOQ was defined as concentration where either CV reached 20% or accuracy left the range of 80-120%. The concentrations of LOQ at accuracy and CV are summarized in Table 3.12. The corresponding data are displayed in Figure 3.33 (FC and CE in fibroblast cells), Figure 3.34 (FC and CE in serum), and Figure 3.35 (DG, TG, and PC in serum). The LOQs of CE, DG, PC, and TG are low enough for accurate and reliable quantification of main lipid species in human plasma, serum, and fibroblast cell matrix. However, the LOQs of FC in plasma (with approximate 200 μ M) and cell matrix (14 nmol/mg protein) are rather high. This is related to the poor ionization efficiency and high rate of in-source fragmentation. Nevertheless, we would like to emphasize that FC is a main component in most mammalian samples with concentrations markedly higher than the LOQ. Thus, despite the high LOQ, MSX can provide accurate quantification of FC in typical samples as shown in Table 3.4.

Table 3.12 LOQ of CE, DG, FC, PC, and TG at accuracy (Acc.) and CV for human plasma and/or cultured human fibroblast cell matrix determined by FIA-FTMS and FIA-MSX/FTMS.

Matrix	Unit	CE		DG		FC		PC		TG	
		Acc.	CV	Acc.	CV	Acc.	CV	Acc.	CV	Acc.	CV
Plasma	[nmol/mL]	1.9	1.4	2.9	1.5	198	65	2.3	0.57	0.48	0.48
Cells	[nmol/mg protein]	0.05	0.01	-	-	4.5	14	-	-	-	-

3.3 Method Validation

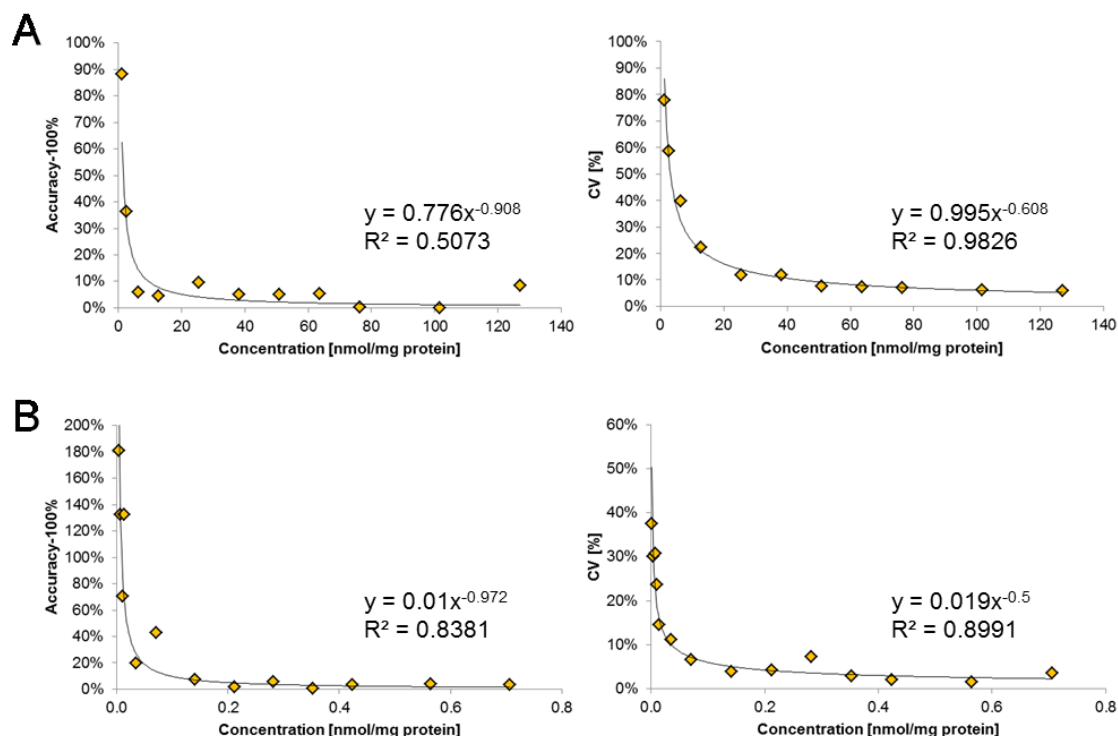


Figure 3.33 Limit of quantification of (A) FC, and (B) CE determined in human fibroblast cells. The left panel shows the absolute values of accuracy-100, and the right panel the measured CV's against the target concentration. Homogenates of cultured human fibroblasts were spiked with (A) D7-FC and (B) CE 22:0 as non-endogenous species at displayed concentration levels. Results were fit by a power function. Each data point was calculated from n=5 technical replicates.

3.3 Method Validation

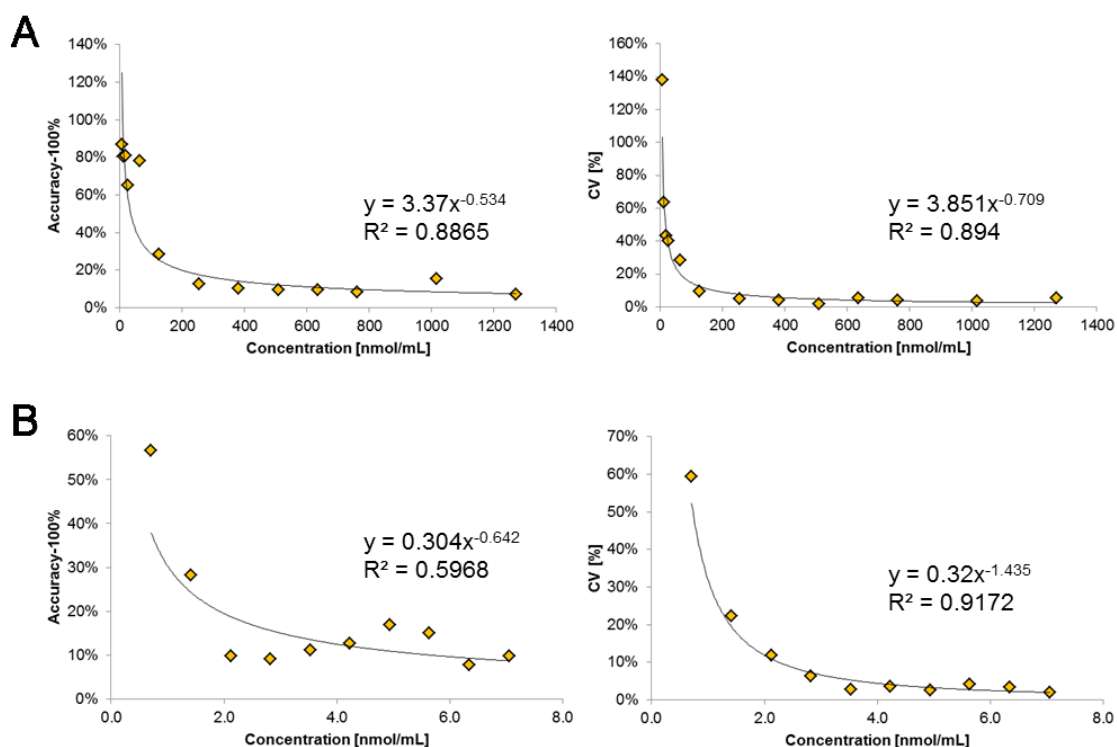


Figure 3.34 Limit of quantification of (A) FC, and (B) CE determined in human serum. The left panel shows the absolute values of accuracy-100, and the right panel the measured CV's against the target concentration. Human serum was spiked with (A) D7-FC and (B) CE 22:0 as non-endogenous species at displayed concentration levels. Results were fit by a power function. Each data point was calculated from n=5 technical replicates.

3.3 Method Validation

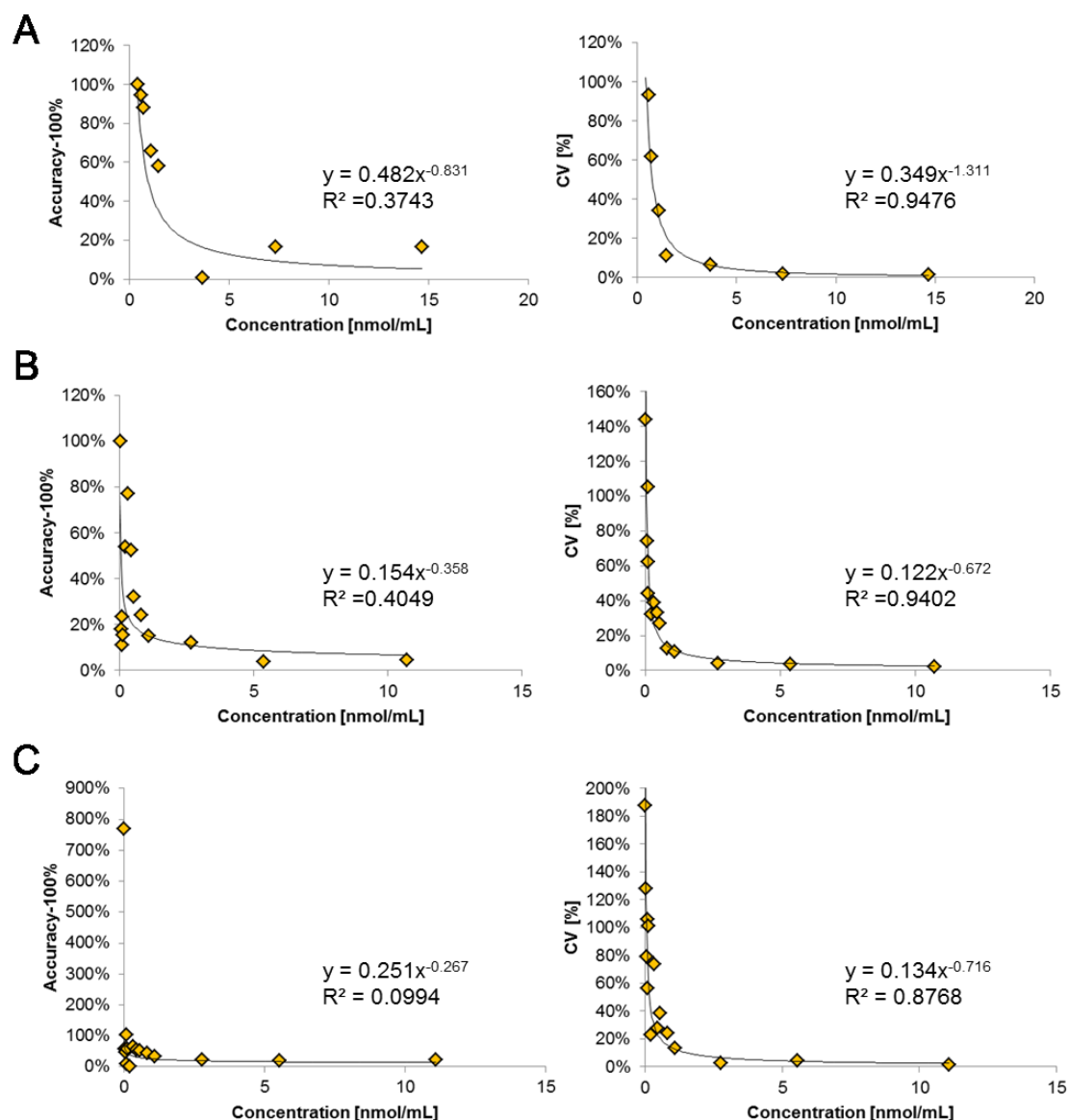


Figure 3.35 Limit of quantification of (A) DG, (B) TG, and (C) PC determined in human serum. The left panel shows the absolute values of accuracy-100, and the right panel the measured CV's against the target concentration. Human serum was spiked with (A) DG 40:0, (B) TG 57:0, and (C) PC 44:0 as non-endogenous species at displayed concentration levels. Results were fit by a power function. Each data point was calculated from n=5 technical replicates.

3.3.3 Dynamic Range of Quantification

The accurate quantification of lipid species is a major goal of high resolution shotgun lipidomics approaches. To evaluate the dynamic range of quantification of FIA-FTMS, synthetic standards without matrix and spiked on murine liver, human plasma, and human skin fibroblast cell samples were analyzed on the Q Exactive (Figure 3.36 and Figure 3.37). Over the spiked range a linear increase was observed with similar slopes for pure standards and matrix containing samples excluding significant effects of the matrix on both linearity and species response. Only for LPE 18:1 added to murine liver slope was almost 15% lower slope than the expected slope of 1. A potential explanation could be the high endogenous amount of this LPE species in the used liver sample or a matrix dependent decreased response.

Notably, the investigated concentration range of each synthetic standard comprises very well the typical concentration range observed in biological samples. Based on these result we conclude that the FIA-FTMS method on the Q Exactive is applicable for quantitative lipidomic analysis of biological samples.

3.3 Method Validation

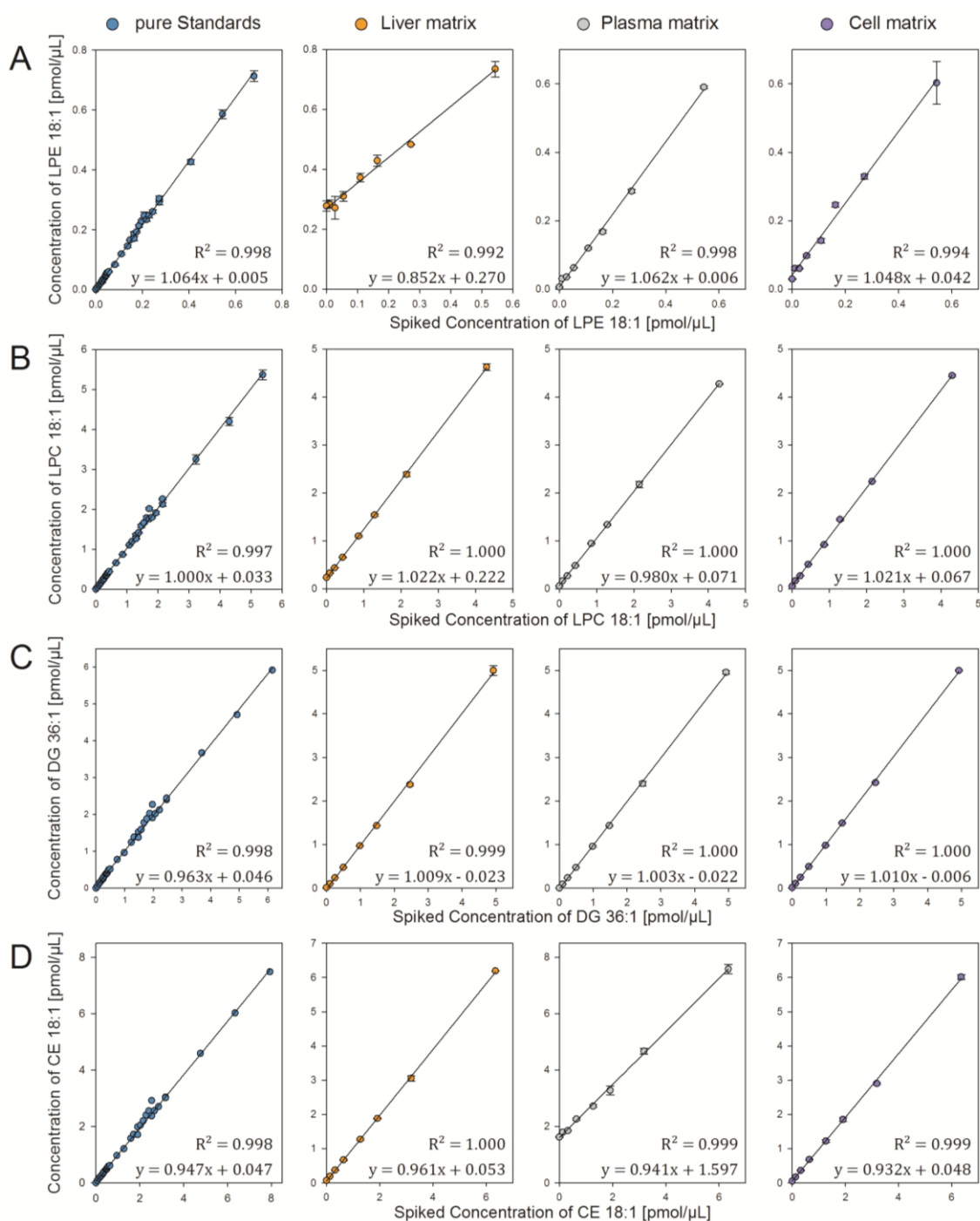


Figure 3.36 Dynamic range of quantification of FTMS analysis of (A) LPE 18:1, (B) LPC 18:1, (C) DG 36:1, and (D) CE 18:1 using a target resolution of 140,000 at m/z 200. Each synthetic standard was analyzed (from left to right) without matrix, and spiked on murine liver, human plasma and human fibroblast cells. The spectra display the correlation of measured and titrated concentration. Each data point represents the average of three replicate analyses per sample.

3.3 Method Validation

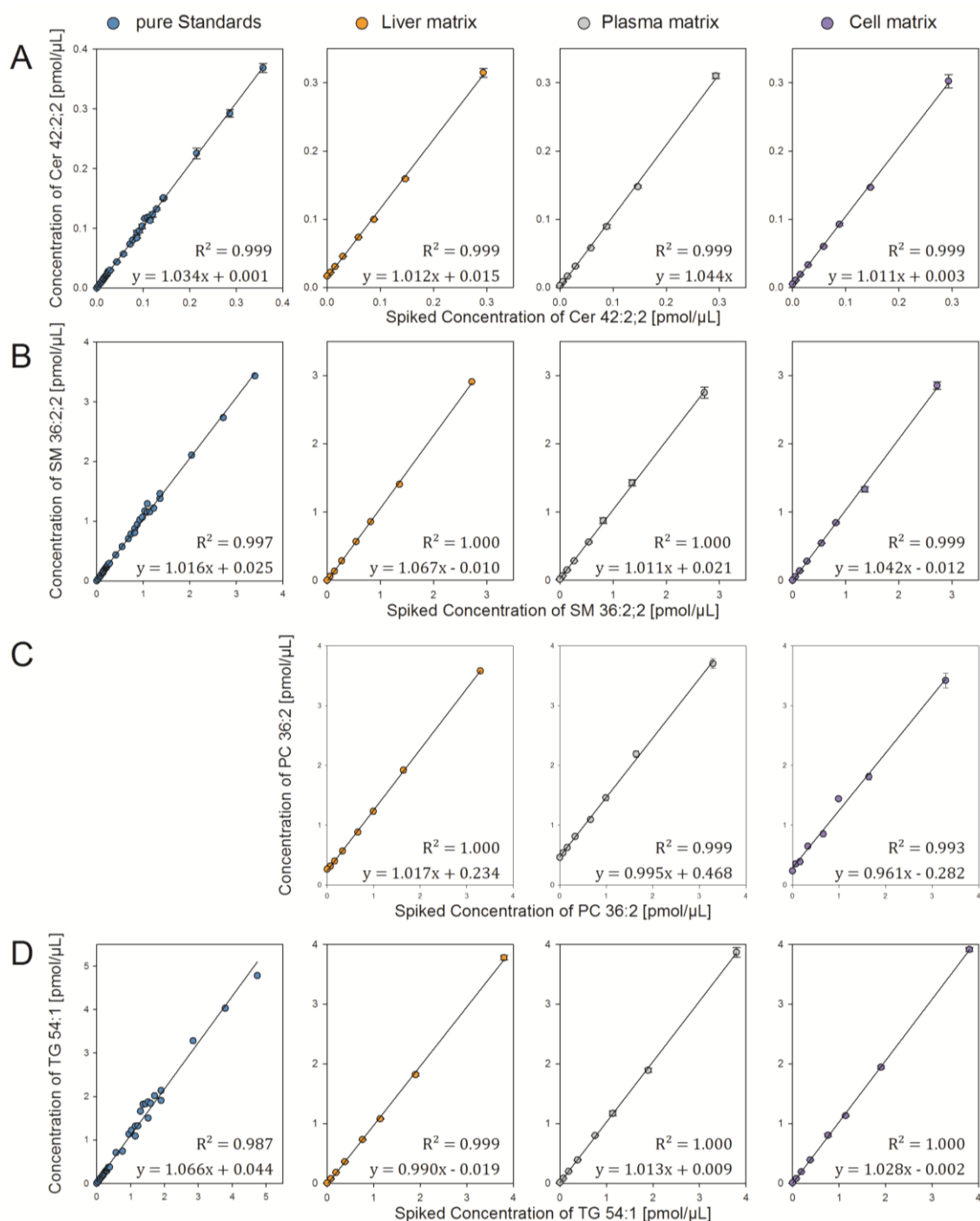


Figure 3.37 Dynamic range of quantification of FTMS analysis of (A) Cer 42:2;2, (B) SM 36:2;2, (C) PC 36:2, and (D) TG 54:1 using a target resolution of 140,000 at m/z 200. Each synthetic standard was analyzed (from left to right) without matrix (not performed for PC 36:2), and spiked on murine liver, human plasma and human fibroblast cells. The spectra display the correlation of measured and titrated concentration. Each data point represents the average of three replicate analyses per sample.

4 Conclusion

This work describes the development of a flow injection analysis Fourier Transform mass spectrometric method (FIA-FTMS) for lipid species quantification, which is – to our knowledge – the first application using a conventional LC pump system instead of a chip-based nano-flow to infuse crude lipid extracts of biological samples.

In order to achieve precise and reliable quantification, an automated isotope correction algorithm was developed. Since isotopic overlap is directly related to mass resolution, which decreases for orbitrap mass spectrometer with m/z , the correction algorithm was developed and evaluated for various mass ranges at the highest mass resolution setting of our instrument (140,000 at m/z 200). An unexpected finding was that peak intensities of near isobaric peaks resulting from DBA did not represent the intensity of both peaks most likely related to the so-called peak coalescence described for FTMS (Kaufmann & Walker, 2012). Here, we demonstrated that despite peak coalescence accurate quantification is possible for a wide range of lipid species. Thus, type II isotope correction is not required for fully overlapping peaks and accuracy of concentrations for partially overlapping peaks could be improved by so-called I/A correction (developed in this thesis). The I/A correction applies a correction factor calculated with intensity and area of the overlapping peaks. These m/z -dependent algorithms implemented in an automated data processing in combination with a simple sample preparation and short analysis time makes the method suitable for a comprehensive high throughput quantification of lipid species in a broad variety of biological samples.

Method comparison to a certified enzymatic test revealed that accurate quantification of CE species by FTMS requires utilization of individual species-specific response factors (illustrated in Figure 4.1). The marked, up to three-fold, differences in their analytical response are related to structural features, like length and double bond number of constituent acyl chains, which affect the susceptibility of CE species to undergo in-source fragmentation processes during electro-spray-ionization. The comparison with a chip-based infusion nano-ESI approach demonstrated that the vast effect of double bond number is

4 Conclusion

not limited to conventional ESI. Remarkably, the response trends observed for both ion sources were similar, despite disparate flow rates of 10 $\mu\text{L}/\text{min}$ and 200 nL/min for ESI and nano-ESI, respectively. This indicates that response correction is highly relevant and should be considered for different instrumental setups, not only for direct infusion methods but also for LC-based quantification. However, CE in-source fragmentation as main cause for response differences could be influenced by the build of the mass spectrometer, gas flow, and temperature. These parameters should also be considered with great care when developing lipidomic methods (Gathungu et al., 2018).

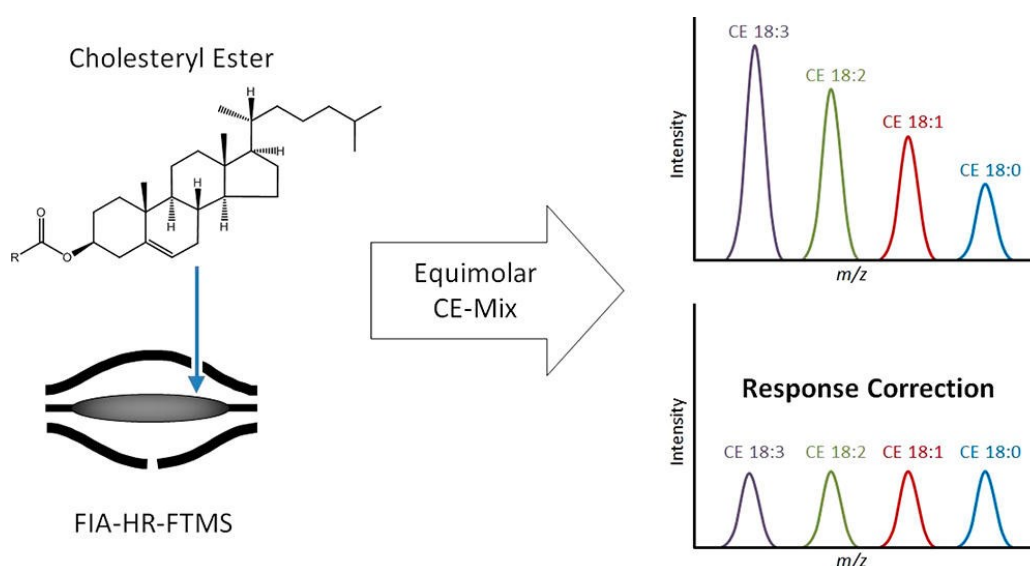


Figure 4.1 Schematic illustration of CE response correction.

Recently, Gallego et al. demonstrated superior performance of free cholesterol determination by MSX/FTMS in comparison with PRM and direct FTMS quantification (Gallego et al., 2017). The evaluation of free cholesterol quantification by MSX/FTMS in our setup demonstrated that the method provides a high accuracy and reproducibility. Comparison with an acetyl chloride derivatization method on a triple-quadrupole mass spectrometer (Liebisch et al., 2006) showed very good alignment of both concentrations.

In summary, validation of the method demonstrated that FIA-FTMS (including MSX/FTMS) is applicable for quantification of lipid species in biological samples

4 Conclusion

used in basic science as well as in clinical studies such as cultured cells, tissue homogenates, plasma, and serum.

5 Bibliography

- Aguilera-Romero, A., Gehin, C., & Riezman, H. (2014). Sphingolipid homeostasis in the web of metabolic routes. *Biochim Biophys Acta*, 1841(5), 647-656. doi:10.1016/j.bbalip.2013.10.014
- Aizikov, K., Mathur, R., & O'Connor, P. B. (2009). The spontaneous loss of coherence catastrophe in Fourier transform ion cyclotron resonance mass spectrometry. *J Am Soc Mass Spectrom*, 20(2), 247-256. doi:10.1016/j.jasms.2008.09.028
- Almeida, R., Pauling, J. K., Sokol, E., Hannibal-Bach, H. K., & Ejsing, C. S. (2015). Comprehensive lipidome analysis by shotgun lipidomics on a hybrid quadrupole-orbitrap-linear ion trap mass spectrometer. *J Am Soc Mass Spectrom*, 26(1), 133-148. doi:10.1007/s13361-014-1013-x
- Alonso, A., & Goni, F. M. (2018). The Physical Properties of Ceramides in Membranes. *Annu Rev Biophys*, 47, 633-654. doi:10.1146/annurev-biophys-070317-033309
- Bielow, C., Mastrobuoni, G., Orioli, M., & Kempa, S. (2017). On Mass Ambiguities in High-Resolution Shotgun Lipidomics. *Anal Chem*, 89(5), 2986-2994. doi:10.1021/acs.analchem.6b04456
- Blanksby, S. J., & Mitchell, T. W. (2010). Advances in mass spectrometry for lipidomics. *Annu Rev Anal Chem (Palo Alto Calif)*, 3, 433-465. doi:10.1146/annurev.anchem.111808.073705
- Bligh, E. G., & Dyer, W. J. (1959). A rapid method of total lipid extraction and purification. *Can J Biochem Physiol*, 37(8), 911-917. doi:10.1139/o59-099
- Bowden, J. A., Bangma, J. T., & Kucklick, J. R. (2014). Development of an automated multi-injection shotgun lipidomics approach using a triple quadrupole mass spectrometer. *Lipids*, 49(6), 609-619. doi:10.1007/s11745-014-3903-x
- Bowden, J. A., Heckert, A., Ulmer, C. Z., Jones, C. M., Koelmel, J. P., Abdullah, L., . . . Zhou, S. (2017). Harmonizing lipidomics: NIST interlaboratory comparison exercise for lipidomics using SRM 1950-Metabolites in Frozen Human Plasma. *J Lipid Res*, 58(12), 2275-2288. doi:10.1194/jlr.M079012
- Brugger, B., Erben, G., Sandhoff, R., Wieland, F. T., & Lehmann, W. D. (1997). Quantitative analysis of biological membrane lipids at the low picomole level by nano-electrospray ionization tandem mass spectrometry. *Proc Natl Acad Sci U S A*, 94(6), 2339-2344.
- Burla, B., Arita, M., Arita, M., Bendt, A. K., Cazenave-Gassiot, A., Dennis, E. A., . . . Wenk, M. R. (2018). MS-based lipidomics of human blood plasma - a community-initiated position paper to develop accepted guidelines. *J Lipid Res*. doi:10.1194/jlr.S087163
- Carta, G., Murru, E., Banni, S., & Manca, C. (2017). Palmitic Acid: Physiological Role, Metabolism and Nutritional Implications. *Front Physiol*, 8, 902. doi:10.3389/fphys.2017.00902
- Chen, J., Green, K. B., & Nichols, K. K. (2013). Quantitative profiling of major neutral lipid classes in human meibum by direct infusion electrospray ionization mass spectrometry. *Invest Ophthalmol Vis Sci*, 54(8), 5730-5753. doi:10.1167/iovs.12-10317

- Coleman, R. A., & Lee, D. P. (2004). Enzymes of triacylglycerol synthesis and their regulation. *Prog Lipid Res*, 43(2), 134-176. doi:https://doi.org/10.1016/S0163-7827(03)00051-1
- Cooper, G. (2000). *The Cell: A Molecular Approach*. 2nd edition. Chapter: *Structure of the Plasma Membrane*. Sinauer Associates.
- Cullen, P., Fobker, M., Tegelkamp, K., Meyer, K., Kannenberg, F., Cignarella, A., . . . Assmann, G. (1997). An improved method for quantification of cholesterol and cholesteryl esters in human monocyte-derived macrophages by high performance liquid chromatography with identification of unassigned cholesteryl ester species by means of secondary ion mass spectrometry. *J Lipid Res*, 38(2), 401-409.
- Dass, C. (2006). *Fundamentals of Contemporary Mass Spectrometry*: John Wiley & Sons, Inc., pp. 15-65.
- Davis, V. W., Bathe, O. F., Schiller, D. E., Slupsky, C. M., & Sawyer, M. B. (2011). Metabolomics and surgical oncology: Potential role for small molecule biomarkers. *J Surg Oncol*, 103(5), 451-459. doi:10.1002/jso.21831
- Dawber, T. R., Moore, F. E., & Mann, G. V. (1957). Coronary heart disease in the Framingham study. *Am J Public Health Nations Health*, 47(4 Pt 2), 4-24.
- Drobnik, W., Liebisch, G., Audebert, F. X., Frohlich, D., Gluck, T., Vogel, P., . . . Schmitz, G. (2003). Plasma ceramide and lysophosphatidylcholine inversely correlate with mortality in sepsis patients. *J Lipid Res*, 44(4), 754-761. doi:10.1194/jlr.M200401-JLR200
- Drobnik, W., Liebisch, G., Biederer, C., Tr mbach, B., Rogler, G., Muller, P., & Schmitz, G. (1999). Growth and cell cycle abnormalities of fibroblasts from Tangier disease patients. *Arterioscler Thromb Vasc Biol*, 19(1), 28-38.
- Ecker, J., Scherer, M., Schmitz, G., & Liebisch, G. (2012). A rapid GC-MS method for quantification of positional and geometric isomers of fatty acid methyl esters. *J Chromatogr B Analyt Technol Biomed Life Sci*, 897, 98-104. doi:10.1016/j.jchromb.2012.04.015
- Ejsing, C. S., Duchoslav, E., Sampaio, J., Simons, K., Bonner, R., Thiele, C., . . . Shevchenko, A. (2006). Automated identification and quantification of glycerophospholipid molecular species by multiple precursor ion scanning. *Anal Chem*, 78(17), 6202-6214. doi:10.1021/ac060545x
- Ejsing, C. S., Sampaio, J. L., Surendranath, V., Duchoslav, E., Ekroos, K., Klemm, R. W., . . . Shevchenko, A. (2009). Global analysis of the yeast lipidome by quantitative shotgun mass spectrometry. *Proc Natl Acad Sci U S A*, 106(7), 2136-2141. doi:10.1073/pnas.0811700106
- Ekroos, K., Janis, M., Tarasov, K., Hurme, R., & Laaksonen, R. (2010). Lipidomics: a tool for studies of atherosclerosis. *Curr Atheroscler Rep*, 12(4), 273-281. doi:10.1007/s11883-010-0110-y
- Fahy, E., Subramaniam, S., Brown, H. A., Glass, C. K., Merrill, A. H., Jr., Murphy, R. C., . . . Dennis, E. A. (2005). A comprehensive classification system for lipids. *J Lipid Res*, 46(5), 839-861. doi:10.1194/jlr.E400004-JLR200
- Fahy, E., Subramaniam, S., Murphy, R. C., Nishijima, M., Raetz, C. R., Shimizu, T., . . . Dennis, E. A. (2009). Update of the LIPID MAPS comprehensive

- classification system for lipids. *J Lipid Res*, 50 Suppl, S9-14. doi:10.1194/jlr.R800095-JLR200
- Fenn, J. B., Mann, M., Meng, C. K., Wong, S. F., & Whitehouse, C. M. (1989). Electrospray ionization for mass spectrometry of large biomolecules. *Science*, 246(4926), 64-71.
- Finnigan, R. E. (1994). Quadrupole mass spectrometers. *Anal Chem*, 66(19), 969A-975A. doi:10.1021/ac00091a002
- Gallego, S. F., Hojlund, K., & Ejsing, C. S. (2017). Easy, Fast, and Reproducible Quantification of Cholesterol and Other Lipids in Human Plasma by Combined High Resolution MSX and FTMS Analysis. *J Am Soc Mass Spectrom*. doi:10.1007/s13361-017-1829-2
- Gathungu, R. M., Larrea, P., Sniatynski, M. J., Marur, V. R., Bowden, J. A., Koelmel, J. P., . . . Kristal, B. S. (2018). Optimization of Electrospray Ionization Source Parameters for Lipidomics To Reduce Misannotation of In-Source Fragments as Precursor Ions. *Anal Chem*, 90(22), 13523-13532. doi:10.1021/acs.analchem.8b03436
- Glatz, J. F., Luiken, J. J., & Bonen, A. (2010). Membrane fatty acid transporters as regulators of lipid metabolism: implications for metabolic disease. *Physiol Rev*, 90(1), 367-417. doi:10.1152/physrev.00003.2009
- Grzybek, M., Palladini, A., Alexaki, V. I., Surma, M. A., Simons, K., Chavakis, T., . . . Coskun, U. (2019). Comprehensive and quantitative analysis of white and brown adipose tissue by shotgun lipidomics. *Mol Metab*. doi:10.1016/j.molmet.2019.01.009
- Haimi, P., Uphoff, A., Hermansson, M., & Somerharju, P. (2006). Software tools for analysis of mass spectrometric lipidome data. *Anal Chem*, 78(24), 8324-8331. doi:10.1021/ac061390w
- Han, X., & Gross, R. W. (2001). Quantitative analysis and molecular species fingerprinting of triacylglyceride molecular species directly from lipid extracts of biological samples by electrospray ionization tandem mass spectrometry. *Anal Biochem*, 295(1), 88-100. doi:10.1006/abio.2001.5178
- Han, X., & Gross, R. W. (2003). Global analyses of cellular lipidomes directly from crude extracts of biological samples by ESI mass spectrometry: a bridge to lipidomics. *J Lipid Res*, 44(6), 1071-1079. doi:10.1194/jlr.R300004-JLR200
- Han, X., & Gross, R. W. (2005). Shotgun lipidomics: electrospray ionization mass spectrometric analysis and quantitation of cellular lipidomes directly from crude extracts of biological samples. *Mass Spectrom Rev*, 24(3), 367-412. doi:10.1002/mas.20023
- Han, X., Yang, K., & Gross, R. W. (2012). Multi-dimensional mass spectrometry-based shotgun lipidomics and novel strategies for lipidomic analyses. *Mass Spectrom Rev*, 31(1), 134-178. doi:10.1002/mas.20342
- Heimerl, S., Fischer, M., Baessler, A., Liebisch, G., Sigrüener, A., Wallner, S., & Schmitz, G. (2014). Alterations of plasma lysophosphatidylcholine species in obesity and weight loss. *PLoS One*, 9(10), e111348. doi:10.1371/journal.pone.0111348
- Herzog, R., Schuhmann, K., Schwudke, D., Sampaio, J. L., Bornstein, S. R., Schroeder, M., & Shevchenko, A. (2012). LipidXplorer: a software for consensual cross-platform lipidomics. *PLoS One*, 7(1), e29851. doi:10.1371/journal.pone.0029851

- Hishikawa, D., Hashidate, T., Shimizu, T., & Shindou, H. (2014). Diversity and function of membrane glycerophospholipids generated by the remodeling pathway in mammalian cells. *J Lipid Res*, 55(5), 799-807. doi:10.1194/jlr.R046094
- Holcapek, M., Liebisch, G., & Ekroos, K. (2018). Lipidomic Analysis. *Anal Chem*, 90(7), 4249-4257. doi:10.1021/acs.analchem.7b05395
- Hopkins, P. N., Heiss, G., Ellison, R. C., Province, M. A., Pankow, J. S., Eckfeldt, J. H., & Hunt, S. C. (2003). Coronary artery disease risk in familial combined hyperlipidemia and familial hypertriglyceridemia: a case-control comparison from the National Heart, Lung, and Blood Institute Family Heart Study. *Circulation*, 108(5), 519-523. doi:10.1161/01.cir.0000081777.17879.85
- Horing, M., Ejasing, C. S., Hermansson, M., & Liebisch, G. (2019). Quantification of Cholesterol and Cholesteryl Ester by Direct Flow Injection High Resolution FTMS Utilizing Species-Specific Response Factors. *Anal Chem*. doi:10.1021/acs.analchem.8b05013
- Horton, J. D., Goldstein, J. L., & Brown, M. S. (2002). SREBPs: activators of the complete program of cholesterol and fatty acid synthesis in the liver. *J Clin Invest*, 109(9), 1125-1131. doi:10.1172/jci15593
- Houjou, T., Yamatani, K., Imagawa, M., Shimizu, T., & Taguchi, R. (2005). A shotgun tandem mass spectrometric analysis of phospholipids with normal-phase and/or reverse-phase liquid chromatography/electrospray ionization mass spectrometry. *Rapid Commun Mass Spectrom*, 19(5), 654-666. doi:10.1002/rcm.1836
- Hu, T., & Zhang, J. L. (2018). Mass-spectrometry-based lipidomics. *J Sep Sci*, 41(1), 351-372. doi:10.1002/jssc.201700709
- Huang, J., Tiedemann, P. W., Land, D. P., McIver, R. T., & Hemminger, J. C. (1994). Dynamics of ion coupling in an FTMS ion trap and resulting effects on mass spectra, including isotope ratios. *International Journal of Mass Spectrometry and Ion Processes*, 134(1), 11-21. doi:https://doi.org/10.1016/0168-1176(94)03964-X
- Hubner, G., Crone, C., & Lindner, B. (2009). lipID--a software tool for automated assignment of lipids in mass spectra. *J Mass Spectrom*, 44(12), 1676-1683. doi:10.1002/jms.1673
- Husen, P., Tarasov, K., Katafiasz, M., Sokol, E., Vogt, J., Baumgart, J., . . . Ejasing, C. S. (2013). Analysis of lipid experiments (ALEX): a software framework for analysis of high-resolution shotgun lipidomics data. *PLoS One*, 8(11), e79736. doi:10.1371/journal.pone.0079736
- Hussain, M. M. (2014). Intestinal lipid absorption and lipoprotein formation. *Curr Opin Lipidol*, 25(3), 200-206. doi:10.1097/mol.0000000000000084
- Hutchins, P. M., Barkley, R. M., & Murphy, R. C. (2008). Separation of cellular nonpolar neutral lipids by normal-phase chromatography and analysis by electrospray ionization mass spectrometry. *J Lipid Res*, 49(4), 804-813. doi:10.1194/jlr.M700521-JLR200
- Jung, H. R., Sylv  nne, T., Koistinen, K. M., Tarasov, K., Kauhanen, D., & Ekroos, K. (2011). High throughput quantitative molecular lipidomics. *Biochimica et Biophysica Acta (BBA) - Molecular and Cell Biology of Lipids*, 1811(11), 925-934. doi:https://doi.org/10.1016/j.bbalip.2011.06.025

- Kaufmann, A., & Walker, S. (2012). Accuracy of relative isotopic abundance and mass measurements in a single-stage orbitrap mass spectrometer. *Rapid Commun Mass Spectrom*, 26(9), 1081-1090. doi:10.1002/rcm.6195
- Kohno, S., Keenan, A. L., Ntambi, J. M., & Miyazaki, M. (2018). Lipidomic insight into cardiovascular diseases. *Biochem Biophys Res Commun*, 504(3), 590-595. doi:10.1016/j.bbrc.2018.04.106
- Koivusalo, M., Haimi, P., Heikinheimo, L., Kostinen, R., & Somerharju, P. (2001). Quantitative determination of phospholipid compositions by ESI-MS: effects of acyl chain length, unsaturation, and lipid concentration on instrument response. *J Lipid Res*, 42(4), 663-672.
- Krakowiak, P. A., Wassif, C. A., Kratz, L., Cozma, D., Kovarova, M., Harris, G., . . . Porter, F. D. (2003). Lathosterolosis: an inborn error of human and murine cholesterol synthesis due to lathosterol 5-desaturase deficiency. *Hum Mol Genet*, 12(13), 1631-1641.
- Krautbauer, S., & Liebisch, G. (2018). LC-MS/MS Analysis of Bile Acids. *Methods Mol Biol*, 1730, 103-110. doi:10.1007/978-1-4939-7592-1_8
- Lagarde, M., Geloën, A., Record, M., Vance, D., & Spener, F. (2003). Lipidomics is emerging. *Biochim Biophys Acta*, 1634(3), 61.
- Leavell, M. D., & Leary, J. A. (2006). Fatty acid analysis tool (FAAT): An FT-ICR MS lipid analysis algorithm. *Anal Chem*, 78(15), 5497-5503. doi:10.1021/ac0604179
- Liebisch, G., Binder, M., Schifferer, R., Langmann, T., Schulz, B., & Schmitz, G. (2006). High throughput quantification of cholesterol and cholesteryl ester by electrospray ionization tandem mass spectrometry (ESI-MS/MS). *Biochim Biophys Acta*, 1761(1), 121-128. doi:10.1016/j.bbalip.2005.12.007
- Liebisch, G., Lieser, B., Rathenber, J., Drobnik, W., & Schmitz, G. (2004). High-throughput quantification of phosphatidylcholine and sphingomyelin by electrospray ionization tandem mass spectrometry coupled with isotope correction algorithm. *Biochim Biophys Acta*, 1686(1-2), 108-117. doi:10.1016/j.bbalip.2004.09.003
- Liebisch, G., & Matysik, S. (2015). Accurate and reliable quantification of 25-hydroxy-vitamin D species by liquid chromatography high-resolution tandem mass spectrometry. *J Lipid Res*, 56(6), 1234-1239. doi:10.1194/jlr.D058511
- Liebisch, G., Vizcaino, J. A., Kofeler, H., Trotschmuller, M., Griffiths, W. J., Schmitz, G., . . . Wakelam, M. J. (2013). Shorthand notation for lipid structures derived from mass spectrometry. *J Lipid Res*, 54(6), 1523-1530. doi:10.1194/jlr.M033506
- Makarov, A. (2000). Electrostatic Axially Harmonic Orbital Trapping: A High-Performance Technique of Mass Analysis. *Anal Chem*, 72(6), 1156-1162. doi:10.1021/ac991131p
- Makarov, A., Denisov, E., Kholomeev, A., Balschun, W., Lange, O., Strupat, K., & Horning, S. (2006). Performance evaluation of a hybrid linear ion trap/orbitrap mass spectrometer. *Anal Chem*, 78(7), 2113-2120. doi:10.1021/ac0518811
- Mapstone, M., Cheema, A. K., Fiandaca, M. S., Zhong, X., Mhyre, T. R., MacArthur, L. H., . . . Federoff, H. J. (2014). Plasma phospholipids

- identify antecedent memory impairment in older adults. *Nat Med*, 20(4), 415-418. doi:10.1038/nm.3466
- Matysik, S., & Liebisch, G. (2017). Quantification of steroid hormones in human serum by liquid chromatography-high resolution tandem mass spectrometry. *J Chromatogr A*, 1526, 112-118. doi:10.1016/j.chroma.2017.10.042
- Merrill, A. H., Jr. (2011). Sphingolipid and glycosphingolipid metabolic pathways in the era of sphingolipidomics. *Chem Rev*, 111(10), 6387-6422. doi:10.1021/cr2002917
- Mu, H., & Hoy, C. E. (2004). The digestion of dietary triacylglycerols. *Prog Lipid Res*, 43(2), 105-133.
- Mullen, T. D., & Obeid, L. M. (2012). Ceramide and apoptosis: exploring the enigmatic connections between sphingolipid metabolism and programmed cell death. *Anticancer Agents Med Chem*, 12(4), 340-363.
- Murphy, R. C. (2015). Tandem Mass Spectrometry of Lipids: Molecular Analysis of Complex Lipids. *Royal Society of Chemistry*, 233-244.
- Myers, D. S., Ivanova, P. T., Milne, S. B., & Brown, H. A. (2011). Quantitative analysis of glycerophospholipids by LC-MS: Acquisition, data handling, and interpretation. *Biochimica et Biophysica Acta (BBA) - Molecular and Cell Biology of Lipids*, 1811(11), 748-757. doi:https://doi.org/10.1016/j.bbalip.2011.05.015
- Nakata, M. T., Hart, G. W., & Peterson, B. G. (2010). Peak coalescence, spontaneous loss of coherence, and quantification of the relative abundances of two species in the plasma regime: particle-in-cell modeling of Fourier transform ion cyclotron resonance mass spectrometry. *J Am Soc Mass Spectrom*, 21(10), 1712-1719. doi:10.1016/j.jasms.2010.06.004
- Paltauf, F. (1994). Ether lipids in biomembranes. *Chemistry and Physics of Lipids*, 74(2), 101-139. doi:https://doi.org/10.1016/0009-3084(94)90054-X
- Pan, X., & Hussain, M. M. (2012). Gut triglyceride production. *Biochim Biophys Acta*, 1821(5), 727-735. doi:10.1016/j.bbalip.2011.09.013
- Peng, B., Geue, S., Coman, C., Munzer, P., Kopczynski, D., Has, C., . . . Ahrends, R. (2018). Identification of key lipids critical for platelet activation by comprehensive analysis of the platelet lipidome. *Blood*, 132(5), e1-e12. doi:10.1182/blood-2017-12-822890
- Prescott, S. M., Zimmerman, G. A., Stafforini, D. M., & McIntyre, T. M. (2000). Platelet-activating factor and related lipid mediators. *Annu Rev Biochem*, 69, 419-445. doi:10.1146/annurev.biochem.69.1.419
- Rockwood, A. L., & Haimi, P. (2006). Efficient calculation of accurate masses of isotopic peaks. *J Am Soc Mass Spectrom*, 17(3), 415-419. doi:10.1016/j.jasms.2005.12.001
- Rosman, K. J. R., & Taylor, P. D. P. (1998). Isotopic Compositions of the Elements. *Pure & Appl. Chem.*, 70(1), 217-235.
- Sales, S., Graessler, J., Ciucci, S., Al-Atrib, R., Vihervaara, T., Schuhmann, K., . . . Shevchenko, A. (2016). Gender, Contraceptives and Individual Metabolic Predisposition Shape a Healthy Plasma Lipidome. *Sci Rep*, 6, 27710. doi:10.1038/srep27710
- Santos, C. R., & Schulze, A. (2012). Lipid metabolism in cancer. *Febs j*, 279(15), 2610-2623. doi:10.1111/j.1742-4658.2012.08644.x

- Schott, H. F., Krautbauer, S., Horing, M., Liebisch, G., & Matysik, S. (2018). A Validated, Fast Method for Quantification of Sterols and Gut Microbiome Derived 5 α /beta-Stanols in Human Feces by Isotope Dilution LC-High-Resolution MS. *Anal Chem*, 90(14), 8487-8494. doi:10.1021/acs.analchem.8b01278
- Schuhmann, K., Srzentic, K., Nagornov, K. O., Thomas, H., Gutmann, T., Coskun, U., . . . Shevchenko, A. (2017). Monitoring Membrane Lipidome Turnover by Metabolic (¹⁵N) Labeling and Shotgun Ultra-High-Resolution Orbitrap Fourier Transform Mass Spectrometry. *Anal Chem*, 89(23), 12857-12865. doi:10.1021/acs.analchem.7b03437
- Schwudke, D., Oegema, J., Burton, L., Entchev, E., Hannich, J. T., Ejsing, C. S., . . . Shevchenko, A. (2006). Lipid profiling by multiple precursor and neutral loss scanning driven by the data-dependent acquisition. *Anal Chem*, 78(2), 585-595. doi:10.1021/ac051605m
- Sigruener, A., Kleber, M. E., Heimerl, S., Liebisch, G., Schmitz, G., & Maerz, W. (2014). Glycerophospholipid and sphingolipid species and mortality: the Ludwigshafen Risk and Cardiovascular Health (LURIC) study. *PLoS One*, 9(1), e85724. doi:10.1371/journal.pone.0085724
- Sokol, E., Almeida, R., Hannibal-Bach, H. K., Kotowska, D., Vogt, J., Baumgart, J., . . . Ejsing, C. S. (2013). Profiling of lipid species by normal-phase liquid chromatography, nanoelectrospray ionization, and ion trap-orbitrap mass spectrometry. *Anal Biochem*, 443(1), 88-96. doi:https://doi.org/10.1016/j.ab.2013.08.020
- Song, H., Hsu, F. F., Ladenson, J., & Turk, J. (2007). Algorithm for processing raw mass spectrometric data to identify and quantitate complex lipid molecular species in mixtures by data-dependent scanning and fragment ion database searching. *J Am Soc Mass Spectrom*, 18(10), 1848-1858. doi:10.1016/j.jasms.2007.07.023
- Staneva, G., Momchilova, A., Wolf, C., Quinn, P. J., & Koumanov, K. (2009). Membrane microdomains: role of ceramides in the maintenance of their structure and functions. *Biochim Biophys Acta*, 1788(3), 666-675. doi:10.1016/j.bbamem.2008.10.026
- Stone, N. J., Robinson, J. G., Lichtenstein, A. H., Bairey Merz, C. N., Blum, C. B., Eckel, R. H., . . . Wilson, P. W. (2014). 2013 ACC/AHA guideline on the treatment of blood cholesterol to reduce atherosclerotic cardiovascular risk in adults: a report of the American College of Cardiology/American Heart Association Task Force on Practice Guidelines. *J Am Coll Cardiol*, 63(25 Pt B), 2889-2934. doi:10.1016/j.jacc.2013.11.002
- Stubbs, C. D., & Smith, A. D. (1984). The modification of mammalian membrane polyunsaturated fatty acid composition in relation to membrane fluidity and function. *Biochim Biophys Acta*, 779(1), 89-137.
- Surma, M. A., Herzog, R., Vasilj, A., Klose, C., Christinat, N., Morin-Rivron, D., . . . Sampaio, J. L. (2015). An automated shotgun lipidomics platform for high throughput, comprehensive, and quantitative analysis of blood plasma intact lipids. *Eur J Lipid Sci Technol*, 117(10), 1540-1549. doi:10.1002/ejlt.201500145
- van Meer, G. (2005). Cellular lipidomics. *Embo j*, 24(18), 3159-3165. doi:10.1038/sj.emboj.7600798

5 Bibliography

- van Meer, G., Voelker, D. R., & Feigenson, G. W. (2008). Membrane lipids: where they are and how they behave. *Nat Rev Mol Cell Biol*, 9(2), 112-124. doi:10.1038/nrm2330
- Wenk, M. R. (2005). The emerging field of lipidomics. *Nat Rev Drug Discov*, 4(7), 594-610. doi:10.1038/nrd1776
- Wiesner, P., Leidl, K., Boettcher, A., Schmitz, G., & Liebisch, G. (2009). Lipid profiling of FPLC-separated lipoprotein fractions by electrospray ionization tandem mass spectrometry. *J Lipid Res*, 50(3), 574-585. doi:10.1194/jlr.D800028-JLR200
- Yang, K., & Han, X. (2011). Accurate quantification of lipid species by electrospray ionization mass spectrometry - Meet a key challenge in lipidomics. *Metabolites*, 1(1), 21-40. doi:10.3390/metabo1010021
- Yang, K., & Han, X. (2016). Lipidomics: Techniques, Applications, and Outcomes Related to Biomedical Sciences. *Trends Biochem Sci*, 41(11), 954-969. doi:10.1016/j.tibs.2016.08.010
- Yetukuri, L., Ekroos, K., Vidal-Puig, A., & Oresic, M. (2008). Informatics and computational strategies for the study of lipids. *Mol Biosyst*, 4(2), 121-127. doi:10.1039/b715468b
- Zubarev, R. A., & Makarov, A. (2013). Orbitrap Mass Spectrometry. *Anal Chem*, 85(11), 5288-5296. doi:10.1021/ac4001223

V Acknowledgement

First of all, I would like to express my sincere gratitude to my supervisor PD Dr. Gerhard Liebisch for giving me the possibility to work on this interesting project and, special thanks, for the continuous and caring support throughout my PhD thesis. I could always count on you, in scientific matters as well as in personal issues.

Beside my supervisor, I would like to thank my thesis committee, Prof. Dr. Christa Büchler and Associate Prof. Christer Ejlsing, for numerous discussions and insightful comments which helped me a lot to understand and widen my perspective on the project. And thank you very much Christer for the cordial welcome in your laboratory in Odense.

Moreover, let me express special thanks to Hans, Sabrina, Silke and Stefan for several constructive discussions and advices, and of course for the enjoyable atmosphere at work.

My sincere thanks also goes to Dr. Josef Ecker who provided different samples of interest that made the basis of extensive method development and involved me in various research projects.

Additionally, I thank my fellow labmates of the Institute of Clinical Chemistry for the pleasant and friendly atmosphere, especially to mention Doreen, Simone, Jürgen and Sebastian for their steady helpfulness in the lab.

Finally, I would particularly like to thank my girlfriend Sibylle, my mother Gerti and my father Thomas for the support in all aspects of life. You have been there for me, always.

VI Lebenslauf

Name: Marcus Domenic Höring
Geboren: 09.03.1989
Geburtsort: Würzburg, Deutschland
Email: marcus.hoering@ukr.de



Bildungsweg

Seit 07/2016

Doktorarbeit

am Institut für klinische Chemie und Laboratoriumsmedizin,
Universitätsklinikum Regensburg
Betreuer: PD Dr. Gerhard Liebisch

10/2013 – 06/2016

Masterstudiengang Biologie

an der Universität Regensburg

Masterarbeit am Institut für Biophysik und physikalische
Biochemie
Thema: Hochdruck-NMR-Spektroskopie am Ras-
Protein

09/2014 – 02/2015

Auslandssemester

an der Université Aix-Marseille (Marseille, Frankreich)

10/2010 – 09/2013

Bachelorstudiengang Biologie

an der Julius-Maximilians-Universität Würzburg

Bachelorarbeit am Institut für Biotechnologie und
Biophysik
Thema: Dielektrische Analyse von humanen
Glioblastomzellen

09/1999 – 07/2009

Allgemeine Hochschulreife

am Städtisches Mozart- und Schönborn Gymnasium Würzburg

Publikationen

Horing, M.; Ejlsing, C. S.; Hermansson, M.; Liebisch, G., Quantification of Cholesterol and Cholesteryl Ester by Direct Flow Injection High Resolution FTMS Utilizing Species-Specific Response Factors. *Analytical chemistry* **2019**.

Schott, H. F.; Krautbauer, S.; **Horing, M.**; Liebisch, G.; Matysik, S., A Validated, Fast Method for Quantification of Sterols and Gut Microbiome Derived 5alpha/beta-Stanols in Human Feces by Isotope Dilution LC-High-Resolution MS. *Analytical chemistry* **2018**, 90 (14), 8487-8494.

Spoerner, M.; Karl, M.; Lopes, P.; **Hoering, M.**; Loeffel, K.; Nuehs, A.; Adelsberger, J.; Kremer, W.; Kalbitzer, H. R., High pressure (31)P NMR spectroscopy on guanine nucleotides. *Journal of biomolecular NMR* **2017**, 67 (1), 1-13.

Memmel, S.; Sukhorukov, V. L.; **Horing, M.**; Westerling, K.; Fiedler, V.; Katzer, A.; Krohne, G.; Flentje, M.; Djuzenova, C. S., Cell surface area and membrane folding in glioblastoma cell lines differing in PTEN and p53 status. *PloS one* **2014**, 9 (1), e87052.

VII Selbständigkeitserklärung

“Ich, Höring, Marcus Domenic geboren am 09.03.1989 in Würzburg, erkläre hiermit, dass ich die vorliegende Arbeit ohne unzulässige Hilfe Dritter und ohne Benutzung anderer als der angegebenen Hilfsmittel angefertigt habe.

Die aus anderen Quellen direkt oder indirekt übernommenen Daten und Konzepte sind unter Angabe der Quelle gekennzeichnet. Insbesondere habe ich nicht die entgeltliche Hilfe von Vermittlungs- bzw. Beratungsdiensten (Promotionsberater oder andere Personen) in Anspruch genommen.

Die Arbeit wurde bisher weder im In- noch im Ausland in gleicher oder ähnlicher Form einer anderen Prüfungsbehörde vorgelegt.

Ort, Datum

eigenhändige Unterschrift
des Promovenden

